FABRICATION, TESTING AND PERFORMANCE ENHANCEMENT OF A SMALL SCALE TIDAL CURRENT TURBINE

NG KAI WERN

DISSERTATION SUBMITTED IN FULFILMENT OF THE REQUIREMENTS FOR THE DEGREEE OF MASTER OF PHILOSOPHY

FACULTY OF ENGINEERING
UNVERSITY OF MALAYA
KUALA LUMPUR

2016

FABRICATION, TESTING AND PERFORMANCE
ENHANCEMENT OF A SMALL SCALE
TIDAL CURRENT TURBINE

NG KAI WERN

DISSERTATION SUBMITTED IN FULFILMENT OF THE
REQUIREMENTS FOR THE DEGREEE OF
MASTER OF PHILOSOPHY

DEPARTMENT OF CIVIL ENGINEERING
FACULTY OF ENGINEERING
UNVERSITY OF MALAYA
KUALA LUMPUR

2016

UNIVERSITY OF MALAYA
ORIGINAL LITERARY WORK DECLARATION

Name of Candidate: NG KAI WERN

Matric No: KHA 120118

Name of Degree: MASTER OF PHILOSOPHY

Title of Project Paper/Research Report/Dissertation/Thesis ("this Work"):

Fabrication, Testing and Performance Enhancement of a Small Scale Tidal Current Turbine

Field of Study: Water Resource Engineering

I do solemnly and sincerely declare that:

(1) I am the sole author/writer of this Work;
(2) This Work is original;
(3) Any use of any work in which copyright exists was done by way of fair dealing and for permitted purposes and any excerpt or extract from, or reference to or reproduction of any copyright work has been disclosed expressly and sufficiently and the title of the Work and its authorship have been acknowledged in this Work;
(4) I do not have any actual knowledge nor do I ought reasonably to know that the making of this work constitutes an infringement of any copyright work;
(5) I hereby assign all and every rights in the copyright to this Work to the University of Malaya ("UM"), who henceforth shall be owner of the copyright in this Work and that any reproduction or use in any form or by any means whatsoever is prohibited without the written consent of UM having been first had and obtained;
(6) I am fully aware that if in the course of making this Work I have infringed any copyright whether intentionally or otherwise, I may be subject to legal action or any other action as may be determined by UM.

Candidate's Signature   Date: 25/4/2018

Subscribed and solemnly declared before,

Witness's Signature   Date:

Name:

Designation:

ABSTRACT

The working concept of a horizontal-axis tidal current turbine (HATCT) is similar to that of wind turbines. The technology used in wind turbine can be readily transferred to tidal current turbines. This is exactly what is going on at the moment in HATCTs industry. Malaysia is a country that can benefit from tidal current turbine, especially in the Straits of Malacca. The current flow in the Straits of Malacca varies from 0.5m/s to 1.5m/s, and reaches 2.0m/s or above at some localities. Considering the benchmark of economic power generation for tidal current turbines to be around 1.5m/s, harnessing tidal current energy looks promising for Malaysia. However, to-date, no study on creating a workable turbine has been reported for Malaysia. Therefore, it is the aim of the current research to study workability and performance of an operational tidal current turbine for Malaysia. The testing and modification of turbine were done with the sponsor and help of Laison Engineering Sdn. Bhd. A 800mm five-bladed turbine was tested at Pangkor Island. The original setting of the prototype turbine was not able to produce steady power output. But after a few modifications on the generator and shaft, a power coefficient of approximately 0.32 was achieved with current velocity of 0.25m/s. Besides the fabrication and testing of the turbine, an innovative method to improve the efficiency of tidal current turbine has also been studied. The innovative method was the use of hydrophobic antifouling paint. Antifouling paint is an important protection measure for tidal current turbine to against marine bio-fouling. Marine bio-fouling has deteriorating effects on the performance of tidal current turbine once they are attached on the turbine blades. Hydrophobic anti-fouling paint is one of the common types of anti-fouling paint that is used. Interestingly, its hydrophobicity has the ability to reduce friction drag over a surface. As such, hydrophobic anti-fouling can potentially provide performance enhancement for a tidal current turbine, meanwhile protects turbine blades

from marine bio-fouling. Two commercial hydrophobic antifouling coatings, Biocyl and a normal hydrophobic coating, Always Dry were used. Experiment has been conducted to understand the effects of hydrophobic coating on hydrofoils and a 350mm diameter three-bladed turbine. It was found that both Biocyl and Always Dry lower the drag coefficient of NACA 63418 by an average of 3% and 3.5%. Biocyl has improved the revolution per minute of the turbine by an average of 1.3%, whereas Always Dry has improved the revolution per minute of the turbine by an average of 2.5%. Last but not least, two commercial antifouling paints, namely Bioycl and Palccoat, have been tested to understand their ability to protect tidal current turbine from marine bio-fouling activities in Pangkor Island. The field test results show that with these anti-fouling paints, the development of thin film on turbine blade can be postponed to 3~4weeks. Up to this stage, the thin film can still be cleaned. However, when barnacles started to grow on the blade, it is difficult to remove the barnacle by simple cleaning.

ABSTRAK

Konsep turbin arus laut (HATCTs) mendatar adalah serupa dengan turbin angin. Turbin digunakan untuk menagkap tenaga kinetik daripade bendalir yang mengalir. Teknologi yang sedang digunakan dalam bidang turbin angina boleh dipindah dan digunakan dalam bidang turbin aras laut. Sebenarnya, inilah yang sedang dijalankan dalam bidang HATCTs. Malaysia merupakan sebuah negara yang boleh mendapat manfaat daripada turbine aras laut, terutamanya di Selat Melaka. Halaju arus laut di Selat Melaka adalah dalam lingkungan 0.5m/s ke 1.5m/s, dan melebihi 2.0m/s di lokaliti tertentu. Memandangkan tanda aras penjanaan kuasa yang berekonomik bagi turbin arus laut adalah lebih kurang 1.5m/s, potensi bagi penangkapan tenaga arus laut di Malaysia adalah cerah. Namun, sehingga kini, tiada pengajian berkaitan dengan penciptaan turbin aras laut yang berfungsi dilaporkan di Malaysia. Oleh sedemikian, matllamt kajian ini adalah untuk menguji prestasi satu turbin arus laut yang berfungsi bagi Malaysia. Pengujian dan pengubahsuaian turbin arus laut telah dilakukan dengan penajaan dan pembantuan daripada Laison Engineering Sdn. Bhd. Sebuah turbin dengan lima bilah telah direka dan diuji di Pulau Pangkor. Pengaturan asal turbin prototaip tidak dapat menjanakan kuasa dengan stabil. Tetapi selepas beberapa pengubahsuaian kepada penjana dan aci, koefisien kuasa berhampir 0.32 telah dicapai dengan 0.25m/s halaju arus laut. Selain daripada perekaan dan pengujian turbin, satu cara innovasi bagi mempertingkatkan kecekapan turbin juga dikaji. Cara innovasi tersebut adalah penggunaan cat antifouling hidrophobik. Cat antifouling merupakan langkah penting bagi melindungi bilah turbin daripada fouling marin. Fouling marin boleh menjejaskan performa turbin arus laut sekali mareka melekat di atas bilah turbin. Cat antifouling hidrophobik merupakan salah satu jenis cat antifouling yang biasa dipakai. Yang menariknya, sifat hidrophobiknya berupaya mengurangkan geseran seret sebuah

permukaan. Oleh demikian, cat ini berpotensi mempertingkatkan performa turbin arus laut, sementaranya melindungi bilah turbin daripada foulind marin. Dua cat antifouling hidrophobik komersial, Biocyl dan Always Dry telah digunakan. Eksperimen telah dilakukan untuk mengaji kesan lapisan hidrophobik terhadap hydrofoils dan sebuah turbin tiga bilah berdiameter 350mm. Adalah didapati bahawa Biocyl dan Always Dry mengurangkan koefisien seret bagi NACA 63418 dengan purata sebanyak 3% dan 3.5%. Biocyl telah meningkatkan revolusi seminit bagi turbin dengan purata sebanyak 1.3%, manakala Always Dry telah meningkatkan revolusi seminit bagi turbin dengan purata sebanyak 2.5%. Akhir sekali, dua cat antifouling komersial, Biocyl dan Palccoat, juga diuji untuk memahami keupayaan mereka bagi melindungi turbin arus laut daripada aktiviti fouling marin di Pulau Pangkor. Keputusan ujian lapangan menunjukkan bahawa kedua-dua cat dapat melambatkan pertumbuhan filem nipis di atas bilah turbin kepada 3~4 minggu. Pada peringkat ini, filem nipis masih dapat dicucikan. Namun, apabila teritip mula bertumbuh di atas bilah, ia adalah susah untuk menghapuskan teritip dengan cara pembersihan biasa.

ACKNOWLEDGEMENT

TABLE OF CONTENTS

LIST OF FIGURES

xiii

LIST OF TABLES

LIST OF ABREVIATIONS/SYMBOLS

HATCT	-	Horizontal-axis tidal current turbine
BEM	-	Blade Element Momentum
F_{dm}	-	Tide-generating force
G	-	Gravitational constant
M_m	-	Mass of the Moon
R_e	-	Radius of the Earth
d_m	-	Distance between the centre of mass of the Moon and the Earth
E	-	Energy per area
ρ	-	Density of seawater
V	-	Velocity of tidal current
A_c	-	Cross-sectional area of a channel
A	-	Swept area of a HATCT
U_o	-	Undisturbed upstream/downstream velocity of a channel
U_1	-	Velocity passing through a HATCT
U_3	-	Velocity within the wake of a HATCT
U_4	-	Velocity outside the wake of a HATCT
P_o	-	Undisturbed upstream pressure of a channel
P_1	-	Pressure immediately before a HATCT
P_2	-	Pressure immediately after a HATCT
P_4	-	Pressure outside the wake of a HATCT
P_5	-	Downstream pressure of a channel
P	-	Power harnessed by a HATCT
r	-	U_3/U_o

$\in$	-	A/A_c
U_∞	-	Free stream velocity
u_s	-	Slip velocity
$\partial u/\partial y$	-	Shear rate
B	-	Slip length
τ_w	-	Shear stress
μ	-	Viscosity of a fluid
v	-	Kinematic viscosity of a fluid
Re	-	Reynolds number
R_D	-	Friction drag reduction rate
C_P	-	Power coefficient of a HATCT
C_L	-	Lift coefficient of a hydrofoil
C_D	-	Drag coefficient of a hydrofoil
C_T	-	Thrust coefficient of a HATCT
AoA	-	Angle of attack
L/D	-	Lift-to-drag ratio
TSR	-	Tip speed ratio
RPM	-	Revolution per minute
CFD	-	Computational fluid dynamics
IG	-	Induction generator
PMSG	-	Permanent magnet synchronous generator
DDPM	-	Direct drive permanent magnet generator
DFIG	-	Doubly-fed induction generator
FBT	-	800mm small scale five-bladed turbine
TBT	-	350mm lab-scale three-bladed turbine

CHAPTER 1: INTRODUCTION

1.1 Overview

The world population has been growing sharply since the past few decades. This growing rate has led to concerns on water security, food security and energy security. The concept of sustainability has been proposed as a solution to achieve balance between consumption and regeneration of the aforementioned resources. Ironically, this is highly dependent on individual behaviour. Practically, no fruitful results have been achieved since the concept of sustainability was proposed. This in turn leads to the need for new methods or technologies that can create more drinkable water, food and energy.

Solving the three concerns simultaneously is rather impractical, even solving one of these requires extremely large efforts. Modern society relies heavily on energy; even the process involved in growing food and producing drinkable water consumes a significant amount of energy. Without sufficient supply of energy, bulk production of food and drinkable water will not be made possible. This is one of the reasons that researchers normally focus more on solving energy concerns compared to the other two. Additionally, most energy sources are of non-renewables, i.e. fossil fuels, which are depleting and produce harmful substances to environment during energy generation process.

All these reasons, couple with the energy crisis in 1970s (Rocks & Runyon, 1972), have driven the world in seek of renewable and environmental friendly energy sources. The common types of renewable energy known by the public are hydropower, solar energy and wind energy. Some of the less known are geothermal energy and ocean energy. Biomass energy and refuse-derived fuels are another branch of renewable

energy which are derived from unwanted organic waste. Among these energy sources, technologies for harnessing hydropower, solar energy and wind energy are the most mature. This is attributed to the higher accessibility of these energy sources and challenges associate with harnessing these sources are relatively easier to address. Hence, a large portion of renewable energy supply is currently coming from these three energy sources, both small scale and commercial scale.

On the other hand, technologies for harnessing geothermal energy and ocean energy are less developed. One of the main reasons is these two energy resources are only available at a certain locations, and those locations are usually far from populated regions. Geothermal energy is only viable for countries located around the Pacific Ring of Fire. For ocean energy, it is only available for countries that have coastal line or surrounded by ocean. Therefore, it is only of interest to limited regions that have access to these energy sources. A lot of knowledge gaps are waiting to be filled for these two energy sources. These two energy sources offer plenty of space for research compared to the other common three energy sources.

For biomass and refuse-derived fuels, the operation concept is similar with conventional coal-fired power plant. The recycled and reused waste materials are burned to generate electricity. The emission of undesired gaseous resulting from burning is one of the obstacles to these renewable energy sources, as the world is looking for environmental friendly renewable energy (Searchinger et al., 2008). This makes these two energy sources less preferable. Nonetheless, for places that have no access to the five energy sources mentioned previously, these two energy sources remain as reasonable option.

On the journey of exploring and utilising the abovementioned renewable energy sources, there are people who aim to replace conventional fossil fuels with renewable energy. However, the replacement of such a huge industry that lays the ground for today's economy and modern living could be disastrous. It is believed that utilisation of renewable energy is essential to diversify and balance the energy supply worldwide, not replacement. Any possible method to harness any available renewable energy should be looked into, disregard how impossible it might be.

1.2 Background

Malaysia is a country graced with abundant natural resources. Plenty of sunlight makes solar energy possible. Seasonal monsoon provides attractive wind energy. Vast rainforest and high precipitation rate bring base for hydropower. The organic wastes from oil palm plantation are the sources for biomass energy. There is even geothermal energy available in selected region (*www.tgepower.com, retrieved Apr 2015*). Almost all the renewable energy sources mentioned in section 1.0 are available and being harnessed at the moment, except for one, ocean energy. Malaysia is surrounded by The Straits of Malacca and The South China Sea. Hence, tapping off ocean energy should not be left behind. It was not until recently that a symposium that discusses on the implementation of ocean energy was held (*www.mima.gov.my, retrieved Apr 2015*).

Ocean energy is available in different forms, including wave energy, tidal energy, salinity gradient and ocean thermal gradient (Ng et al., 2013a). Wave energy is the energy from wave motion on the surface of the ocean. It can be harnessed by using submerged pressure differential, oscillating wave surge and oscillating water column (Drew et al., 2009). Tidal energy is the energy results from motion of tides. It can be harnessed in two ways, which are tidal barrage that harnesses the potential energy and

tidal current turbines that harness the kinetic energy (Ng et al., 2013a). Salinity gradient exists at the mouth of river where freshwater and ocean water meets. Energy conversion from salinity gradient is done by using a specially designed membrane to achieve reverse electrodialysis (Hong et al., 2015). For ocean thermal gradient, the energy is harnessed by utilising temperature difference between the surface of the ocean and deep sea.

Of the four forms of ocean energy, research and development on wave energy and tidal current energy are the fastest growing worldwide. Echoing this growth, some researchers in Malaysia have started studying the feasibility of tapping these two types of energy since 2010 (Lim and Koh, 2010; Mirzaei et al., 2014). It is estimated that an annual average of 2.5kW/m of wave energy are available to be harnessed along the East Coast of Peninsular Malaysia. Studies have also suggested that tidal current energy from selected sites could be harnessed with specially designed devices and can provide electricity of up to 14.5GWh/year. For comparison, the Ministry of Energy, Green Technology and Water of Malaysia has targeted to achieve electricity generation of 985MW from renewable energy in the 10th Malaysia Plan 2011-2015. It is clear that both wave energy and tidal current energy can contribute significantly to renewable energy supply for Malaysia.

Currently, there are various designs of wave energy converter being developed and used worldwide. Depending on the sites, the design of wave energy converter can be very much different. This can be seen from Pelamis designed by Pelamis Wave Power (Figure 1.1) and CETO designed by Carnegie Wave Energy Limited (Figure 1.2).

Figure 1.1: Pelamis
(*source:www.emec.org.uk*)

Figure 1.2: CETO
(*source*: *www.carnegiewave.com*)

On the other hand, there are only two major designs for tidal current energy converter, which are horizontal-axis turbine and vertical-axis turbine. The horizontal-axis turbine type is the most common one in this field as can be seen from the design of SeaGen by Marine Current Turbines Ltd. (Figure 1.3) and HS1000 by ANDRITZ HYDRO Hammerfest (Figure 1.4).

Figure 1.3: SeaGen
(*source: www.marineturbines.com*)
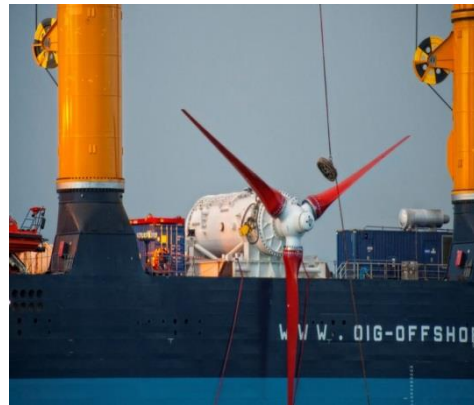
Figure 1.4: HS1000
(*source: www.hammerfeststrom.com*)

Apparently, if a wave energy converter is to be developed for Malaysia, it would take greater time to come out with an appropriate design that suits Malaysia. Whereas, realising tidal current energy for Malaysia by developing horizontal-axis tidal current turbines would be much easier, as the design is comparatively straight forward. Hence, the current work is going to focus on tidal current turbines for Malaysia.

1.3 Problem Statement

The working concept of a horizontal-axis tidal current turbine (hereinafter known as HATCT) is similar to that of wind turbines. A turbine is used to harness kinetic energy from a moving fluid. Theory like actuator disc theory and Blade Element Momentum (BEM) theory are applicable for both HATCTs and wind turbines (Fraenkel, 2002; Winter, 2011; Ng et al., 2013a). The technology used in wind turbine industry can be readily transferred to tidal current turbine industry, and this is exactly what is going on at the moment in HATCTs industry. The working fluid for tidal current turbines is water, which is approximately 823 times denser than air. This means a higher energy potential can be harnessed by HATCT from tidal current.

Despite the similarities, there is one major difference between HATCTs and wind turbines, which is the working environment. HATCTs operate in a harsher environment. Being a device that needs to be submerged and work under the sea, installation, operation and maintenance of HATCTs are more difficult compared with wind turbines. The higher loading results from denser working fluids make HATCTs' installation and operation a challenge. The wakes development is also different from normal wind turbines due to the confine effects from sea surface, not to mention additional effects from wave. Biofouling is also an issue for HATCTs (Ng et al., 2013b; Walker et al., 2014). But before addressing all these challenges, the utmost priority would be to design and build a HATCT that is operational, cost-effectiveness and useful for community in Malaysia.

Obviously, cost-effectiveness relies on the maturity of a technology, but at current stage, cost-effectiveness of HATCTs depends on the tidal current speed. A high tidal current speed possesses more energy and allows HATCTs to give higher electricity

output. For tidal current with low speed, the electricity output from HATCTs becomes less appealing. Years back, a tidal current speed of 2-3m/s was suggested to be cost-effective for tidal current turbine operation (Fraenkel, 2007). For SeaGen, its cut-in speed is approximately 0.8m/s and achieves its rated power at approximately 2.5m/s (MacEnri et al., 2013). This implies that a turbine may be able to operate in low tidal current flow, but it does not mean that it can produce sufficient amount of electricity that can covers the construction cost. However, if more energy could be harness from low tidal current flow, the required flow speed for cost-effectiveness can be lower down further.

For Malaysia, the range of tidal current speed at the Strait of Malacca varies from 0.2m/s to 1.5m/s, and reaches 2.0m/s or above at some localities (*http://www1.american.edu/ted/malacca.htm*, *retrieved April 2015*). Figure 1.6 and Figure 1.7 show the averaged ocean surface current of selected regions over the Straits of Malacca between 2009 to 2014 (Bonjean & Lagerloef, 2002). According to the current state-of-the-art, apparently, Malaysia's tidal current speed is considerably less appealing. Hence, besides making an operational HATCT, there is also need to explore alternatives that help HATCT to operate effectively at low tidal current flow. In addition, marine bio-fouling is a great threat to HATCTs' performance. There is need to understand the marine bio-fouling rate in Malaysia and identify proper measure to overcome these issues. As such, it is the aim of the current research to address these three issues.
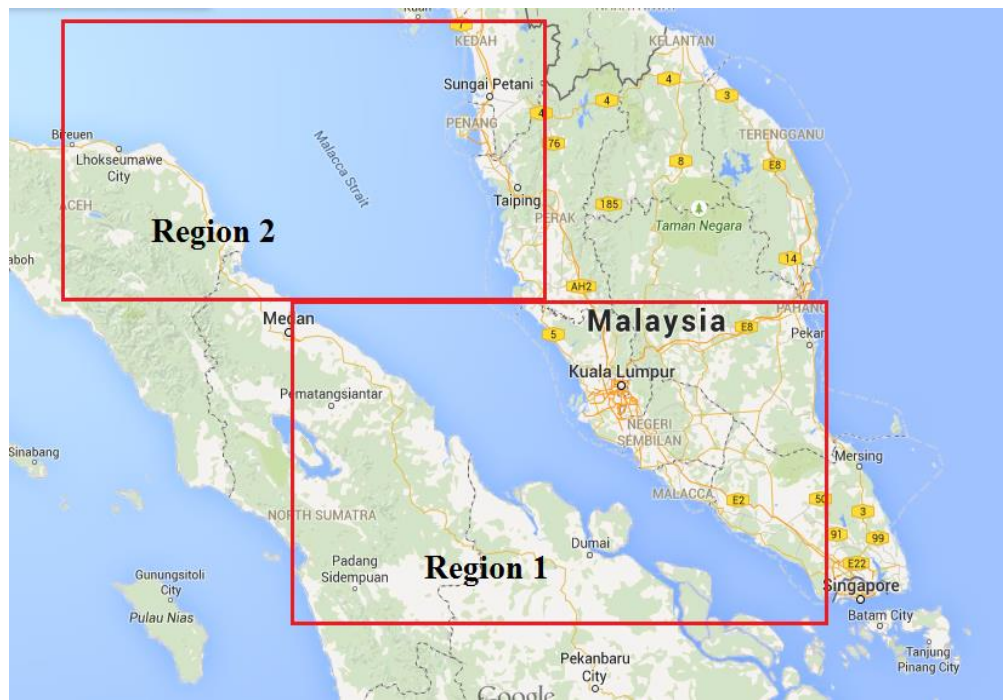
Figure 1.5: Map of Peninsular Malaysia (source: www.google.com.my/map)
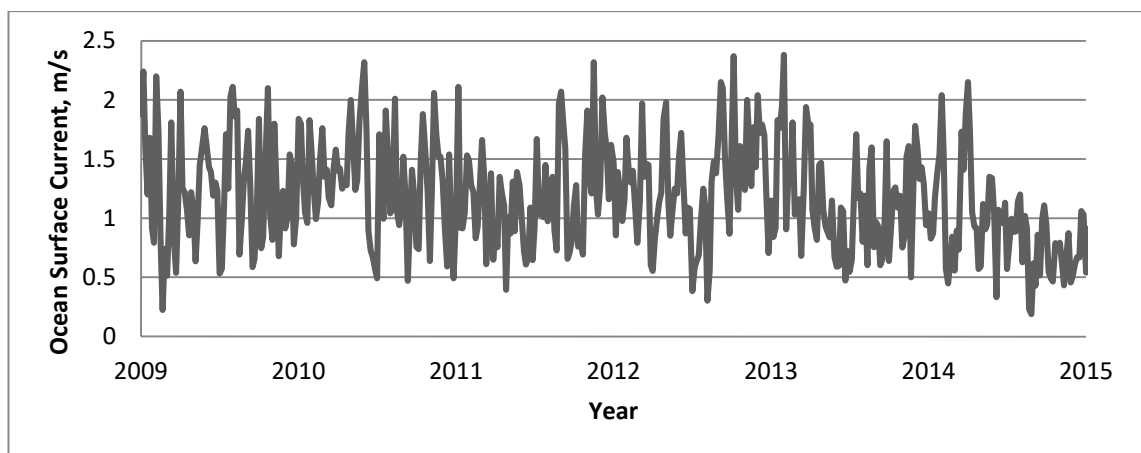
Figure 1.6: Averaged mean ocean surface current for region 1
(99.8E – 101.8E, 2.2N – 4.2N)
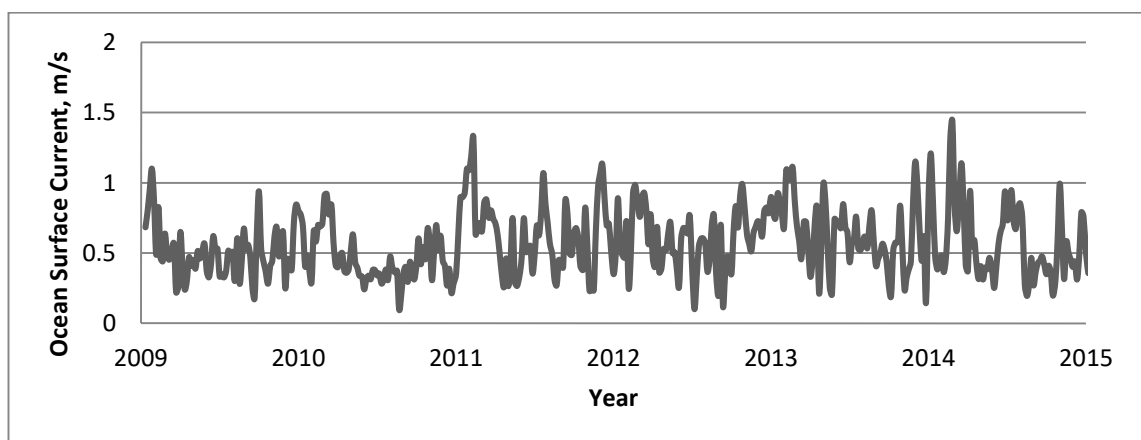
Figure 1.7: Averaged mean ocean surface current for region 2
(97.8E – 100.8E, 4.2N – 6.2N)

1.4 Objectives

The main aim of the current study is to create a small scale HATCT that is operational and to establish understanding on relevant information related to its operation. A small scale five-bladed turbine was built and its performance was tested at Pangkor Island in Perak State. Study on the use of hydrophobic coating for performance enhancements and study on marine bio-fouling will be conducted in parallel. The detailed objectives are listed as follows,

1. To run field side test of a small-scale HATCT,

2. To study performance enhancement methods to improve the efficiency of HATCT,

3. To study and understand marine bio-fouling activity in Pangkor Island

The following steps were taken to achieved the three objectives above,

➢ **Field Testing of HATCT:** A 800mm five-bladed HATCT provided by Laison Engineering Sdn. Bhd.. It was brought to Pangkor Island to test its performance characteristics.

➢ **Performance Enhancements:** Different gearing systems were tested for the 800mm five-bladed HATCT in Pangkor Island. Effects of hydrophobic coating on performance of a HATCT were examined by using another 350mm three-bladed turbine in lab test. Both numerical and experimental analyses were adopted for the study on hydrophobic coating.

➢ **Marine bio-fouling test:** The test was conducted in Pangkor Island. Stainless steel plates, dummy turbines and the 800mm five-bladed turbine were submerged in seawater to observe the marine bio-fouling activity for 3 months.

1.5 Scope and Study

The current research focuses on the use of numerical tools and experimental works to study performance of a HATCT. The 800mm small scale HATCT is a prototype designed and built together with the assistant from a local engineering company – Laison Engineering Sdn. Bhd. All materials are purchased from market. No synthesis of new materials is involved in this study. The main targeted parameter is the power output in Watt for the 800mm small scale HATCT at different tidal current velocity. Other parameters that could affect performance of turbine are made constant in all experiment to minimise the effects on data. The experiment is conducted at a selected site located in Pangkor Island. The main variables include incoming velocity ranging from 0.05m/s - 0.25m/s.

For the study on effects of hydrophobic coating, numerical study of hydrofoil performance is done by using ANSYS Fluent. The main variables include slip wall, no-slip wall and angle of attack (AoA). The hydrofoil models for the numerical and experimental study are NACA 63418. Lab-scale study on effects of hydrophobic coating towards lift and drag forces of hydrofoils is conducted in Centre of Advanced Material and Green Technology inside Multimedia University in Melaka. The main variables include coated hydrofoil, uncoated hydrofoil and AoA. Numerical simulation and experimental data is compared for validation purpose.

Numerical study on power coefficient of a 350mm three-bladed turbine with and without hydrophobic coating is done by using WT_Perf. The turbine model proposed by Pinon et al. (2012) was adopted in the study. Lab-scale experiment is also conducted for the 350mm three-bladed turbine to measure its power coefficient and revolution per minute (RPM) with and without hydrophobic coating. The main variables include

incoming velocity ranging from 0.2m/s -0.7m/s. Lab-scale experiment for turbine is conducted in Hydraulic Lab inside University Malaya.

Study on marine bio-fouling activities includes the testing of fouling rate at the selected site in Pangkor Island and investigation on the effectiveness of anti-fouling paints currently available in the market.

1.6 Significance of Study

The current study produces an operational 800mm diameter small scale HATCT for Malaysia. It also explores the possibility of utilising different techniques to improve performance of a HATCT. This effort helps in addressing issues related to cost-effectiveness of tidal current turbines for low tidal current speed region. Meanwhile, it helps in gaining understanding on the marine bio-fouling activity in Malaysia. Success of the current study produces a readily usable prototype HATCT that can generate electricity for small community. Additionally, results from performance modifications provide alternatives for countries like Malaysia to tap on low tidal current flow. Last but not least, this study helps in providing baseline data on the marine bio-fouling pattern on HATCT.

1.7 Outlines of Thesis

This thesis is structured as following. It has six chapters. Chapter one is introduction. Chapter two explains in details the literature review related to HATCTs. Methodologies will be covered in chapter three. Chapter four shows results and discussions for each objective. Chapter 5 is conclusion, which serves to summarise the findings of current research and provides recommendation for future works.

CHAPTER 2: LITERATURE REVIEW

2.1 Rationale for Tidal Current Energy Research

Against the backdrop of global warming resulting from environmental pollutions related to conventional energy sources, the world is currently in pursuit of sustainable and environmental friendly renewable energy sources. Tidal current energy is capable of providing a predictable zero carbon emission electricity. Its operation also has a minimal visual impact since it will be submerged under the sea during its operation. It is a clean and sustainable energy source when harnessed in a correct way. Coupled with the reasons discussed in section 1.2, it is clear that there is a need to push forward research in the field of tidal current energy for Malaysia and for the world.

2.2 Condition of Tidal Current in Malaysia

.

In Malaysia, the tide pattern at the east coast and part of the lower west coast of peninsula is dominantly mixed. The rest of the west coast of peninsula is semi-diurnal type. For Sabah and Sarawak, the tide pattern is mixed type (Lim and Koh, 2010). This means all coastlines will have two high tides and two low tides daily. The tidal current will be flowing in one direction until the tide reaches maximum (or minimum) and flow in the opposite direction afterwards. This process occurs two times daily. When the tide is at maximum (or minimum) and prepares to change direction, there will be a short slack water period where no tidal current movement will be taking place.

At the Strait of Malacca, there is non-tidal current flowing at a mean speed of approximately 0.5m/s and a maximum speed around 1m/s towards Northwest direction.

The current is strongest from December to February and weakest from June to August. The northern part of the strait has a relatively higher current speed. Although the geographical features of the Strait of Malacca that connects the Andaman Sea and Java Sea should provide venturi effects on the current flow, the water exchange remains low (Pauly & Martosubroto, 1996; National Geospatial-intelligence Agency, 2005). The average surface current, as mentioned in section 1.3, is relatively low.

2.3 HATCTs

As mentioned in section 1.3, the working concept of HATCTs has similarity with wind turbines. This type of energy harnessed by HATCTs is known as tidal current energy. Nonetheless, due to different working environment, in depth research and development is still essential to come out with a robust operational HATCT. This is exactly what researchers worldwide have been doing for the past decade. In recent years, the efforts are even more and obvious, which can be seen from the reports published by Implementing Agreement on Ocean Energy Systems (IA-OES) (2010, 2011, 2012, 2013). In this section, a concise review of past researches on HATCTs will be presented.

2.3.1 Energy Resource Assessment

As all the exploration of new energy goes, tidal current energy also started with the quest to identify locations that possess potential energy resource that can be harnessed through implementation of HATCTs. The earliest record of modern HATCTs research on tidal current energy resource assessment was around the late 1970s (Blunden and Bahaj, 2007). At that time, major activities were concentrating on the northwest European. Various approaches were developed and used by different researchers in estimating the available tidal current energy resources.

Pioneering works in tidal current energy resource assessment by European countries and North America was not surprising as this type of new renewable energy had captured their interest during the energy crisis period (Ben Elghali et al., 2007: Bedard et al., 2010). Even to date, majority of the countries that study the potential of tidal current energy are from the abovementioned two areas (Implementing Agreement on Ocean Energy Systems, 2010, 2011, 2012, 2013). Generally, after a potential site is identified, the tidal current velocity and tide height will be measured or modelled. The potential energy density is then estimated by using the kinetic energy flux formula,

$$E = \frac{1}{2}\rho V^3 \qquad\qquad (2.1)$$

where E is the energy per area expressed in unit W/m^2, ρ is the density of seawater which is approximately 1024kg/m^3 and V is the velocity of tidal current. But, this equation is later proven to be unsuitable to be used for estimation of potential energy, which will be discussed in details in later part of this session.

There are two types of estimation that the researchers were studying. One is the total available energy and the other one is the extractable energy. The total available energy is the energy available in the undisturbed current flow, whereas, the extractable energy is the energy that can be harnessed from a tidal current flow by using a turbine along with the consideration of turbine efficiency, effects on surrounding environment and hydrodynamic factors.

2.3.1.1 Theoretical Extractable Energy

Estimation of the available energy is relatively straightforward. With known tidal current speed, the kinetic energy flux can be determined using eqn. 2.1. The tidal

current speed can be obtained via in-situ measurement or numerical modelling (will be discussed further in section 2.3.1.2). On the other hand, estimation of the extractable energy involves much tedious works, where many factors need to be considered. Research on theoretical extractable energy in the past decade focused more on analytical works. Formulas have been derived by different researchers to estimate the theoretically extractable energy.

Bryden, Couch and their team was some of the earliest researchers that studied the theoretical extractable energy (Bryden et al., 2004; Bryden & Melville, 2004; Couch & Bryden, 2004; Bryden & Couch, 2006; Couch & Bryden, 2006; Bryden & Couch, 2007; Bryden et al., 2007). They derived a simple analytical formula to study the changes in flow condition over a channel. The model that they considered is a simple rectangular channel that connects two oceans. The flow is considered to be driven by the static head difference between both ends of the channel. The power extraction activity of a turbine is considered to be exerting a certain amount of retarding force on the flow. The resulting friction of the channel is the sum of seabed friction and the turbine blockage. Readers are referred to Bryden et al. (2004) and Bryden & Melville (2004) for detail derivation.

Bryden et al. (2004) showed that a 10% energy extraction would cause a 3% reduction in tidal current flow speed. Though 3% is seemingly a small amount, it may cause significant impact on microorganisms and marine organisms that rely on tidal current flow movement. From HATCT arrays point of view, thorough understanding on changes in tidal current speed after passing a row of HATCTs is crucial to determine the layout and the optimum efficiency of an array. Couch & Bryden (2006) extended their study to larger scale effects of HATCTs on the hydrodynamic of tidal current flow by

using Tidal Flow Development (TED), a numerical model developed at the University of Strathclyde (Bryden & Couch, 2006; Bryden & Couch, 2007; Bryden et al., 2007). Their findings still suggest no apparent changes in water elevation will appear if single HATCT is used, even when energy extraction causes a 10% reduction in tidal flow speed.

Besides Bryden and Couch's team, Garrett, Cummins and their team were also some of the earliest researchers that worked on theoretical extractable energy (Garrett & Cummins, 2004; Garrett & Cummins, 2005; Garrett & Cummins, 2007; Slutherland et al., 2007; Blanchfield et al., 2008a; Blanchfield et al., 2008b, Garrett & Cummins, 2008). Similarly, they have developed models for a channel connecting a bay and ocean, and a channel connecting two oceans. Their focus was to determine the possible maximum extractable energy by using a fence of HATCTs in a channel. Equations were developed for both models. Similar to Brydan and Couch's model on a bay and ocean, Garrett and Cummins's considered the flow in the model is driven by pressure gradient results from surface elevation changes from sinusoidal tide.

For the model on a channel connecting two basins, their derivation is more complicated compared to Bryden and Couch's model, where they took into consideration of different drag laws and separation effects at the outlet of channel. Readers are referred to Garrett and Cummins (2005) for detail on derivation of their formula. Their major outcomes from the study was that the maximum extractable energy, for a channel occupied by a fence of turbines, generally ranges from 0.24% - 0.21% of the channel's peak tidal pressure head times the peak volume flux of an undisturbed channel as the natural regime varies from no background friction to one dominated by friction. In this model, they ignored the possible positive effects on head

change that could be caused by presence of turbines. It is said the potential power would be slightly higher if that is taken into consideration. This finding is similar to that of Bryden and Couch's model.

For the model on a channel connecting a bay and ocean, the detail on derivation of formula is presented by Blanchfield et al., (2008b). Similar to the model for channel connecting two oceans, they studied the extractable energy for three different scenarios which are: (1) bottom drag and flow separation effects are negligible with linear proportionality between turbine drag and flowrate; (2) bottom drag and flow separation effects are negligible with quadratic relation between turbine drag and flowrate; and (3) bottom drag and flow separation effects are considered with quadratic relation between turbine drag and flowrate. The main finding is that the average extractable energy ranges from 0.25% - 0.22% of the magnitude of dominant tidal constituent times the peak volume flux of an undisturbed channel for the three scenarios.

A reminder is that although the multiplier of the formula of both models is almost identical, the terms in the formulas are different. For channel connecting two oceans, the tidal head across the channel plays important role in providing the energy. For channel connecting a bay and ocean, the magnitude (or more commonly known to be amplitude) of the dominant tidal constituent just outside the channel plays important role in providing the energy. Normally, amplitude of the dominant tidal constituent is larger compared to tidal head across a channel, hence allows a channel that connects a bay and ocean to provide higher energy. Nonetheless, in reality, a channel connecting two oceans does not necessarily provide lesser extractable energy. There is always a trade-off between extractable energy and impact on environment, in this case, the alteration of tides (Ng et al., 2013a).

There are few worth noticing arguments by Garrett and Cummins' team based on their studies. They pointed out that the kinetic energy flux equation (which is eqn. 2.1) is insufficient to estimate the available energy, and hence unsuitable to be used for estimation of extractable energy. The kinetic flux equation does not cover the term for tidal head and any possible positive feedback caused by presence of turbines. There is also no term to cover the possible effects brought by diversion of flow and separation of flow in a channel. The kinetic flux equation is likely to significantly over-estimate or under-estimate the available/extractable energy of a particular tidal channel.

Here are some examples on the difference of estimation made by using kinetic energy flux equation and the formula derived by Garrett and Cummins. Karsten et al. (2008) studied extractable energy for Minas Passage of the Bay of Fundy by applying the formula derived by Garrett and Cummins (2004) and the value they obtained a is 7GW. When kinetic energy flux equation is used, the extractable energy is merely 1.9GW. The significant difference is apparent. When Karsten et al. (2008) considered only to allow 5% changes in tidal amplitude, the extractable energy decreases to 2.5GW.

Another example is the study conducted by Blanchfield et al. (2008a) to check the formula derived by Garrett and Cummins (2008), which is a formula for channel connecting a bay and ocean. They applied the formula for Masset Sound, Haida Gwaii and obtained an extractable energy of 79MW. They did not make comparison to the kinetic energy flux equation. A cross-checking has found that the value estimated by using kinetic energy flux equation is two times lower than

Blanchfield et al. results. Therefore, for a proper energy resource assessment of any selected site, it is inappropriate to directly apply eqn. 2.1.

After Bryden and Couch's team and Garrett and Cummins's team, there are other researchers who continue to work on theoretical extractable energy for HATCTs in the past five years. They include Vennell from New Zealand (Vennell, 2010; Vennell 2011a; Vennell 2011b; Vennell 2012) and Thomas Adcock's team from The UK (Adcock, 2012; Adcock et al., 2013; Draper et al. 2014; Vennell & Adcock, 2014). A worth noticing point is that the Garrett and Cummins's works have had significant influences on their work. Both Vennell and Adcock's team have extended Garrett and Cummins's works with more complexity. Unlike Bryden and Couch or Garrett and Cummins, they have included the operation factors of HATCTs in their analysis. This makes their analysis even closer to reality and further pushes forward the understanding on theoretical extractable energy.

Vennell (2010, 2011a) has argued that to maximise the potential of a channel, HATCTs must occupy most of the cross-section or to place as many rows of HATCTs as possible. Apparently, occupying most cross-section of a channel is not viable as clearance is required for marine activities like navigation. Placing as many rows as possible may be possible, if the associated flow reduction at a particular channel is not going to cause environmental problems. Vennell (2011b) showed that it is possible to increase the total efficiency of a HATCT farm by optimally tuning the value of r and number of HATCT rows. If every HATCT in all rows are tuned to the classic Lanchester-Betz limit $r = 1/3$, increasing the number of rows will only results in lower total efficiency.

For Adcock's team, they have conducted a study similar to Vennell (2011a) whereby equations are derived to estimate theoretical available energy of a particular channel, either connecting two oceans or a bay connecting to ocean. (Draper et al., 2014) They have derived three equations where each only requires either two of the following three parameters to estimate the available energy,

i.   The amplitude of water elevation across a channel

ii.   The undisturbed peak flow rate across a channel

iii.   The geometry of channel and seabed drag coefficient.

These equations are useful for preliminary estimation of available energy for potential sites that only have basic information. The reliability of these equations has also been checked by Adcock's team.

In a later work by Vennell and Adcock, they demonstrated that the theoretical extractable limit can be further enhanced by varying HATCT farm overall drag coefficient (Vennell & Adcock, 2014). Varying the overall drag coefficient effectively delays extraction by building up the inertia of tidal flow. The energy within the tidal flow is then 'stored' until the HATCT farm started to extract energy. But, a period of low or nearly no energy extraction is needed for the storage process. Such strategy can yield high extractable energy at a desired period, such as during the peak demand. Theoretically, this strategy is possible. Technically, it would require high-end technology to realise.

2.3.1.2 Numerical Energy Assessment

Apart from study on theoretical extractable energy, development and application of numerical solutions to model tidal current flow is also an important part in resource energy assessment. Normally, there will be tidal stations at selected point to record data

on tidal range, tidal current and perhaps temperature. The purpose is to monitor changes on sea and provide reference for shipping activities throughout years. When it comes to tidal energy assessment, it requires tidal current flow data for a wide area. It is impractical to install large number of stations over a large area to measure tidal current flow. In order to obtain data on tidal flow for sites of interest, numerical method acts as a useful tool.

Table 2.1 is a table retrieved from Ng et al. (2013a) that tabulates different numerical models used by various researchers for modelling of tidal flow. Those researchers include: Blunden & Bahaj (2006), Ben Elghali et al. (2007), Karsten et al. (2008), Carballo et al. (2009), Grabbe et al. (2009), Polagye et al. (2009), O'Rourke et al. (2010), Xia et al. (2010), Lim & Koh (2010), Defne et al. (2011), Abundo et al. (2011), Li et al. (2012) and Work et al. (2013). A closer look will find that some researchers directly use well-known models, such as Delft 3D-FLOW and Princeton Ocean Model (POM), which is relatively straightforward. Nonetheless, many researchers are willing to spend time to develop their own models.

A reminder is that numerical modelling only serves as a prediction of tidal current flow. Its accuracy must be cross-checked with data recorded from tidal station. Generally, after the data from numerical modelling is validated, the value of tidal current flow for the sites o interested will be used to determine the available energy. Although Bryden and Couch's team and Garrett and Cummins's team have commented on the suitability of the kinetic energy flux for estimation of available energy, most of the abovementioned researchers still used kinetic energy flux for their energy resource assessment. This shows that research recognition between researchers back at that time was weak. In the selection of limit on

extractable energy, most of them merely assumed a value that is lower than Lanchester-Betz limit. As discussed in section 2.3.1.1, such a simplified assumption will lead to an over or underestimation of extractable energy.

Table 2.1: Numerical models used by various researchers in the past decades (Ng et al., 2013a).

Year	Place	Model	Developer
2006	Portland Bill, UK	TÉLÉMAC	Électricité de France
2007	Raz de Sein, Brittany, France	Matlab-Simulink	MathWorks
2008	Minas Passage, Bay of Fundy, Canada	2-D finite-volume model (FVCOM)	C. S. Chen, Cowles G & Beardsley
2009	Ría de Muros, Spain	Delft 3D-FLOW	Delft Hydraulics
	Various sites in Norway	Bergen Ocean Model & High Resolution Tidal Model	University of Bergen & University of Oslo
	Puget Sound, Washington, USA	1-D time dependant model	University of Washington
2010	Various sites in Ireland	2-D depth-integrated numerical model	RPS Kirk McClure Morton
	South Wales coast, UK	Refined finite volume numerical model	Cardiff University
	Various sites in Malaysia	Princeton Ocean Model (POM)	Princeton University
2011	Georgia coast, USA	Regional Ocean Modelling System (ROMS)	Rutgers IMCS Ocean Modelling Group
	Verde Island Passage, Philippines	Delft 3D	Delft Hydraulics
2012	Langyatai Strait, China	Delft 3D-FLOW	Delft Hydraulics
	South Carolina coast, USA	Regional Ocean Modelling System (ROMS)	Rutgers IMCS Ocean Modelling Group

While aims of most numerical modelling is to obtain tidal current profile, there were also studies that aim to develop that can model effects of tidal energy extraction. The one-dimensional time dependant model developed by Polagye et al. (2009) is used to quantify effects from tidal energy extraction. They argued that tidal energy extraction at multiple sites along a channel with several branches can considerably alter tidal regime of one another. They also emphasize that the energy dissipated by turbine will not be fully harnessed by turbine, as there will be losses due to drag imposed by support structure and wakes. When a particular

amount of energy dissipates and causes reduction in tidal transport, it is necessary to ensure those dissipated energy can be harnessed as much as possible.

To date, although guidelines on preliminary energy resource assessment have been published in Europe and the USA after almost a decade of study since early 2000s, research in resource assessment is still undergoing. For instance, Hou et al. (2015) conducted both extractable energy assessment and study on effects of tidal energy extraction in Zhoushan. Lin et al. (2015) even go into detail on predicting distribution of velocity deficit and study the relation of this distribution with extractable energy. More factors are being taken into consideration in recent study on energy resource assessment. Some of the factors have not been considered by the researchers discussed in section 2.3.1, which include the actual design, types, mechanical and electrical efficiency of HATCTs. These factors are closely related to performance of HATCTs and will be discussed in section 2.3.2.

2.3.2 Performance of HATCTs

Performance of HATCTs depends on many factors. On the hydrodynamic side, periodical variation of current speed, wave interaction, wake pattern and effects of turbulence intensity can affect the performance of turbine positively or negatively. On the mechanical side, design of turbine blade, efficiency of mechanical parts and yaw/fix govern the efficiency of turbine. On the electrical side, generator selection, power storage and loading sequence determine the power output of a HATCT. The nature of a particular potential site can also affect the performance of HATCTs, such as fouling activity.

This is a rather complicated topic and is almost impossible to solve it all at once. Early research focused more on aspects that can be study in lab, such as the design of turbine blade and wake interaction. Studies on complex issues like wave interaction and turbulence intensity only started in the past 2 years. Thorough understanding on these subjects is extremely useful and forms the fundamental for optimisation of HATCTs, either individual HATCT or HATCTs farm. In the following sub-sections, research outcomes by various researchers on some of the abovementioned subjects will be discussed.

2.3.2.2 Design of HATCTs

As mentioned in section 2.3.2.1, it is not difficult to design a HATCT with high C_p. Utilisation of different hydrofoils section with proper configuration can help achieve desired C_p. Sometimes, a HATCT blade that consists of same hydrofoil sections, but with different length and pitch can yield different C_p value. In year 2007, Bahaj et al. (2007b) designed and tested a 800mm diameter three-bladed horizontal-axis turbine. The turbine blade was made of NACA 63-8xx series, namely NACA 63-812, NACA 63-815, NACA 63-818, NACA 63-821 and NACA 63-824. Readers are referred to Bahaj et al. (2007b) for the details on the pitch distribution and configuration of hydrofoil sections.

They tested their turbine with different hub pitch angle. At 0° pitch angle, the turbine has maximum C_P of approximately 0.45 at tip speed ratio (TSR) 5. At 5° pitch angle, the turbine has maximum C_P of approximately 0.45 at TSR 5. At 10° pitch angle, the turbine's maximum C_P drops to approximately 0.38 at TSR 5. At 12° pitch angle, the turbine's maximum C_P drops further to approximately 0.3 at TSR 4.5. This is an obvious example where changing pitch can have significant impact on the efficiency of

HATCTs. Their experiment results also showed that increase in pitch for their turbine leads to drop in thrust coefficient (C_T). Figure 2.1 shows the C_P and C_T values from Bahaj et al. (2007).

In the same experiment, Bahaj et al. (2007b) also examined effects of water surface proximity, dual turbine and yaw on the performance of turbine. For water surface proximity, they compared efficiency of turbine with shallow immersion and deep immersion. The distance from water surface and turbine tip is only 20% of the turbine diameter for shallow immersion. They observed a 10-15% drop in efficiency when turbine is operating near to water surface. They argued that the reason for drops in efficiency is due to the surface that restricts the expansion of wake, which in turn interfere the pressure difference across turbine and leads to reduction in power produced. Additionally, the wave motion of water surface also adds on the turbulence of flow approaching turbine and cause lower efficiency.

(a)
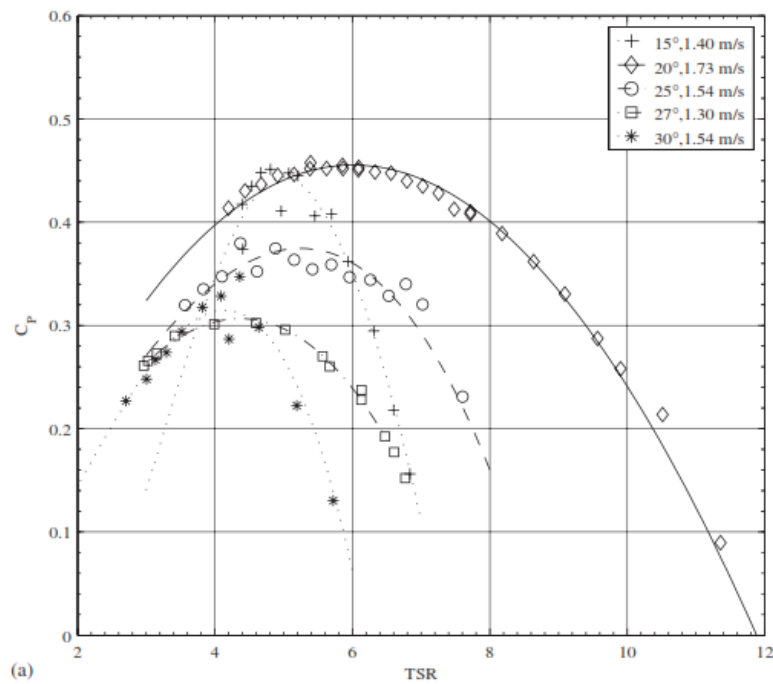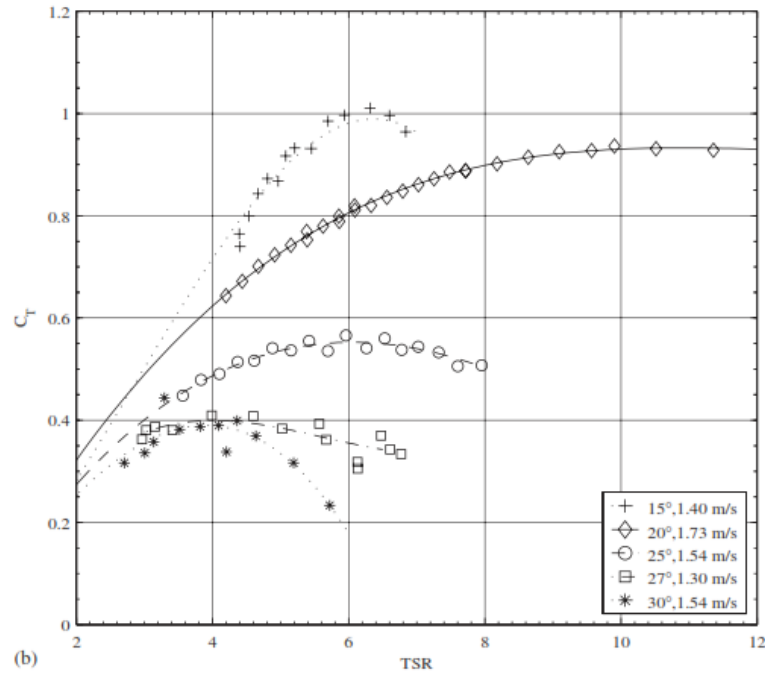
Figure 2.1: (a) C_P and (b) C_T for Bahaj et al. (2007b) turbine at different pitch angle.

For comparison between turbine with yaw and fix, they found the efficiency decreases as the yaw angle increases. It is observed that a 30° yaw angle can cause 30% decrease in efficiency, disregard the pitch angle. For dual turbine, they placed an extra turbine next to the main tested turbine. Three distances were tested, which include 100mm, 200mm and 400mm. It is reported that the rotation and TSR or the extra turbine, whether similar to the main turbine or not, has little influence to the efficiency of the main turbine. As the tested turbines are lab-scale, the applicability of this finding for large scale HATCTs remains questionable.

A worth noticing thing is that these series of work by Bahaj's team has been one of the earliest reported results that is widely used and referred by other researchers. Based on the presentations in the 2nd Asian Wave and Tidal Energy Conference (EWTEC) in August 2014, it was found that many simulation and experimental works still used the results from Bahaj's team to validate their results. Their work on wake

expansion (which will be discussed in section 2.3.2.4) is also a popular source of reference among HATCTs community.

Besides Bahaj's team, Coiro et al. (2006) also built and tested a small-scale tidal current turbine in year 2006. They also built a 800mm diameter three-bladed turbine, but the hydrofoils used by them were *ad-hoc* style and S805. C_P for their turbine is as shown in figure 2.2. Their turbine can achieve a C_P of 0.45 at a TSR of 3. A reminder is that Bahaj et al. (2007b) turbine achieves a C_P 0.45 at a TSR of 6. This implies Coiro's turbine is better than Bahaj's turbine as it can achieve similar performance at lower speed. The overall loading that needs to be bear by turbine is much lower at low rotational speed. Additionally, Coiro's results show that proper selection of pitch angle can affect efficiency significantly.
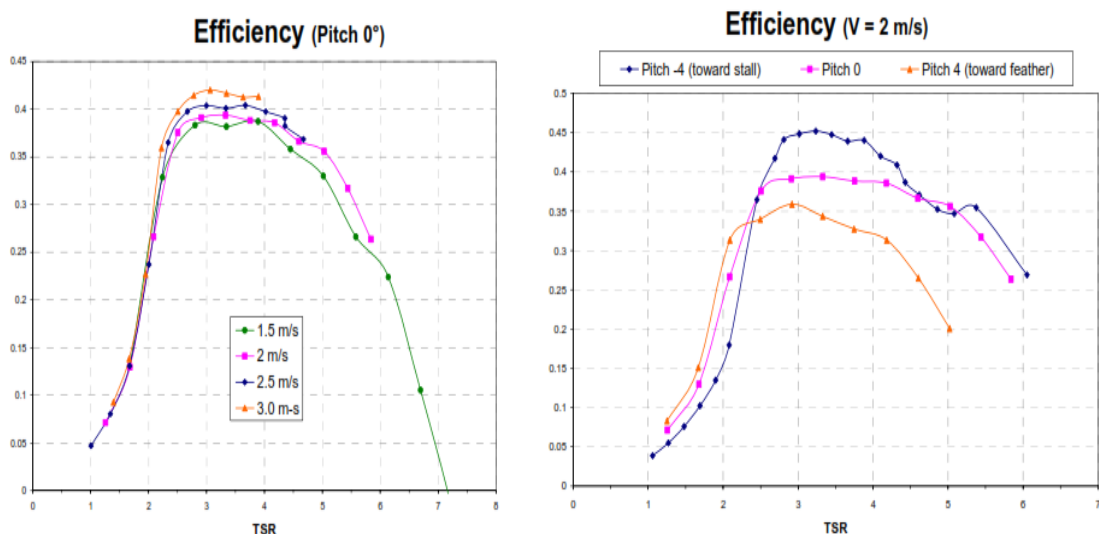
Figure 2.2: C_P for Coiro et al. (2006) turbine at different pitch angle.

In another recent study by Jo et al. (2012). They were able to achieve a C_P of 0.5 at a TSR of 5 for their turbine. Their turbine was a 500mm diameter three-bladed turbine made from hydrofoil S814. Both S814 and S805 are originally aerofoil section developed by National Renewable Energy Laboratory (NREL) from the USA. S814 exhibits better lift-to-drag ratio compared to S805. This may be the reason that Jo's

turbine has better performance than Coiro's turbine. A reminder is that Jo et al. (2012) only conducted computational fluid dynamics (CFD) analysis for their turbine. No experiment was conducted for their turbine and therefore, the actual performance for their turbine may be lesser than 0.51.

Nonetheless, the above three examples have clearly shown that designing a turbine with good efficiency is achievable with a variety of hydrofoils and different blade configurations. Hence, it can be said that there is no such thing as 'universal perfect design' for HATCTs. Design of HATCTs can vary accordingly based on the needs. As long as the extracted power from a site of interest can meet the power demand of a community, any design of HATCTs can be used.

2.3.2.4 Effects of Wakes

When a fluid flows past or around an object, its flow immediately after the object, which has a lower velocity compared to the upstream flow, is known as wake. The formation, pattern and extension of wake depends on many factors, such as the shape of objects, motion of object and presence of obstacle along downstream. The flow within the wake region has a lower velocity and energy. Mixing occurs at the edge where the wake and by-pass flow meets. As the mixing goes on, a wake will gradually regain energy. It will continue to expand until its velocity is recovered to its initial velocity or same to adjacent flow.

Study of wakes is important in the field of HATCT to determine the optimum layout of a HATCT farm. The distance needed for full wake recovery will determine the distance between a HATCT located at upstream and a HATCT located at downstream. This helps in ensuring the downstream HATCT can also be fed with a flow that has

similar energy as far upstream flow. With this optimum distance, a HATCT farm will be able to harness the tidal current energy optimally for a given site. Likewise, if a given site has limitation on space, understanding on wakes can help determine the maximum unit of HATCTs that can be installed for that particular site.

Research team led by Bahaj has conducted a series of study to understand the wake of HATCTs (Myers & Bahaj, 2007; Bahaj et al., 2007c; Myers et al., 2008a; Myers et al., 2008b; Myers & Bahaj, 2009; Blunden et al., 2009; Myers & Bahaj, 2010; Myers et al., 2011; Myers & Bahaj 2012). They focus on thorough understanding of wake development and recovery for single and multiple arrays HATCT, with the aim to develop a suitable computational tool for predicting wake of HATCTs at initial design stage.

Based on the discussion made by Myers & Bahaj (2007), the factors that affect wake pattern include performance of HATCT itself, the turbulence of surrounding flow field, geometry of site, seabed boundary layer and velocity of incoming flow. They also highlighted that direct use of a small scale turbine to study wake pattern of large scale turbine may be impractical, especially when one wishes to consider the tip speed scaling effects. Consider a 10m HATCT with a design TSR of 5 and subjected to tidal current speed of 1.5m/s, its tip speed at design TSR will be 7.5m/s. This is equivalent to a RPM of approximately 5.7. If one wishes to maintain the tip speed scaling with a small scale turbine with 300mm diameter, the RPM of the small scale turbine will be above 230. This relatively high rpm will cause greater swirl to the downstream wake. For this reason, they suggested the use of actuator mesh disc rotor simulator as an alternative for the study of HATCT wake.

In one of their earliest tests, it was found that velocity deficit of a wake can persist to far downstream. At a distance of 20 turbine diameters downstream, the velocity was only 90% to that of the upstream undisturbed flow. In year 2008, they studied and reported the effects of surface proximity on wakes pattern (Myers et al., 2008a; Myers et al., 2008b). When they immersed actuator mesh disc near to the bottom of test flume, it was found that the wake persists further downstream. Contrarily, wake from an actuator mesh disc immersed close to water surface has a similar wake pattern compared with the wake from an actuator mesh disc at half depth.

Following the above test, they further tested the effects of channel depth on wake pattern. One shallow test flume with a depth of 0.4m and another one deep test flume with a depth of 2m were used. For both tests, they placed a 100mm actuator mesh disc 200mm below the water surface. To their surprise, the wake persists further downstream for the test flume with deeper depth. They explained this difference is attributed to the accelerated flow for shallow flume. The comparatively constrained space between the actuator mesh disc and the bottom of the shallow flume causes flow around the actuator mesh disc to accelerate. The accelerated flow increases the mixing of wake and breaks the wake earlier. For deeper flume, the large space between the actuator mesh disc and bottom of the flume does not accelerate flow to the same degree, and therefore wake persists further downstream under this condition.

After they had investigated far field wake pattern of HATCT, they moved to study the combined effects of support structure and turbine towards wake pattern immediately downstream of a turbine (Myers & Bahaj, 2009). This time, they used a 800mm three-bladed turbine instead of an actuator mesh disc. The illustration of their turbine and support structures is shown in Figure 2.3. Figure 2.4 show the wake pattern

resulting from the support structure when the turbine was non-operational. A reminder is that the flow speed of their flume was set to be approximately 0.8m/s.
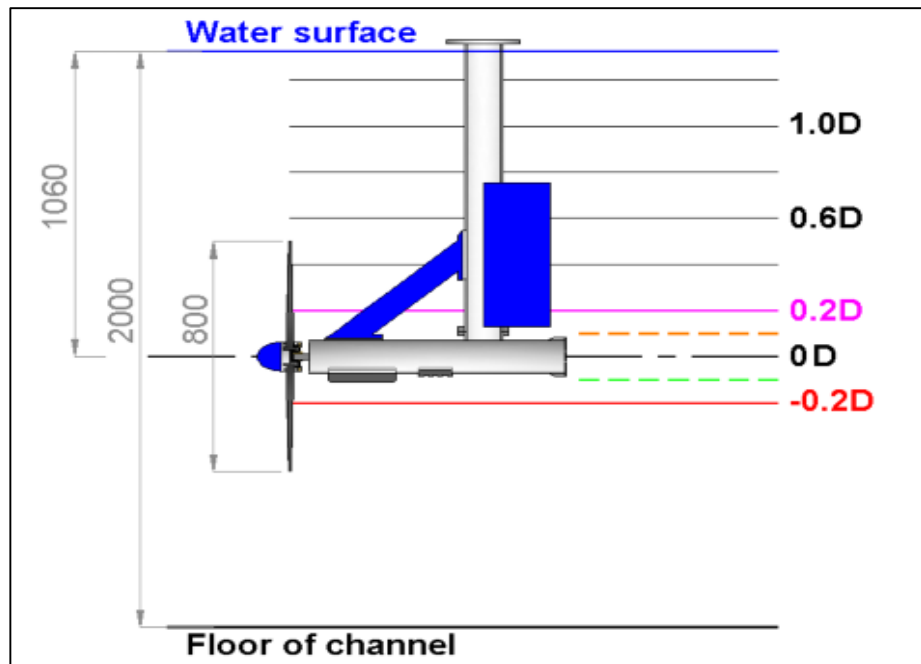
Figure 2.3: Side elevation of 800mm turbine (Myers & Bahaj, 2009).
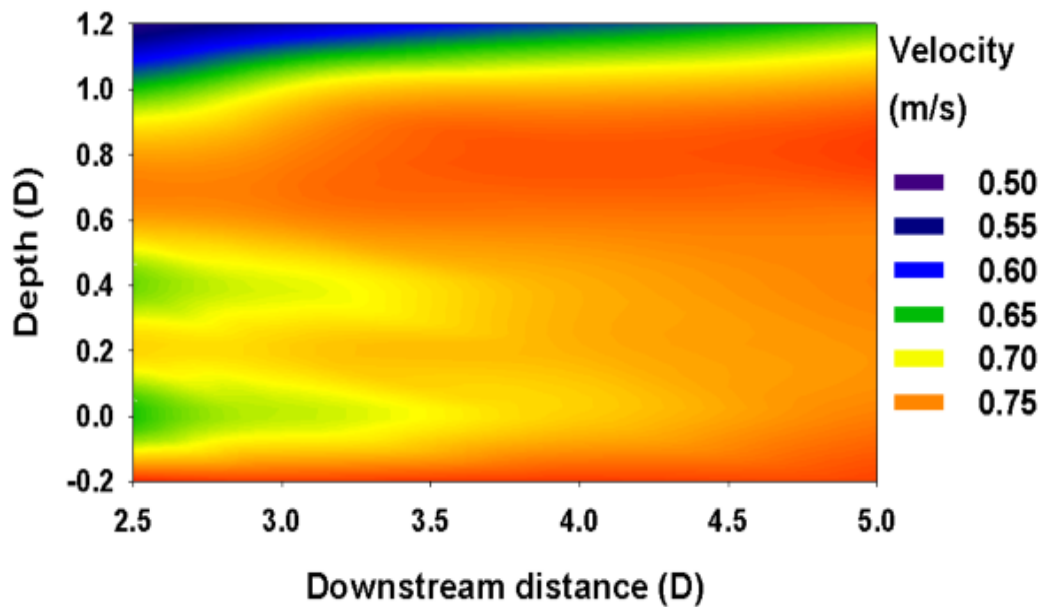
Figure 2.4: Wake pattern at centre plane of turbine support structure
(Myers & Bahaj, 2009).

In Figure 2.4, the two triangular flow field at D=0.0 and D=0.4 are results from turbine nacelle and the reinforcement strut. The wake from circular support at D=1.2 is even significant and persists down to a distance of 5 turbine diameters. When turbine is in operation, the resultant combined wake at the turbine centreline is shown in Figure 2.5. The blue line represents the velocity deficit when turbine is in operation. It is clear that from D= -0.4 to D= 1.2, the velocity deficit is exaggerated. Below D= -0.4, the velocity deficit pattern is identical to the black line. The difference at D=0.0 and D=1.0 are most obvious.
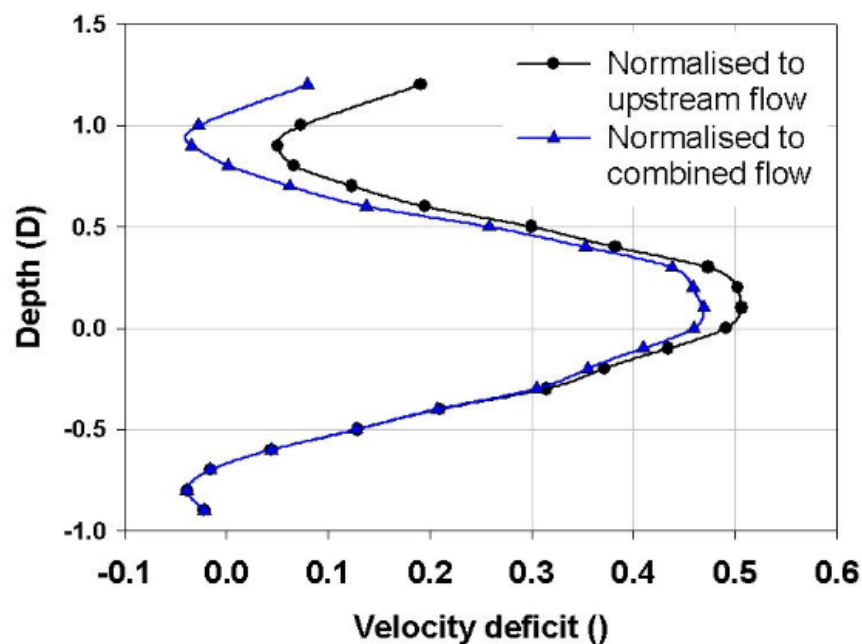
Figure 2.5: Combined wake at a distance of 5 turbine diameters downstream
(Myers & Bahaj, 2009).

As the study of wake is to understand the wake pattern to help determine the optimum HATCT farm's layout, Bahaj's team has also studied the interaction of wake between two turbines (Myers et al., 2011; Myers & Bahaj 2012). They placed two 100mm diameter actuator mesh discs side by side with different lateral spacing. Figure 2.6 shows the wake pattern results from the two actuator mesh discs. As a reminder, the x-axis of Figure 2.6 denotes the horizontal width of the test flume, with 0 as the centreline of the test flume.

When the discs were spaced with a distance of 0.5 diameter, wakes from the two discs merge and form a greater velocity deficit alongside centreline. With 1.0 diameter lateral spacing, although there is no merger between two wakes, the prolonged velocity deficit is still obvious and sensible down to a 25 diameters distance. When a 1.5 diameter lateral spacing is used, the interaction between two wakes is minimal.
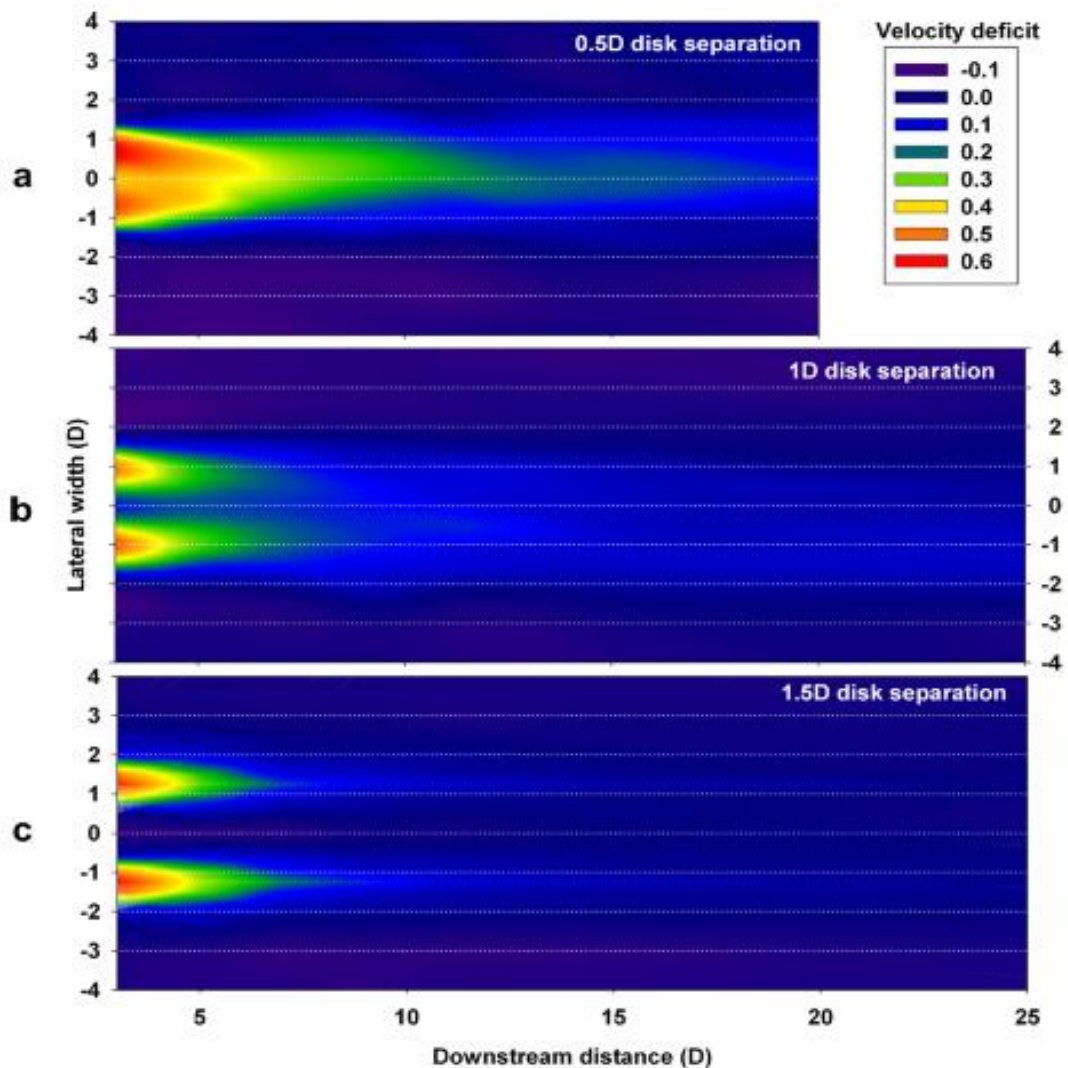
Figure 2.6: Plan view of wake pattern from two actuator mesh discs with different spacing (Myers & Bahaj 2012).

For a standard HATCT farm, there will be multiple rows of HATCTs. Results from Bahaj's team suggest that the minimum lateral spacing between adjacent HATCT should be 1.5 diameters, so that the HATCT of the following row can be placed at the centreline of the spacing to harness the undisturbed tidal current flow. Figure 2.7 shows the schematic diagram of the HATCT farm layout. Figure 2.8 shows the comparison of

wake pattern between a single row two actuator mesh discs and a three actuator mesh discs array by Myers & Bahaj (2012).
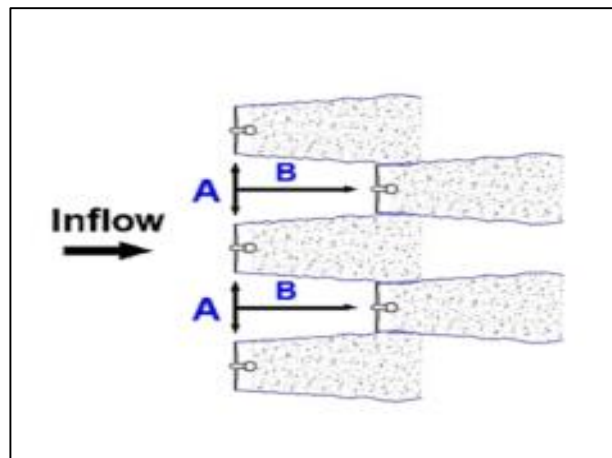
Figure 2.7: Schematic diagram of HATCT farm suggested by Bahaj's team (Myers & Bahaj 2012).
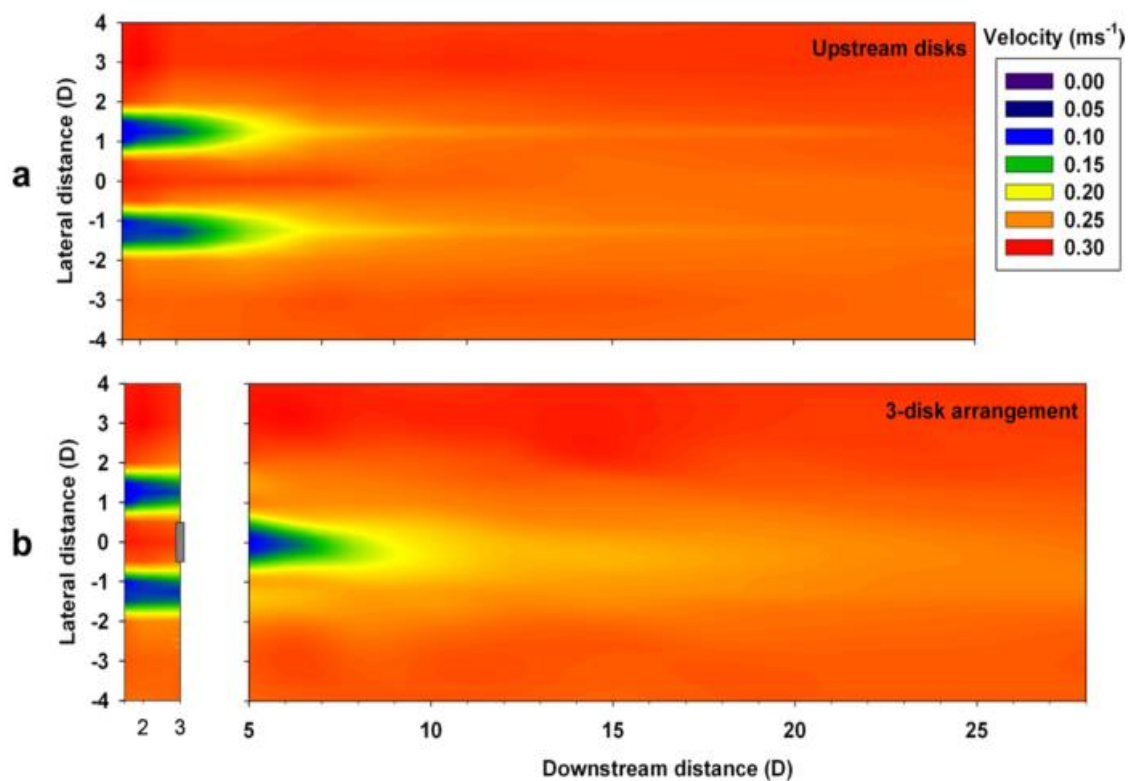
Figure 2.8: Wake pattern with (a) two actuator mesh discs and (b) three actuator mesh discs array (Myers & Bahaj 2012).

Beside Bahaj's team, there were also other researchers who have studied the wake of HATCTs. Macleod et al. (2002) has studied wake of HATCTs earlier than

Bahaj's team back in year 2002. They used an in-house CFD code to simulate the wake of HATCTs. Similar results were obtained by them such as higher C_T value corresponds to higher velocity deficit. An interesting finding by them is that they studied the velocity pattern when a turbine is placed behind another turbine with different distance. Figure 2.9 show their results on double turbine. They studied two different spacing, namely 5 diameters spacing and 8 diameters spacing.
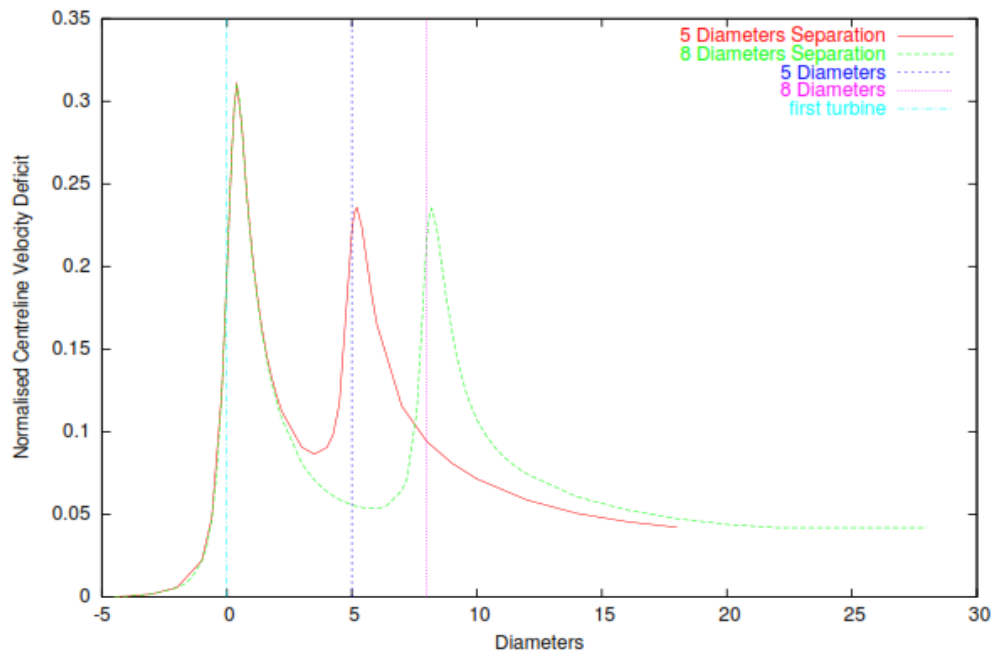
Figure 2.9: Velocity deficit for two turbines placed in-line (Macleaod et al., 2002).

Figure 2.9 has provided two messages. First, regardless the downstream spacing between two turbines, the centreline velocity deficit eventually recovers to 5% of the initial flow after a distance of 15 diameters downstream from the first turbine. Second, although the velocity deficit immediately after both downstream turbines are approximately 23%, but the energy harnessed by turbine at 5 diameters downstream and 8 diameters downstream is totally different. For 5 diameters downstream, the flow only recovers to 90% of initial flow velocity. For 8 diameters downstream, the flow has sufficient space to regain velocity to almost 95% of initial flow velocity. The different in percentage may seem insignificant, but bear in mind, kinetic energy flux is directly

proportional to cubic velocity. Assume an initial flow velocity of 1.0m/s, the difference between 0.9 cubic velocity and 0.95 cubic velocity after the first turbine can be up to almost 17%. This directly highlights the need to consider the turbine spacing correctly.

Another team of researchers from the French Research Institute for Exploitation of the Sea, known as ifremer in French, has also been studying wake pattern of HATCTs since 2008 (Maganga et al., 2008a; Maganga et al., 2008b; Maganga et al., 2009; Maganga et al. 2010a; Maganga et al., 2010b; Pinon et al., 2012; Mycek et al. 2013). Their works include the development of an in-house CFD code that can simulate the wake pattern of HATCTs, experimental study on performance of HATCTs and wake. Their series of efforts in developing and optimising their own numerical method is a good example for one to have more understanding on CFD method. In the following, their work will be used as a reference to describe the conveniences and limitations of using CFD in modelling the hydrodynamic parameters for HATCTs.

In year 2008, they reported the use of an unsteady Lagrangian method coupled with the Vortex method to simulate the wake pattern of a three bladed HATCT subjected to uniform upstream flow. Readers are referred to Maganga et al. (2008a) and Maganga et al. (2008b) for the details of their methodology. For comparison purpose, they defined their blades shapes and configurations similar to that of Bahaj et al. (2007a). Comparison of C_p values obtained by their numerical method and Bahaj's results is as shown in Figure 2.10. It is clear that although the general trend is in good agreement and the simulation has predicted the optimum TSR considerably accurate, Maganga's numerical model has under-predicted the overall C_p value by more than 20%.
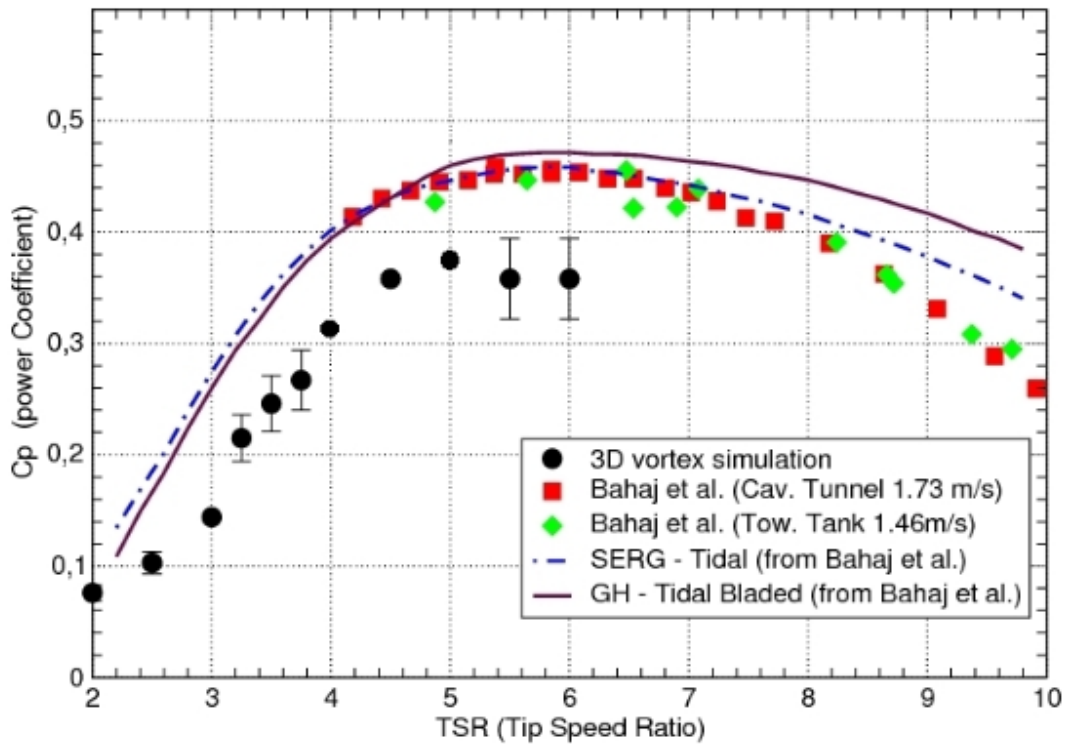
Figure 2.10: Comparison of C_p between Maganga's results and Bahaj's results (Maganga et al. 2008b).

They have attributed this difference to the fact that they have not meshed the turbine hub in their simulation. However, their explanation is questionable. The influence of turbine hub in a simulation is limited towards C_p value as it is not the main part that provides the torque. A properly streamlined turbine hub may more or less improve the C_p of a turbine, but the difference should be minimal. The reasons for the difference must be associated with the improper defined equations, turbulence models and/or mesh density. For the same study, they also simulated wake pattern but they did not show the comparison of the wake pattern predicted by their model with Bahaj's result. They only claimed that the difference is within 5%.

In year 2012 that Maganga's team reported a numerical method that is capable of predicting more accurate results (Pinon et al., 2012). They implemented simple Large Eddy Simulation (LES) as their turbulence model. In addition, they used the unsteady Bernoulli relation in their vortex method. Figure 2.11 shows their numerical results.

They used back the experimental data on C_p value reported by Bahaj's team for different pitch angle to validate their numerical results. As a gentle reminder, reader can refer back to Figure 2.1 for the complete experimental C_p value reported by Bahaj's team for different pitch angle.

(a)

(b)
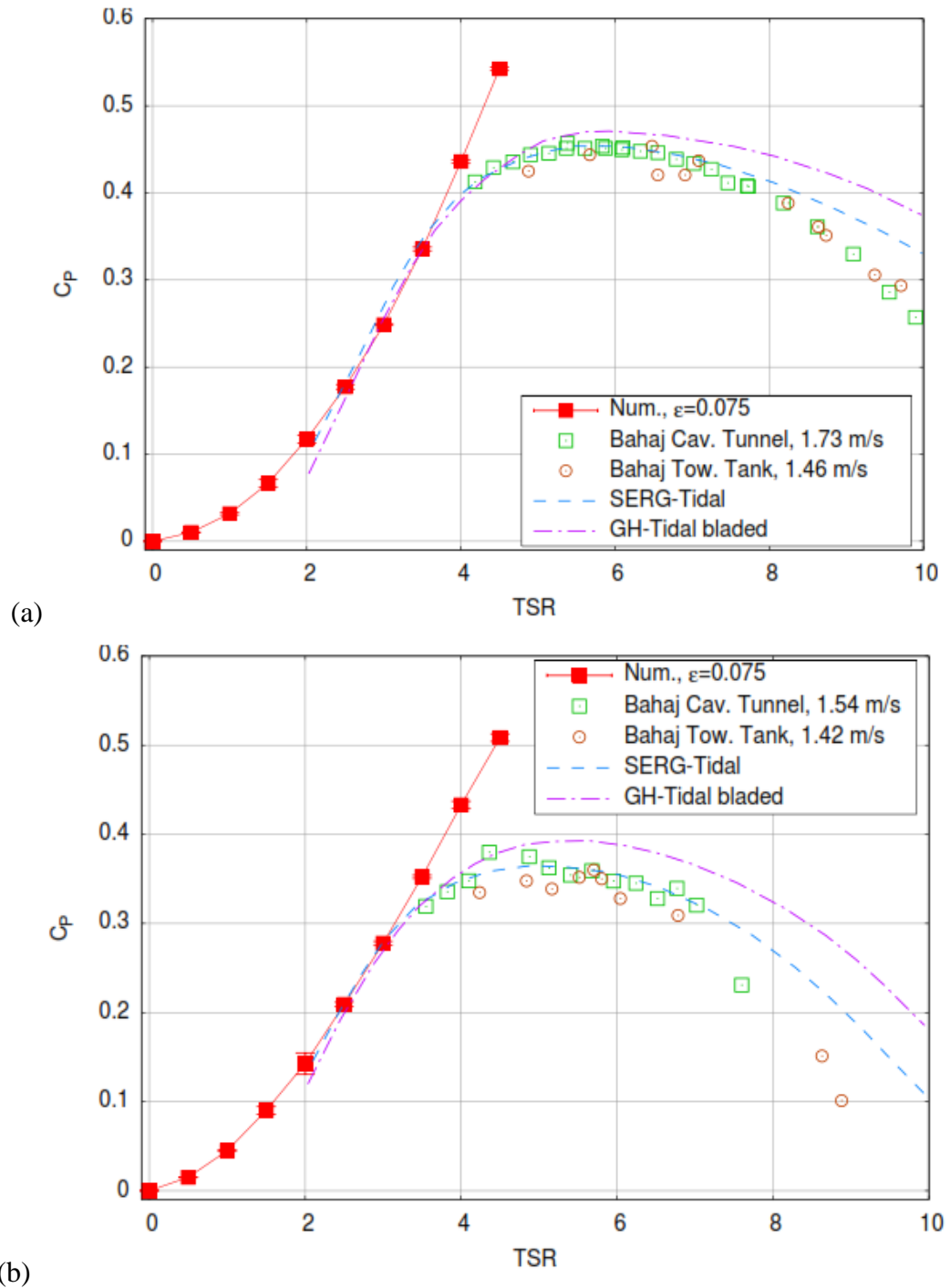
Figure 2.11: C_p Comparison between numerical results by Maganga's team.and experimental data by Bahaj's team. (a) 5° pitch angle (b) 10° pitch angle (Pinon et al. 2012).

As can be seen from Figure 2.11, the prediction of numerical model is in good agreement with the experimental results reported by Bahaj's team for TSR below 4. Above TSR 4, their numerical model fails to predict the optimum C_p value, as well as the decrease of C_p value at higher TSR. They have explained this limitation in their work, whereby they did not consider flow separation effect and vortices losses in their numerical model. Flow separation occurs at high angle of attack (AoA) and induces higher pressure drag on the blade.

Apart from the numerical study, Maganga's team has also studied the wake pattern of HATCTs experimentally. In year 2011, they reported the measurement of wake pattern behind a 0.7m three-bladed turbine (Mycek et al., 2011). This is different with Bahaj's team, where Bahaj's team has been using actuator mesh disc in their wake study. The flume used by Maganga has a depth of 2m and they positioned their small-scale turbine at the centre with 1D distance from the tip of the turbine to the bottom of the flume.

A comparison between Maganga's group data and Bahaj's group data reveals that the velocity deficit at the near wake region ($1.0 < D < 4.0$) behind an actual turbine is larger than those generated by an actuator mesh disc. Nonetheless, beyond 8D distance, the velocity deficit is approximately similar. This comparison suggests that the near wake pattern behind a turbine and an actuator mesh disc is different. Generally, the findings on wake pattern by Maganga's team are in agreement with Bahaj's team.

In the same study, Maganga's team also studied the wake interaction between two HATCTs placed in-line. This is similar to that what Macleod et al. (2002) has done. They did not present the velocity deficit between two turbines, but they presented the C_p value of the second turbine with different spacing. Figure 2.12 shows the C_p value of second turbine at different spacing. Note that a denotes the spacing between turbines and D denotes the diameter of turbine. The red line represents the C_p value of the upstream turbine. It is obvious that with a larger spacing, the downstream turbine can have better efficiency. This finding is similar with Macleaod et al. (2002). Note that the upstream turbine is in operation for all the measurements.
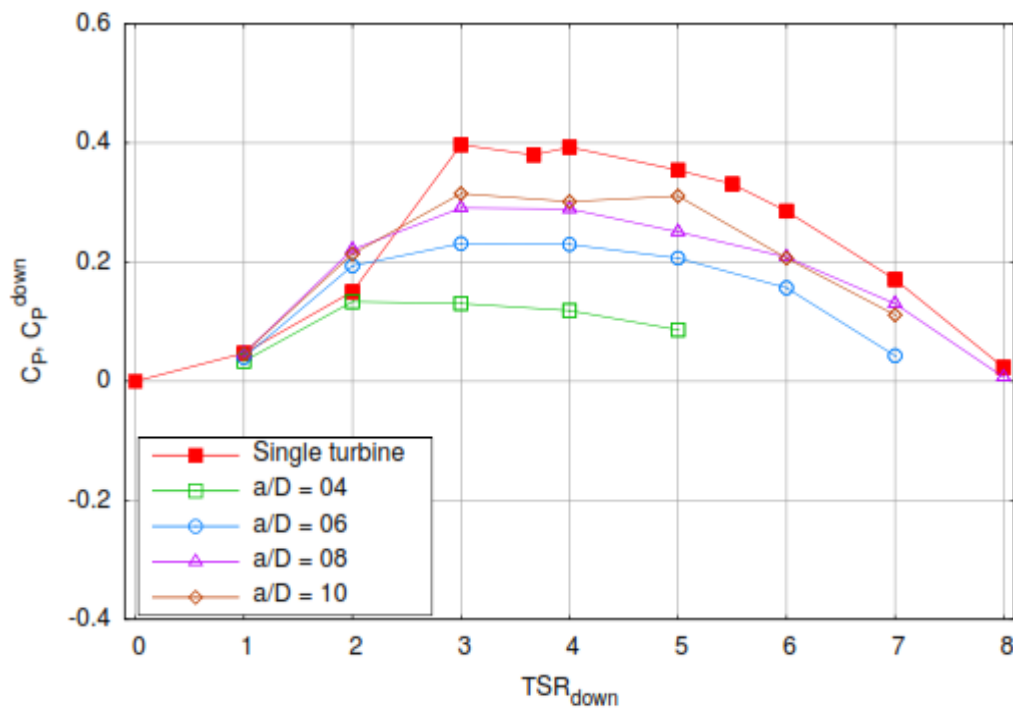
Figure 2.12: C_p value of downstream turbine with different spacing from upstream turbine (Mycek et al., 2011).

Based on their findings, Maganga's team suggested that there may be a need to compromise the efficiency of a single HATCT to optimise or maximise the total output of a HATCT farm. For instance, a HATCT with an optimum C_p value of 0.45 may generate a wake that only recovers after 15 diameters downstream. Therefore, the next HATCT can only be placed after 15 diameters downstream to obtain a similar C_p value.

Contrarily, a HATCT with an optimum C_p value of 0.35 may generate a wake that recovers after 10 diameters downstream.

For a channel with a length of 30m that requires 5m clearance at both the entrance and the exit; the first scenario can only get an efficiency of 2 x 0.45 = 0.9, whereas, the second scenario can get an efficiency of 3 x 0.35 = 1.05. This makes the second scenario has a slightly higher total efficiency than the first scenario. This idea surprisingly matches with the idea of Vennell (2011b), discussed in section 2.3.1.1, which is maximizing every single turbine in a HATCT farm may not necessarily give the best optimized power output.

Despite these continuous investigations on HATCTs' wake pattern by Bahaj's team and Maganga's team, researchers have yet to come to consent. This is especially true for near wake region and in-line HATCTs' wake interaction. In year 2011, Jo and his team from Korea also reported study on wake interaction (Jo et al., 2011a; Jo et al., 2011b). They used three 500mm diameter three-bladed turbines and placed them in-line with a spacing of 1.5D to study the influence of wake on performance of a downstream turbines.

They measured the performance of turbine in term of RPM. The RPM of the 2nd and 3rd turbine under different free stream velocity were measured. Figure 2.13 shows the RPM of the 1st turbine that is subjected to undisturbed flow. Table 2.2 shows the RPM measured for all the three turbines. Their data presentation is not that clear. A data reduction is required to have a clearer picture. In their experiment, they allow the turbines to rotate freely without the need to turn a generator. The corresponding TSR of the turbine for the range of velocity shown in Table 2.2 ranges between 6.7~7.1. At

such a high TSR, the disturbance level on the flow should be high and the velocity

deficit immediately after the 1st turbine should also be significant.
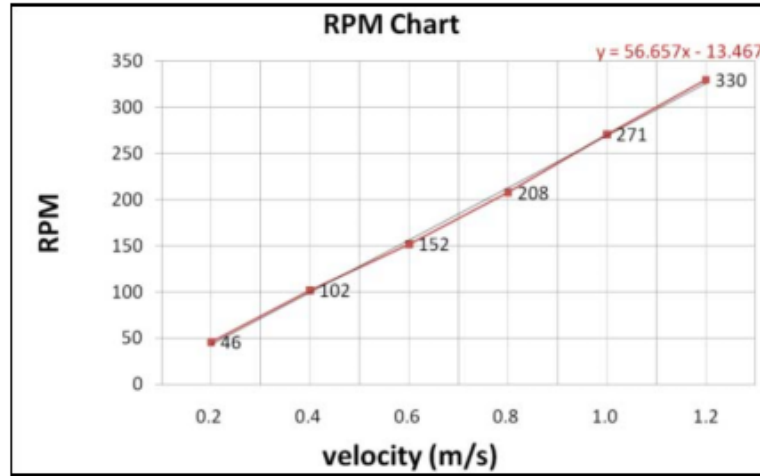
Figure 2.13: RPM of Jo et al. turbine subjected to different free stream velocity
(Jo et al., 2011a).

Table 2.2: Measured RPM for the three turbines used by Jo et al. (2011b).

Rotor Interval (1.5D)			
Flow velocity(m/s)	1st turbine (RPM)	2nd turbine (RPM)	3rd turbine (RPM)
0.2	47	33	0
0.4	103	83	65
0.6	157	131	112
0.8	212	180	158
1.0	270	231	206
1.2	330	289	258

Consider the data set for flow velocity at 1.0m/s and 1.2m/s. The RPM for the

2nd turbine are 231 and 289 respectively. The RPM for the 3rd turbine are 206 and 258

respectively. According to Table 2.2, the velocity corresponds to a RPM of 231 and 206

are approximately 0.88m/s and 0.81m/s. This suggests that at a velocity of 1.0m/s, the

velocity deficit after 1.5D from the 1st turbine is only about 12%. Even after 3.0D with

the blockage of the 2nd turbine, the velocity deficit only increases to about 20%. Similar

condition occurs for data set at 1.2m/s. The velocity corresponds to a RPM of 289 and

258 are approximately 1.08m/s and 0.95m/s. This suggests a 12% velocity deficit after

1.5D and 20% velocity deficit after 3.0D. The velocity deficit becomes greater at lower flow velocity.

Jo et al. (2011b) findings have huge difference with that of Bahaj's team and Maganga's team. Based on the previous results reported by Bahaj's team and Maganga's team, one would expect that the velocity deficit at 3.0D downstream should be around 40% ~ 50%. If findings by Jo et al. (2011b) are accurate, their experimental data suggests that the velocity deficit at near wake region is lower than the common perception. Close placement of in-line HATCT might be workable.

One may question the reliability of such comparison as very often, the experimental data are affected by many factors which include the dimension of test rig, the potential faster wake recovery due to higher turbulence intensity of the used flow and the design of turbine itself. Nonetheless, such comparison implies that the wake pattern and optimal spacing may vary significantly for different type of HATCT farm's configuration. Moreover, Jo and co-workers are not the only researchers that reported different findings on HATCTs' wake pattern.

A research team from the UK also has different findings compared with Bahaj's team on the wake interaction between multiple HATCTs (Whelan & Stallard, 2011; Stallard et al., 2013). They used a 270mm diameter three-bladed turbine in their experiment. They studied the wake pattern generated by a row of turbines with different lateral spacing which includes 1.5D, 2.0D and 3.0D. Their findings show that the wakes generated by two turbines with 1.5D lateral spacing merge after 6.0D diameter downstream. This is contradictory to the experimental results reported by Bahaj's team,

where merger of wakes from two actuator mesh discs with a lateral spacing of 1.5D does not take place.

Note that the actuator mesh disc used by Bahaj's team was 100mm and the turbine used by Stallard et al. (2013) was 270mm. The lateral spacing of turbine in Stallard et al. (2013) is definitely larger than Bahaj's team, but wake merger occurs. This suggests the swirling effect of rotating turbine plays significant role in wake expansion. An actuator mesh disc cannot reproduce this swirling effect. This may be the reason for no wake merger was observed by Bahaj's team. Stallard et al. (2013) has tested that for three turbines in a row and five turbines in a row. Wake merger happens in both settings.

Recently, Jeffcoate et al. (2016) reported their field test data on performance of turbines placed in-line and in-plane. Note that all the findings discussed so far are obtained from lab experiment and numerical modelling. This field test provides insights on the actual effects of wake interaction upon HATCTs performance. They built a test platform on a lake, in order to provide steady state for the test, to study the performance of two 1.5m four-bladed turbines. For in-plane setting, they tested 1.5D and 2D lateral spacing. For in-line setting, they tested 2.0D and 6.0D spacing. They also tested a setting where a downstream turbine, with a 6.0D downstream distance from the upstream turbine, is placed 1.5D and 3.0D offset from the centreline of the upstream turbine to study the effects of wake expansion from the upstream turbine towards the downstream turbine.

Figure 2.14 shows the C_p values for the two turbines when placed in-plane with a spacing of 1.5D. C_p values recorded for both turbines are in good agreement with no significant difference. Figure 2.15 shows the C_p values for the two turbines when placed in-line with a spacing of 2.0D and 6.0D. Here, the wake effect is apparent as the C_p values decrease significantly for the downstream turbine. Figure 2.16 shows the C_p values for 1.5D and 3.0D offset. The results suggest that the effect of wake expansion becomes negligible at 6.0D downstream as the C_p values of downstream turbine is almost identical to the upstream turbine. Note that the terms *P* and *SB* in Figure 2.16 are used by Jeffcoate et al. (2016) to denote whether the second turbine is placed to the right or left-hand side of the first turbine.

Results in Figure 2.15 contradict with the results reported by Jo et al. (2011a). Figure 2.15 clearly shows that a HATCT placed in-line behind another HATCT will suffer a loss of efficiency up to almost 40%. No doubt, such a significant loss is a result of high velocity deficit. Note that this effect remains strong even at 6.0D downstream. In their field test, turbine's diameter is 1.5m. This translates to a distance of 9.0m. Since Jeffcoate et al. (2016) reported their findings based on a field test, their data should be closer to reality compared to Jo et al. (2011a).
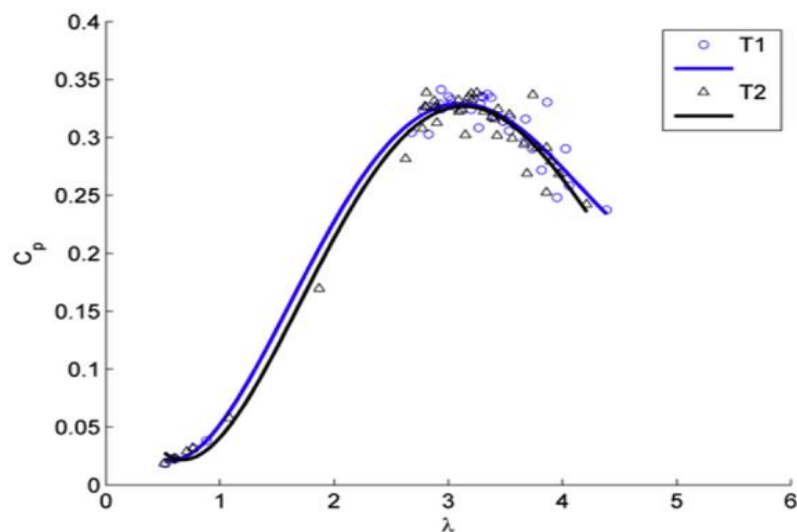
Figure 2.14: C_p values for turbines placed in-plane with 1.5D spacing (Jeffcoate et al., 2016).
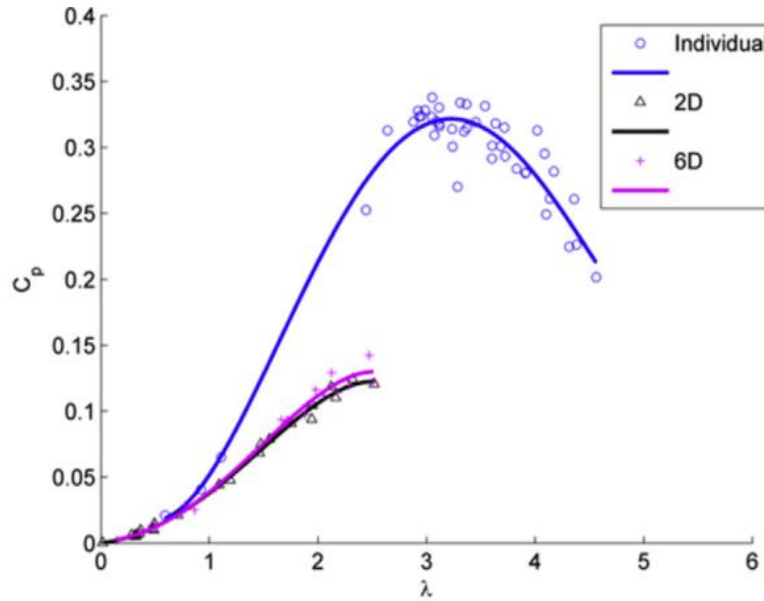
Figure 2.15: C_p values for turbines placed in-line with different spacing
(Jeffcoate et al., 2016).
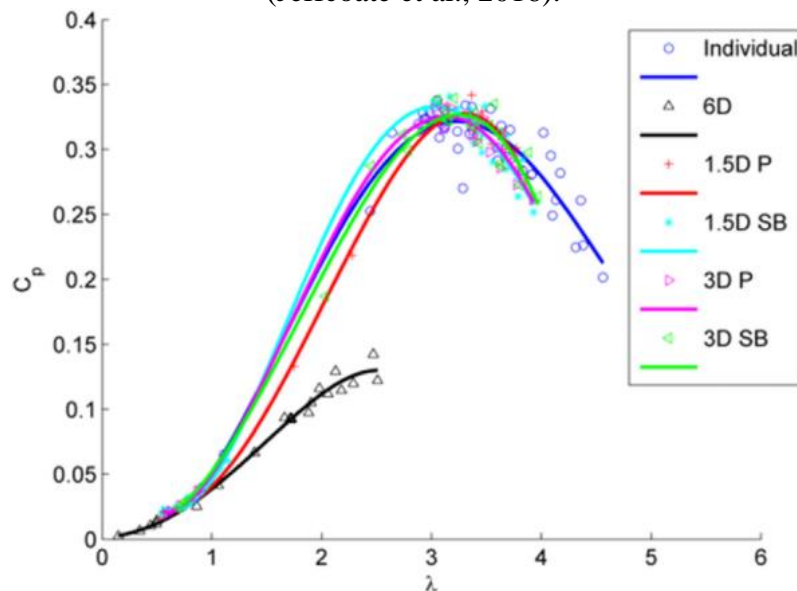
Figure 2.16: C_p values for turbines placed with different offset spacing from the first
turbine's centreline at a downstream distance of 6.0D (Jeffcoate et al., 2016).

At the moment, works by Jeffcoate et al. (2016) can be considered as a summary of what the research community has been doing to understand the wake pattern. Their field test has proven most of the findings obtained from lab work and is in good agreement. At the moment, what is known for sure is that the impacts of wake from an upstream HATCT on the performance of a downstream HATCT are significant. A suitable spacing, depending on the design of HATCT, is required for wake recovery in

order to optimise the total output of a HATCT farm. This can be achieved via experimental test or CFD modelling.

2.3.2.5 Generator Issues

In this section, the research on HATCTs' generator will be discussed. Generator is the key component that transforms the rotational energy of HATCTs' turbine into useful electrical energy. Despite its important role in HATCTs, not many researchers have conducted study on it. The main reason for this is that generator technology is a mature field. Generator is the common part shared by all electricity generating devices such as the conventional power plant and wind turbines. Research on design modification and efficiency optimisation has already been done far before this and therefore, the potential operating issues associated with HATCTs' generator is minimal.

The only challenge in HATCTs' generator is the sizing and selection of generator based on the designed efficiency of turbine blade. In fact, such study is also common in wind turbines field. For wind turbines, the fluctuation of incoming wind speed is high. There are many circumstances where a wind turbine will encounter extremely high wind speed or highly turbulent wind where velocity fluctuates vigorously within a short period. Under such extreme conditions, generator will be subjected to high loading. For HATCTs, tidal current flow is relatively constant and falls within a predictable range. Nonetheless, the effects of waves and surges can also cause high degree of velocity fluctuation in a short period. Hence, the sizing must be appropriate and take into consideration safety factor for such extreme condition. Otherwise, extra mechanisms may be needed to control the generator output.

A review in 2012 shows that the type of generator used by different developers includes Induction Generator (IG), Permanent Magnet Synchronous Generator (PMSG) and Direct Drive Permanent Magnet Generator (DDPM) (Chen. et al., 2012). These are the common type of generators used in wind turbines. Basically, the main difference between IG and PMSG is that IG requires external current to create its rotating magnetic field (either from a grid or a capacitor bank), whereas PMSG has a built-in permanent magnet to induce electrical current. There is another more widely used IG known as Doubly-Fed Induction Generator (DFIG) in wind turbines field. The difference between IG and DFIG is that IG only has winding on its stator, but DFIG has winding on both its stator and rotor, hence the term Doubly-Fed.

Table 2.3 are the main differences between DFIG and PMSG tabulated by the company called The Switch, which is a company that specialises in electrical drive train technology for wind turbines (The Switch, 2014).

Table 2.3: Overview of DFIG and PMSG (The Switch, 2014).

Performance	Machine Type	
	DFIG	PMSG
Stator	Same	Same
Rotor	Rotor Coil	Permanent Magnet
Bearing	Same	Same
Slip Ring	Available	Not Needed
Manufacturing	Complicated process to manufacture rotor	Simple process to manufacture rotor
Maintenance	Heavy maintenance work and high cost for rotor slip rings	No need for rotor maintenance
Converter	25% ~ 30% output power	Full power
Reactive power and adjustment ability	Varies according to the generator speed	100% across the entire speed range
Ability to connect and support power grid	Poor	Very good
Advantages	The initial investment is lower	1. Rotor is made of magnet; no coils, coil connection or slip ring needed. 2. No need for rotor maintenance. 3. Applicable to high-, medium- and low-speed

		generator.
		4. High efficiency
		5. Generator is lighter and size is smaller
		6. Smaller cogging force
Disadvantages	1. Difficult to service rotor, especially problems associated with the rotor coil and rotor wire connection 2. Not applicable to medium- and low-speed generator 3. Low efficiency 4. Large unstable cogging force 5. Large bearing current.	1. The initial investment is higher 2. Requires professional design software for complicated calculation 3. Requires more sophisticated process

Based on Table 2.3, it is clear that both DFIG and PMSG are suitable for HATCTs depending on the design and desired output. Based on the available open literature, Ben Elghali's team from France have conducted study to understand which generator is more suitable for HATCTs (Ben Elghali et al., 2008a; Ben Elghali et al., 2008b; Ben Elghali et al., 2009; Ben Elghali et al., 2010a; Ben Elghali et al., 2010b, Ben Elghali et al., 2011a; Ben Elghali et al., 2011b; Mekri et al., 2011; Ben Elghali et al., 2012; Drouen et al., 2012).

They first started with DFIG back in year 2008. They proposed the use of a sensor free control for the DFIG to operate under turbulence condition (Ben Elghali et al., 2008a; Ben Elghali et al., 2008b). They first used a Maximum Power Point Tracking (MPPT) strategy where the pre-calculated power output of a turbine at different tidal current speed and the projected average tidal current speed are fed into the control system. The projected average tidal current speed serves to control the output of DFIG. Their MPPT uses a first order model to predict the tidal current speed and uses it as the reference to control the operation of DFIG. The model takes into consideration effects from the tidal current speed, the swell disturbance and included a term that represents any other disturbances in a flow.

In year 2010, they made a comparison with traditional controlling system, known as Proportional Integral (PI) control, to showcase how their MPPT strategy can improve the efficiency of HATCTs (Ben Elghali et al., 2010a). They showed that under normal condition, PI gives a slightly higher output compared to their second-order sliding mode MPPT. However, when swell and other disturbance are present, their MPPT strategy yields an output that is 8% ~ 9% higher than PI (Ben Elghali et al., 2010a).

After their attempt on DFIG, they started looking into the use of PMSG in year 2010. A study to compare these two types of generator was reported by them (Ben Elghali et al., 2010b). They also listed out the pros and cons for IG, DFIG and PMSG, as tabulated in Table 2.4. Their comparison is quite similar to that listed in Table 2.3. They used the simulated performance of their second-order sliding mode MPPT for both DFIG and PMSG to calculate the annual power of a 10.0m diameter turbine with a rated power of 100kW. The tidal current velocity input was taken from the Raz de Sein tidal site. The calculated power is shown in Figure 2.34. It was found that the calculated power for DFIG-based is about 1530MWh/year, whereas PMSG-based is about 1916MWh/year.

Table 2.4: Comparison of pros and cons for IG, DFIG and PMSG (Ben Elghali et al., 2010b).

Type	IG	DFIG	PMSG
Pros	- Full speed range - No brushes on the generator - Complete control of reactive and active power	- Limited speed range, $\pm 30\%$ around synchronous speed - Inexpensive small capacity PWM Inverter - Complete control of reactive power and active power	- Full speed range - Possible to avoid gear - Complete control of reactive power and active power - Brushless (low maintenance) - No power converter for field
Cons	- Full scale power converter	- Need slip rings - Need for gear	- Full scale power converter

	- Need for gear		- Multipole generator (Big and heavy) - Permanent magnet needed

The difference for annual power output is as high as 25%. Ben Elghali's team attributed this difference to the fact that the speed reference for DFIG was limited to $\pm 30\%$ of the rated power. This is obvious in Figure 2.17, where DFIG has no output for tidal velocity lower than 1.25m/s. Another point that the team highlighted is that the generator for HATCTs should be robust and preferably require less maintenance. For this reason, PMSG appears to be a better candidate for HATCTs. From that point onwards, they put more efforts in the study of PMSG, which include study on the difference between three- and five-phase PMSG (Ben Elghali et al., 2011a), as well as developing a fault-tolerant system for multiphase PMSG (Mekri et al., 2011).
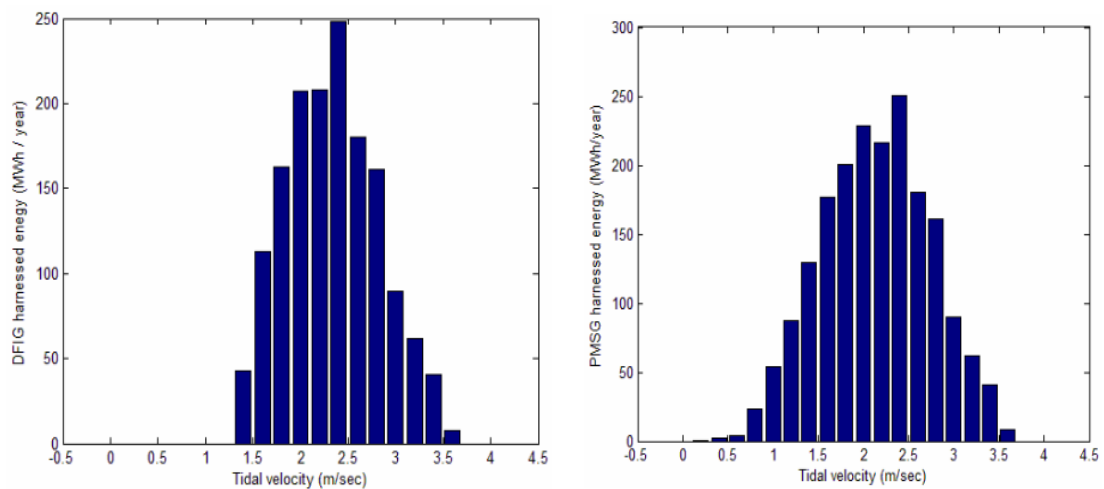
Figure 2.17: Comparison of harnessed power between DFIG and PMSG (Ben Elghali et al., 2010b).

A more recent work by Sousounis et al. (2015) also shows that PMSG is a better candidate for HATCTs' generator. They make comparison between PMSG and IG. Their study shows that PMSG reach its maximum efficiency faster than IG. PMSG is also capable to capture more energy at low tidal current velocity compared to IG. They also reported that the overall system losses at each component for IG are higher than

PMSG. Their findings are in good agreement with Ben Elghali's team. All these point out that PMSG has a better prospect to be used as the generator for HATCTs.

Based on the findings by Ben Elghali's team and Sousounis et al. (2015), PMSG appears to have more advantages compared to DSIG. This is especially true for HATCTs that are built for remote area where a reactive power from grid is less likely. Looking back at the situation in Malaysia, a relatively low tidal current speed implies the need for PMSG, which is capable of producing power effectively even with low tidal current speed. Hence, it is believed that PMSG should be used as the generator for HATCT that is built for Malaysia.

2.3.2.6 Design Modifications

Up to the previous sub-section, all the major factors that affect the performance of HATCTs have been discussed. The optimisation of HATCTs' performance depends largely on the tidal current resources, turbine design and generator. Although loading and cavitation have impact on performance, the possibility for having these problems may be minimal for potential sites where the tidal current speed is mild. Nonetheless, driven by the interest to optimise the efficiency of a HATCT, new design ideas have also been reported by researchers from time to time.

One common idea to improve the total power output of HATCTs is to provide the device with higher tidal current speed. This can be done by accelerating the incoming tidal current flow with auxiliary part such as a duct, or more commonly called as diffuser in the field of wind turbines. A circular duct with large diameter inlet facing upstream and small diameter facing downstream can help accelerate a flow that passes through it. Figure 2.18 shows the illustration of such setting. According to conservation

of mass, *V2* will be faster than *V1*, hence providing a higher energy for the turbine placed at the middle to harness.
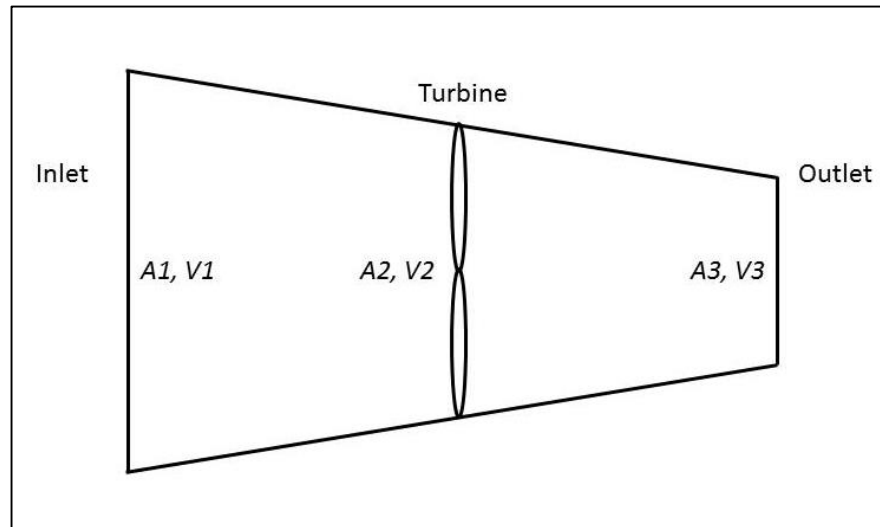
Figure 2.18: Illustration of diffuser augmented HATCT.

Some earliest research in the design of diffuser augmented HATCTs can be traced back to year 2003. Lawn (2003) reported the use of a one-dimensional model to analyse the efficiency of a diffuser augmented HATCT. The reported enhancement is more than 30% of a HATCT without the diffuser. In year 2004, Setoguchi et al. (2004) reported a study on two-way diffuser augmented HATCT to account for the nature of tidal stream which is bi-directional. They showed that the outside shape of a diffuser has effects on the performance of the diffuser. The best configuration of their diffuser yielded a flow velocity that is 1.3 times faster than the undisturbed flow.

Shives & Crawford (2010) reported the use of ANSYS CFX to study the overall efficiency of a diffuser augmented HATCT. They showed that the presence of the diffuser structure increases the drag over the entire system. In a later work, they developed an empirical model to study the hydrodynamic parameters associated with diffuser. Their model showed that the flow separation near the diffuser section has significant impact on the efficiency of diffuser. A worth noticing point is that they

argued that diffuser augmented HATCT may not be suitable for array deployment due to higher drag losses associated with the auxiliary structure. This has been confirmed recently by Cresswell et al. (2015).

In order to make this idea workable, there are many challenges that need to be addressed. Besides the issue of drag, there are many other factors that make the use of diffuser less appealing. The making of diffuser itself is cost-intensive and the extra structure imposes higher load on the overall structure. This in turn needs a stronger foundation, which also means a higher cost of construction. Additionally, diffuser also needs to operate in the harsh marine environment. Its maintenance will be challenging in case of any failure. Last but not least, the diffuser can easily trap ocean rubbish. This is especially true for HATCTs that deployed near to a location with intensive human activities.

Besides provision of diffuser, there were researches that aim to design a HATCT that is different from the conventional types. Clarke and co-workers from the UK have designed, developed and tested a contra-rotating HATCT (Clarke et al., 2007a; Clarke et al., 2007b, Clarke et al., 2008; Clarke et al., 2010). Their design idea was to put a three-blade turbine facing upstream and another four-bladed turbine facing downstream. The four-bladed turbine will rotate in the opposite direction of the three-bladed turbine. Their aim is to design a HATCT that imposes near-zero reactive torque on the foundation structure and near-zero swirls.

As mentioned several times previously, the more the mechanical parts that expose to the open marine environment, the more vulnerable a HATCT could become. Therefore, maintenance will be an issue for contra-rotating turbine. Despite the

challenge, there are still researchers who recently reported their study on contra-rotating HATCT (Lee et al., 2015; Huang & Kanemoto, 2015).

2.3.3 Maintenance of HATCTs

Building a robust HATCT that can operate effectively under the harsh marine environment is one challenge. Maintaining its performance and ensuring its lifespan through proper maintenance is a more challenging one. Any mechanical parts will inevitably suffer fatigue loading and has a definite lifespan. Based on the current state-of-the-art of HATCTs, an economically viable commercial-scale HATCTs must be able to operate for a design lifespan of more than 15~20 years (Fraenkel et al., 2002). Certainly, this depends on the scale of HATCTs and design output. The idea is that a HATCT must be able to achieve its design lifespan without major failure and capable to deliver its designed output.

A colonisation activity of benthic marine organisms on HATCTs support structure will become a marine bio-fouling that can cause HATCTs to lose their efficiency. Smoothness of turbine blade's surface is crucial to ensure hydrodynamic performance. Presence of roughness due to corrosion or marine bio-fouling will affect the flow field past the surface of turbine blade. This in turn causes the turbine blade to lose its hydrodynamic efficiency.

In year 2001, Orme et al. (2001) already reported the effects of marine bio-fouling on HATCTs performance. They used a NACA4424 aerofoil, with 0.2m chord length and 0.22m span, to study the effects of marine bio-fouling on lift coefficient (C_L) and drag coefficient (C_D). They studied the effects of bio-fouling density and size of fouling species on C_L value and C_D value of NACA4424. Figure 2.19 and Figure 2.20

show their results. Their results clearly show that the presence of fouling species leads to a decrease in C_L and increase in C_D. Note that the C_P value of HATCTs is directly proportional to lift-to-drag ratio (L/D).
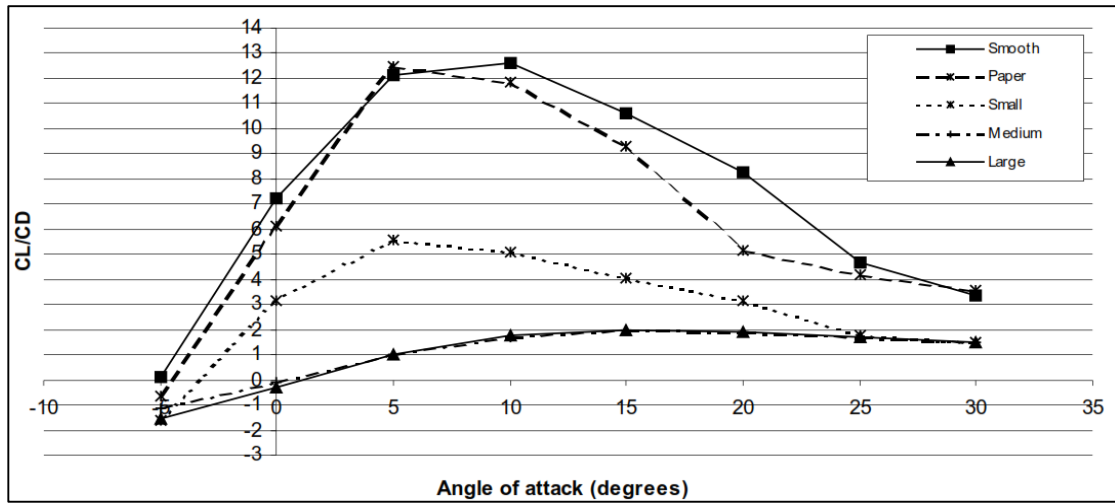
Figure 2.19: L/D ratio of NACA4424 with different fouling species' size (Orme et al. 2001).
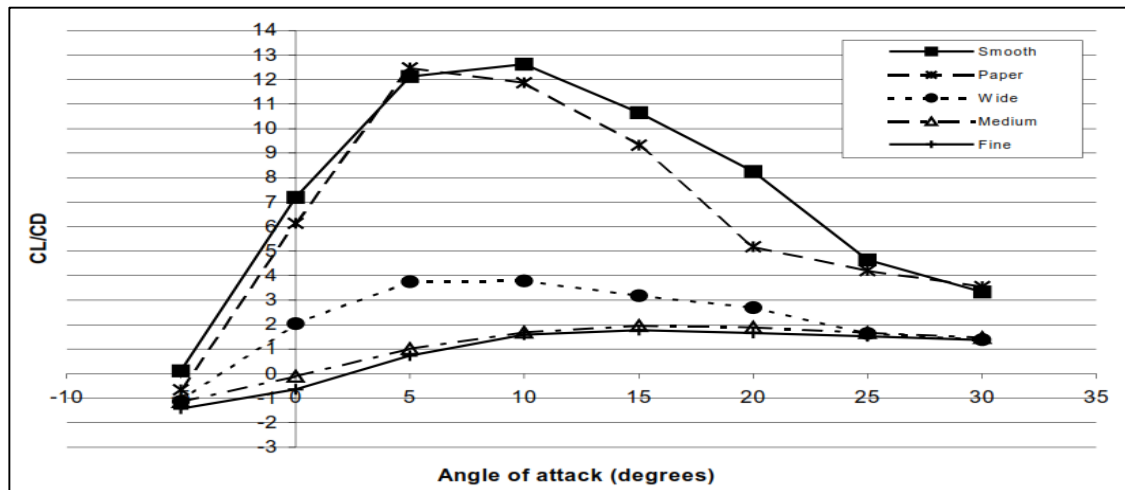
Figure 2.20: L/D ratio of NACA4424 with different fouling species' density (Orme et al. 2001).

Recently, Walker et al. (2014) also reported their experimental and numerical study on the effects of marine bio-fouling on the performance of HATCTs. Their results are shown in Figure 2.21. It can be seen that the optimum C_P value of HATCTs drops more than 20% when it is covered by marine bio-fouling. Another recent study by Kyozuka et al. (2014b) has also shown similar findings. All these studies point out the importance of ensuring a smooth turbine blade surface. Based on the available literature,

there is no study to determine the best measure to minimise occurrence of marine bio-fouling on turbine blades of HATCTs from (Ng et al. 2013a).
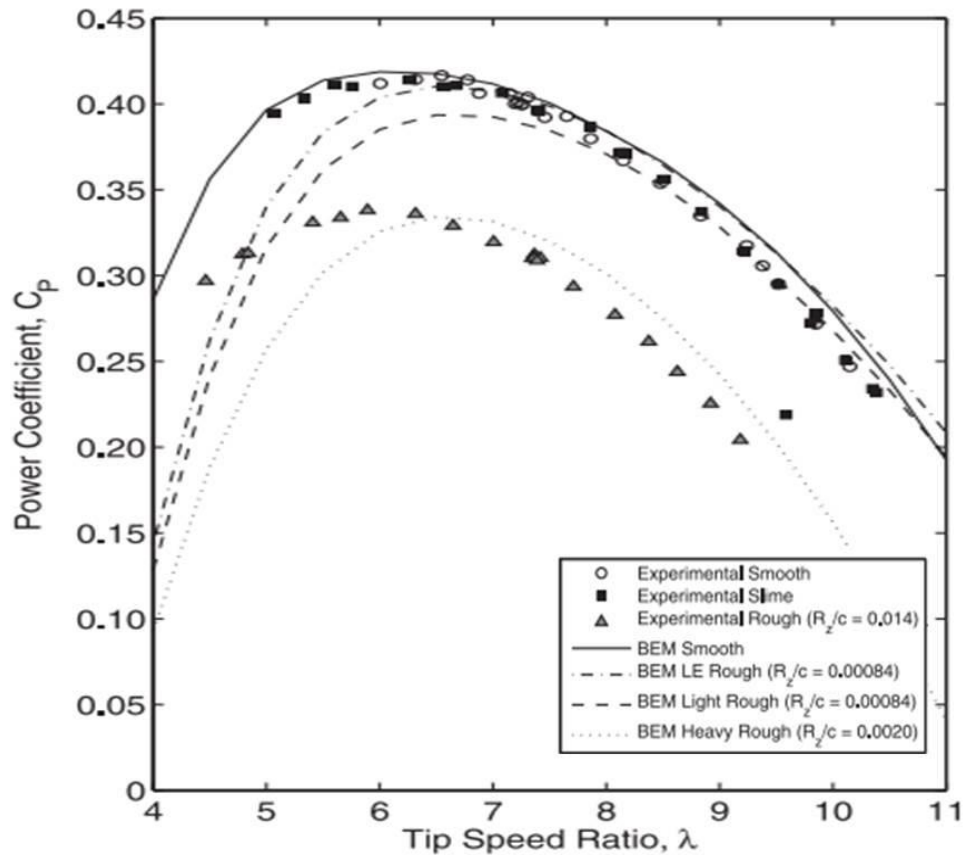
Figure 2.21: C_P value of HATCTs with different surface roughness of turbine blade
(Walker et al., 2014).

The current measure that HATCTs developers, including Marine Current Turbines Ltd., are using is the application of anti-fouling paint or fouling release paint (Ng et al. 2013b). Anti-fouling paint in the market can usually last for 3-5 years. It is effective in preventing soft fouling, which is the colonisation of thin algae film. But, it is not effective in preventing hard fouling present, which is the colonisation of organisms like barnacles. Once barnacles attach on a surface, it can only be removed manually. Hence, even when turbine blades and other important parts that should be made clear from marine bio-fouling are coated with anti-fouling paint, intensive maintenance is still needed to ensure the anti-fouling paint to performance effectively.

Similar to energy resources, marine bio-fouling rate is also site-specific. In colder water, the marine organisms' activity will be limited by temperature. In warmer water like those located in the tropical region, the fouling rate is expected to be fast. Hence, site investigation is required to identify the fouling rate of a site prior to deployment of HATCTs. In addition, for a HATCT that is designed with no auxiliary system to recover its turbine blade onto sea surface for schedule cleaning, failure of HATCT blade will be just a matter of time. From this point of view, it implies that a HATCT must be built in a way that it can be readily recovered from the ocean, just like the SeaGen.

The above statement on turbine recovery from the ocean is not only limited to marine bio-fouling issue. An auxiliary system is also needed for maintenance on turbine blade's condition. Routine maintenance is necessary to examine whether turbine blades suffer from natural corrosion process, scratching from ocean sediments, rubbish trapping and fatigue cracks. It is undoubtedly not cost-effective to send divers down to do such checking, especially for HATCT farm where there can be more than 10 units of HATCT. Furthermore, underwater repair work is also tedious and cost intensive. This indirectly suggests that it is unsuitable to build a HATCT device that will be fixed permanently underwater.

Studies on maintenance issues are lacking. This is simply due to the fact that there are not many commercial scale HATCTs currently in operation. While some monitoring methods from wind turbines field can be transferred and applied directly, there is still need for monitoring techniques that specially designed for HATCTs. This area has only been addressed by researchers recently (Prickett et al., 2011). In fact, possible causes for HATCTs failure are not well understood. What can be done at the

moment will be limited to the well-known maintenance issues associated with mechanical parts.

2.4 Summary

A concise review of past researches on HATCTs has been discussed in this chapter. Some knowledge gaps have also been identified, such as the maintenance issues and environmental impacts. From this review, some important points to be highlighted are as following:

1. At current stage, no model can predict available energy resources accurately;

2. It is possible to get a higher total power output for HATCT farm by tuning individual HATCT accordingly;

3. Design of turbine for HATCTs can vary according to needs. There is no universal best turbine design for HATCTs;

4. For HATCT farm, the optimum downstream spacing depends on the efficiency of individual turbine. A shorter wake is possible with a lower C_P value;

5. A minimum lateral spacing of 1.5 diameter is preferable for two adjacent HATCTs;

6. PMSG is the preferable generator for HATCTs;

7. A single HATCT is unlikely to have significant negative environmental impacts;

8. More studies on maintenance issues of HATCTs are required; and

9. Marine bio-fouling on turbine blade is a serious issue for HATCTs' maintenance.

This review provides sufficient guidelines for the current study, especially for the purpose of field testing of HATCT for Malaysia. Suitable methodologies for efficiency

testing and performance modification are adapted from these literatures. This includes

the use of CFD, hydrofoil testing, turbine testing and field test.

CHAPTER 3: METHODOLOGY

3.1 Overview

In this chapter, the methodologies used in achieving the three objectives of the current research will be discussed. The methodologies consist of analytical analysis, numerical analysis and experiment. Analytical analysis involves the derivation of equation. Numerical analysis involves the use of commercial CFD code. Experiments include lab test and field test. A flowchart is shown below to provide the general ideas of current methodology and relations between each objective. In the following sub-sections, each section explains the methodologies used to achieve each objective respectively.
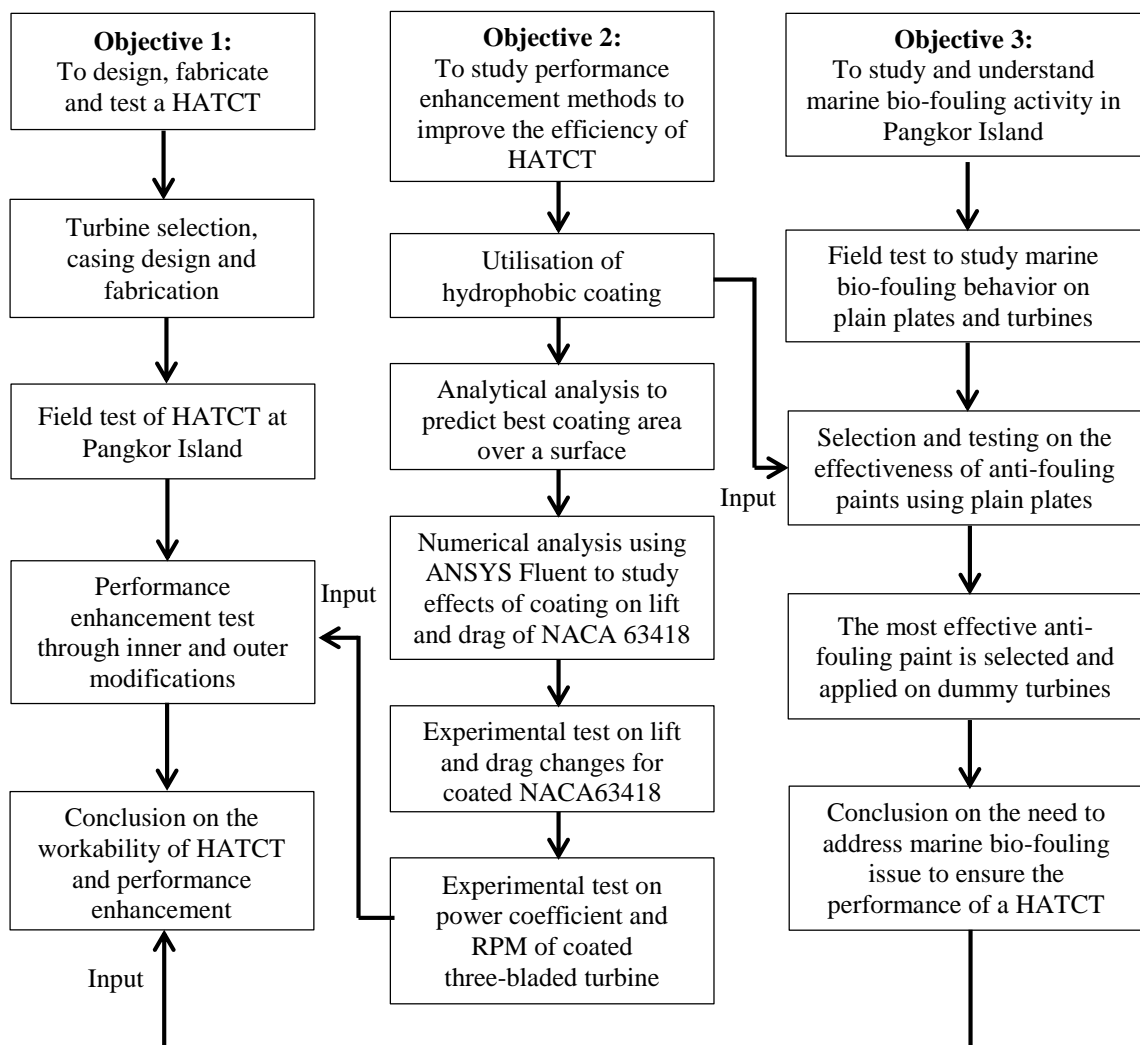
Figure 3.1: Flowchart of methodologies.

3.2 Field Test of Small Scale HATCT

This sub-section discusses the fabrication of a small scale HATCT. As indicated in Chapter 1, one of the aims of the current work is to fabricate a HATCT that can operate in the sea of Malaysia. It is essential to design and fabricate this HATCT locally so that more insights on HATCT fabrication can be gained from the process and form the basis for future works. But for the current study a small scale HATCT provided by a local engineering company – Laison Engineering Sdn. Bhd (hereinafter known as Laison) was utilised for field test.

3.2.1 Turbine Blades

It is widely accepted that a three-bladed turbine blade are most suitable for large scale wind turbines, especially for wind turbine farm. The main reason behind this is because three-bladed turbines offer good stability during operation, especially when it involves yawing control (Manwell et al., 2009). Such setting also allows a wind turbine to extract just enough energy form a flow and allows the flow to regain energy before reaching the subsequent wind turbine. If most energy from a flow has been extracted, it would require longer distance for wake recovery and affect the total output of a wind turbine farm.

In small-scale wind turbines, the numbers of blades are relatively flexible. For a small-scale wind turbine that operates alone, more numbers of blade are preferable as it allows the turbine to extract more energy from wind. Higher numbers of blade also provide more energy for a turbine to start its rotation. This is particularly helpful for turbine that needs to operate at low wind speed. This is also applicable for small-scale HATCTs. The selection of blade number depends on the desired output and purpose of a small-scale HATCT.

Since the ultimate goal of the current study is to test an operational small-scale HATCT on field, it is believed that use of a turbine with more than three blades will be comparatively safer. In addition, a larger chord length from blade's root to tip is preferable. This helps ensure its start-up at low tidal current speed and provides sufficient robustness to prevent undesired breakdown during field test. After considering the allowable timeframe, cost constraint and technology barriers, Laison suggested to use a modified five-bladed axial propeller as the turbine for the small-scale HATCT.

Figure 3.2 shows the five-bladed turbine (hereinafter known as FBT). This turbine is originally an industrial axial ventilation fan with a diameter of 800mm and a hub diameter of 150mm. Its chord length varies from 80mm at tip to 100mm at root. Its pitch angle is adjustable but must be fixed during operation. Under normal configuration, it works as an axial ventilation fan when power is supplied to it. When all the blades are turned to opposite direction, it effectively works as a lift turbine that rotates when sufficient fluids flow cross it. The characterisation test conducted by Laison found that a pitch angle of 8° allows the FBT to achieve the highest RPM when subjected to a wind speed of 2m/s. Hence, 8° pitch angle was used throughout the field test.

Figure 3.2: Five-bladed turbine used for the field test.

3.2.2 Drive System and Generator

A direct drive system with the shaft of a HATCTs directly connected to generator is most effective as it avoids unwanted mechanical loses from gearbox. In the current study, there are two major considerations on using direct drive system. First consideration is sealing. A small clearance is needed between the shaft and the casing to allow shaft's rotation. A mechanical seal plays an important role in providing this clearance while preventing leakage of water from outside to inside the casing. Second consideration is the relatively slow tidal current flow at the selected site in Pangkor Island. A direct drive system may not be able to provide sufficient rotational speed to run a generator.

For the first consideration, it is unsure that how effective a mechanical seal would be in preventing water leakage for a HATCT casing that needs to be submerged at least 1.0m from sea surface. For safety consideration, installing generator on a platform above sea water level is preferable. For the second consideration, a scaling up of rotational speed is necessary to ensure sufficient torque is provided to the generator.

Hence, a direct drive system was deemed unsuitable for the current study and a gear system was used.

The initial design aims to scale up twice the rotational speed from the FBT. A large pulley with 160mm diameter and a small pulley with 80mm were used. The reason for using a 160mm was to provide allowance for further scale up when needed. For example, if a two-times scale up is still insufficient, the smaller pulley can be replaced by pulley with even smaller diameter such as 20mm or 10mm. This allows a wide range of scaling from 2 ~16 times. After obtained the basic dimension for main components, the dimension of casing can be determined.

As the generator must be above water level, the small scale HATCT was designed to be a hanging type where it can be directly fixed on a bracket on a floating platform. This has an additional advantage of easy recovery. If the small scale HATCT was to be designed to be fixed at the seabed, it would be extremely difficult to observe its operation, access to it for necessary modification and to recover it in case of any emergency. Based on this idea, the shaft would be located at the bottom of the casing, with one end connected to the FBT and a pulley attached to its body. A timing belt will connect the shaft's pulley to the smaller shaft attached to the generator located at the top of the casing.

The diameter of the FBT is 800mm and a clearance of 800mm from water surface to the tip of the FBT is required to minimise effects from wave on the turbine itself. However, due to the concern on mechanical seal, it was decided to set the distance between shaft and the sea surface to be within 1.0m. In this case, the clearance between the tip of the FBT and the sea surface reduces to about 600mm. A set of

hangers will be welded to the casing about 1.0m from the centre of the shaft. Therefore, the height of the casing should be at least higher than 1.0m.

Figure 3.3 shows the side view of the casing along with the main components, except the FBT and pulley. Green colour denotes the casing, red colour denotes the shaft, blue colour denotes the stuffing box that house the mechanical seal, pink colour denotes the bearing and the purple colour denotes the portable support flange for generator. All these components were designed specifically for the current study and fabricated by Laison, except for the bearing. Readers are referred to APPENDIX A for the engineering drawings with dimensions for all relevant components. As can be seen, the casing is divided into two parts. This is done for the ease of transportation and the ease of modification of inner components when needed.

Figure 3.4 shows the outer look of the bottom casing and top casing. They are made of 6mm width stainless steel. Figure 3.5 shows the bottom casing with shaft, pulley and bearings installed inside. Figure 3.6 shows its front view. The stuffing box is next to the bottom casing. Stuffing box is also made of stainless steel. Both the design of the shaft and stuffing box was based on the mechanical seal selected. Figure 3.7 shows the mechanical seal which is commonly known as O ring. It comprises of a spring, a middle ring that holds on to shaft and an outer ring that fixes to the inner wall of stuffing box. The inner diameter of the middle ring is 25mm and the outer diameter of the outer ring is 41mm. This makes the diameter of the shaft to be 25mm and the inner diameter of the stuffing box to be 41mm (refer APPENDIX A).
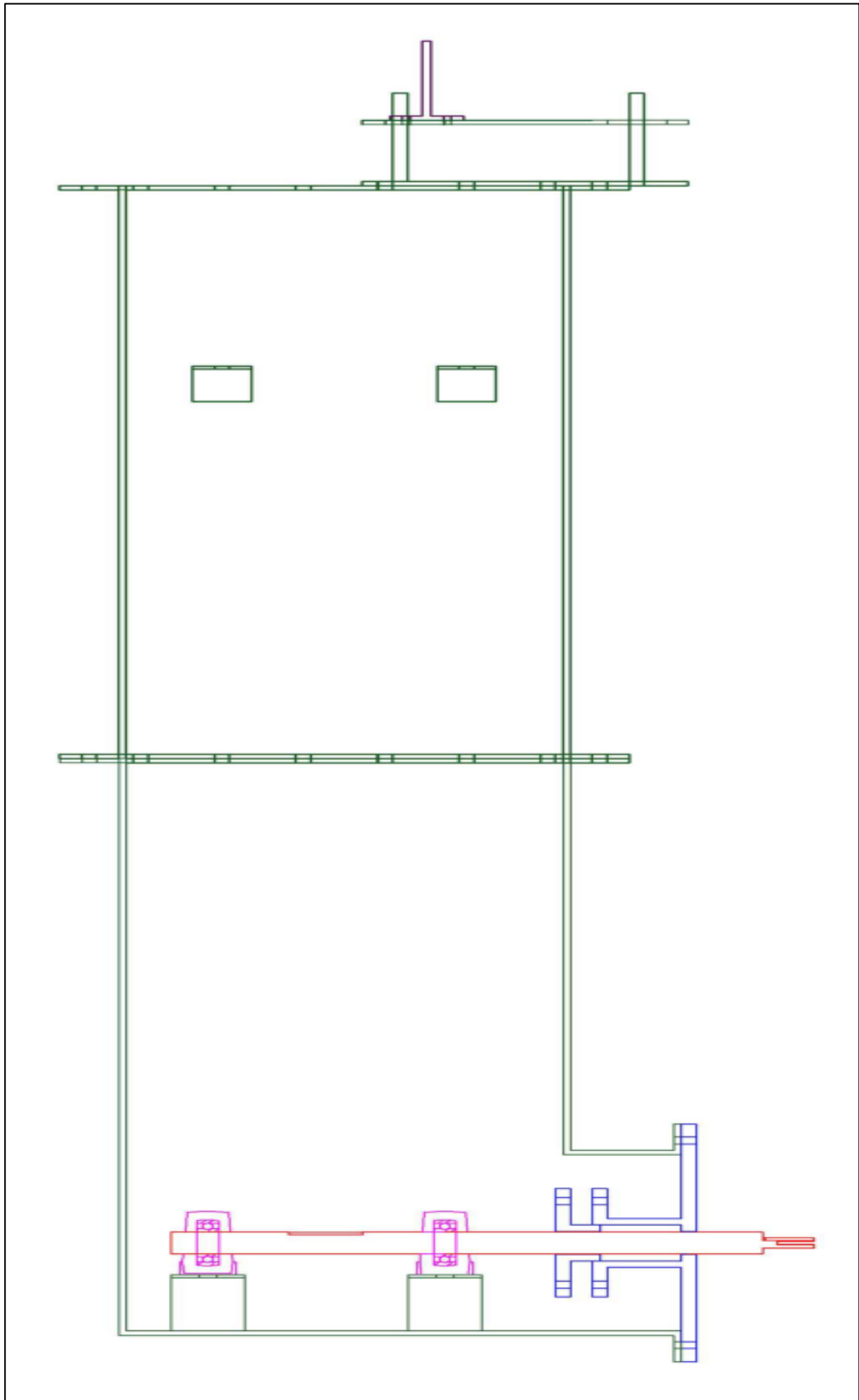
Figure 3.3: Side view of complete assemble of the small scale turbine's components

Figure 3.4: Bottom casing (right) and top casing (left) of the small scale HATCT.

Figure 3.5: Plan view of bottom casing of the small scale HATCT
with shaft, pulley and bearings.
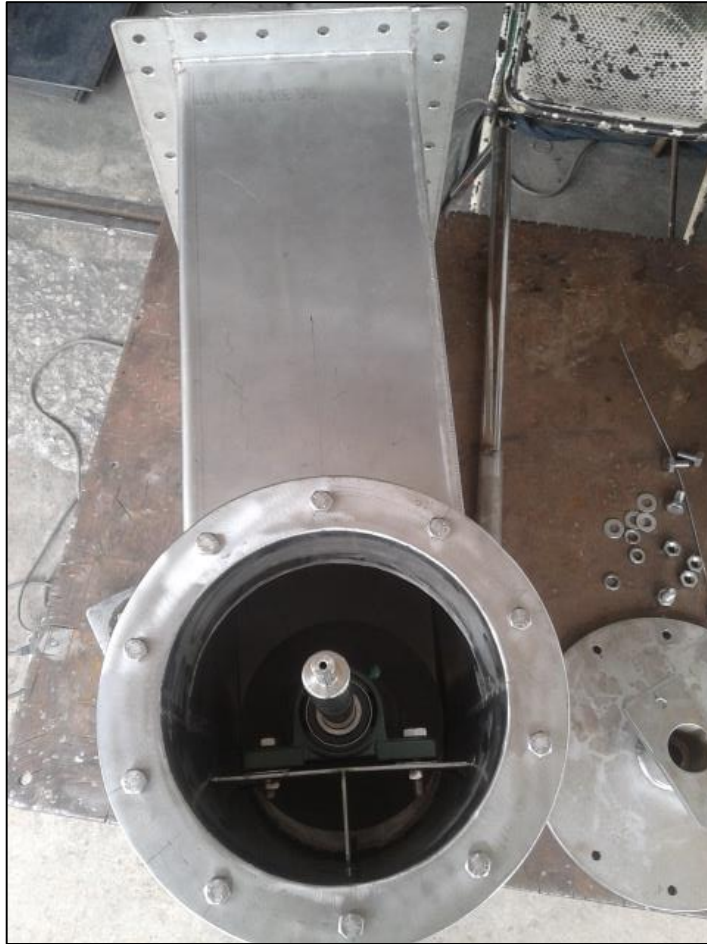
Figure 3.6: Front view of bottom casing of the small scale HATCT
with shaft, pulley and bearings.

Figure 3.7: Mechanical seal used in the small scale HATCT.

The workability of the FBT was tested to ensure the shaft and bearing are functional without vibration. Figure 3.8 shows one of the photos taken during the rotational test. The mechanical seal was also tested prior to the actual field test to ensure its workability. Figure 3.9 and Figure 3.10 show the bottom casing with all relevant

components installed submerges inside a tank with water. As can be seen from Figure 3.10, there is no water leaking into the casing. Nonetheless, this test only shows the mechanical seal works find at a relatively shallow water depth. Its functionality for field test will be affected by the rotational of the shaft and a deeper water depth with higher static pressure.

Figure 3.8: Testing of the FBT.

As can be seen from Figure 3.3, there will be an adjustable platform for generator at the top of the casing. The area of the platform is 220mm x 290mm (refer APPENDIX A, Fig. A12). It can accommodate any generator within that size. However, for the current study, the rotational speed of the FBT in field is believed to be relatively slow. Therefore, the generator used in the study is a small generator with low output. The generator is a customised PMSG with a maximum output of 4W. The reason for using PMSG for the current study has been discussed in section 2.3.2.5. Figure 3.11 shows the generator and generator platform. The portable support flange fixed on the generator support was purposely designed to hold the small generator. The black pulley

in Figure 3.11 is the smaller pulley that will be connected to the larger pulley on shaft through a timing belt. Due to the nature of the pulleys, a standard V-belt was used.

Figure3.9: Bottom casing submerged in water
to test the suitability of mechanical seal-1.

Figure 3.10: Bottom casing submerged in water
to test the suitability of mechanical seal -2.
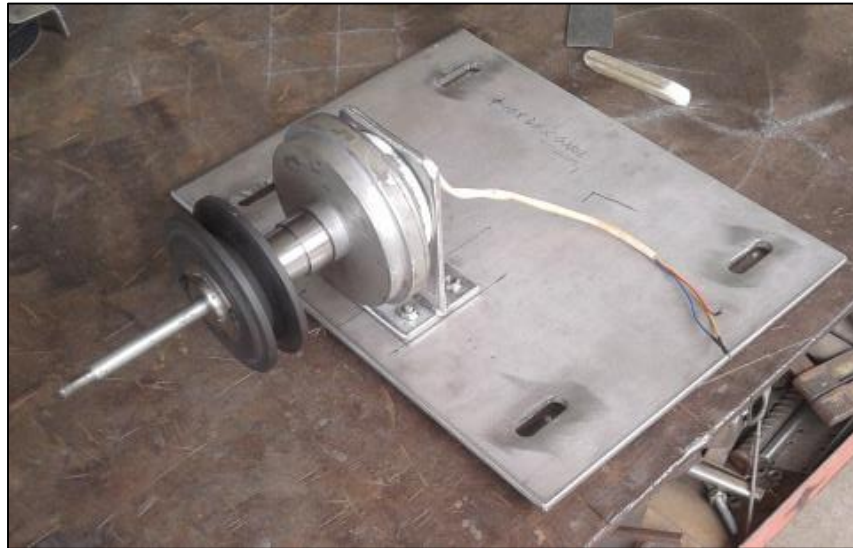
Figure 3.11: Generator with platform support for the small scale HATCT.

3.2.3 Field Test Platform

The field test was carried out at a floating fishing platform outside a guest house, called Pangkor Fish House, in Pangkor Island. Figure 3.12 shows the bridge connected to the platform and Figure 3.13 shows a closer look on the floating fishing platform. Tourists who stay in the guesthouse can walk to the platform freely for fish feeding or fishing. Figure 3.14 shows its location on Google Map. Generally, the tidal current flows from South to North for 12hours and North to South for the other 12 hours every day. If looking at Figure 3.12, the direction is from right to left and vice-versa.
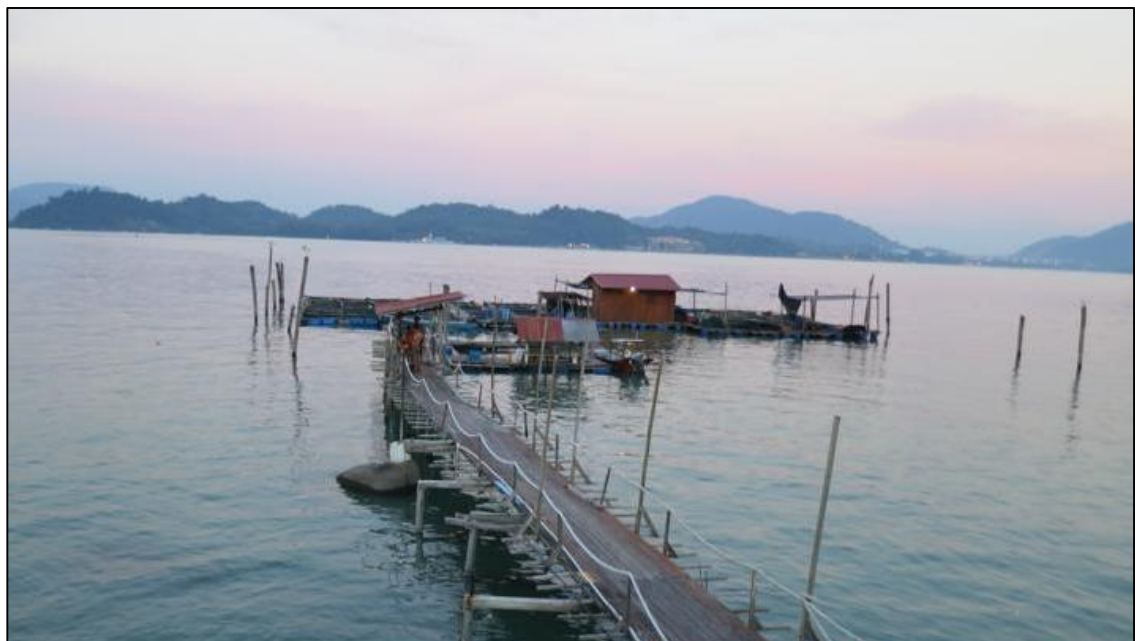
Figure 3.12: Bridge to the small fishing platform

Figure 3.13: Closer view of the fishing platform with people on it.
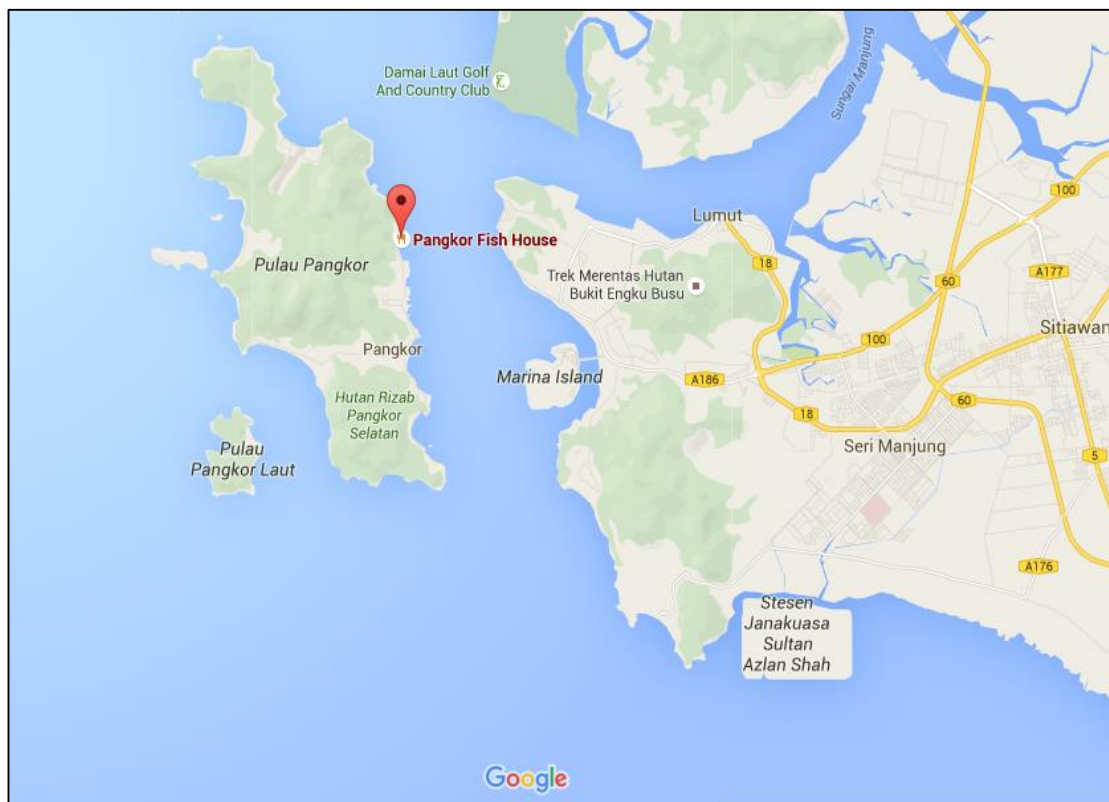
Figure 3.14: Location of Pangkor Fish House from Google Maps
(*Source: www.google.com/maps/*).

The relatively high tidal ranges around this region generally occurs about 14~16 days per month (*source: www.jupem.gov.my*). The tidal current flow in these days is relatively higher which generally ranges between 0.2m/s ~ 0.4m/s, with occasional high speed of up to 0.5m/s. The tidal current flow on the other days is much slower and

sometimes falls below 0.1m/s. Note that Pangkor Island located in the region 2 as discussed in section 1.3. The relatively fast flowing tidal current occurs during the change of tidal current's direction. This means, theoretically, it is possible to harness this relatively fast tidal current twice per day with unidirectional HATCTs and four times per day with bi-directional HATCTs. The small scale HATCTs designed in the current study is unidirectional, hence it can only harness twice per day.

Figure 3.15 illustrates the concept of the field test. The small scale HATCT was fixed on one of the fishing platform's edge. It was allowed to float together with the fishing platform. The depth from the sea surface to the centre point of small scale HATCT's shaft was approximately 900mm. The generator was connected to a digital multi-meter to record the output. The focus of current study was given to the workability of HATCT, hence the test only covers basic characterisation of the small scale HATCT's operation and its power output. The device was not tested for a complete lunar cycle.
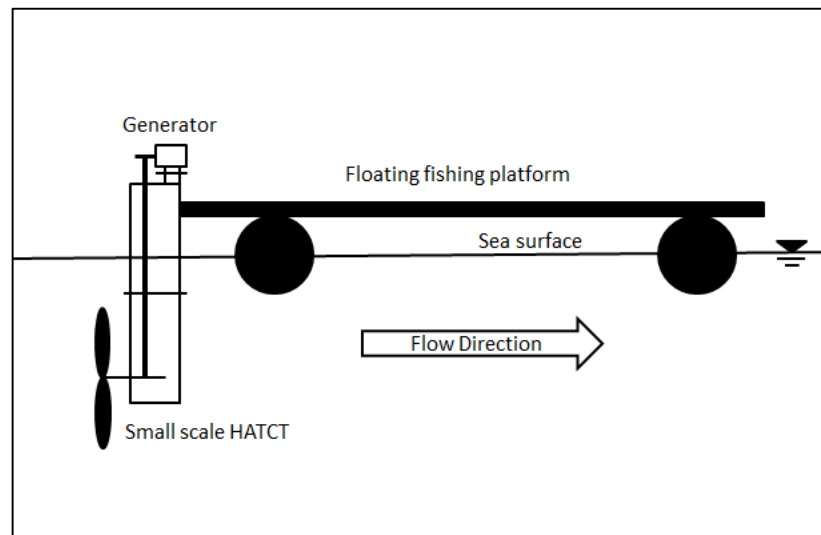
Figure 3.15: Illustration of field test platform.

3.3 Design Modifications for Performance Enhancement

Although the second objective of the current study focuses on the effects of hydrophobic coating towards performance enhancement, it is believed that a simple design modification to enhance a turbine's performance is necessary to ensure the HATCT's operation under slow tidal current flow. The novel approach of hydrophobic coating can be considered as outer modifications as it alters turbine blades' surface. To date, no study on the use of hydrophobic coating in HATCTs has been done. The other simple modification is by modifying the gearing system, which is a typical mechanical modification that can be considered as inner modifications. In the following sub-sections, the modifications will be discussed in details.

3.3.1 Inner Modifications

Inner modification is simple and straightforward. The smaller pulley attached on the generator was replaced by other pulleys with smaller size to scale up the rotational speed. The original diameter of large pulley is 160mm and diameter of small pulley is 80mm. During the field test, small pulley with a diameter of 40mm and 20mm were also used to improve the total power output of the generator.

3.3.2 Outer Modifications

There are various methods to modify a HATCT's performance from outside, such as those discussed in section 2.3.2.6. Provision of an augmented diffuser to accelerate incoming flow is one of the methods. Applying blade pitch control is also one of the methods to obtain better efficiency. However, there are some downsides for these modifications. For diffuser, it requires more space to accommodate the auxiliary parts and there is likelihood to trap ocean trash. Once it is blocked, it will lose its purpose. Certainly, every method has its pros and cons. These methods are still favourable

depends on the need. This is the reason that many researchers still study on diffuser (Shives & Crawford, 2010; Cresswell et al., 2015)

Apart from the common methods, it is possible to improve the performance of a HATCT through modification of turbine blade. There is study that tries to improve the hydrodynamic performance of a turbine blade via mimicking whale's tubercles. It is said that the features of whale's tubercles can improve the L/D ratio (Gruber et al., 2011). Such modification effectively alters the friction behaviour over the surface of turbine blade and leads to enhanced L/D ratio. Despite its good effect, understanding the correct design and fabricating the complex structure can be difficult. Hence, it is the aim of current study to explore other similar methods that can improve L/D ratio of a turbine blade through surface modification. The proposed method is the use of hydrophobic coating.

3.3.2.1 Hydrophobic Coating

Hydrophobic coating is a coating with surface that can repel water. It will form a contact angle of larger than 90° with water. When contact angle goes above 150°, the surface is said to be super-hydrophobic. The surface energy of hydrophobic surface is lower than water such that the surface is 'unwilling' to do more works to attract water on it. Under such condition, the cohesion forces of the water molecules cause the water to form sphere to lower its own energy. This is why the water is repelled by a hydrophobic surface and makes the wetting process an ineffective one. This type of hydrophobic coating can be said as chemically hydrophobic coating. With proper measures, it is possible to achieve adhesion of water or liquid on a surface with low surface energy.

Another type of hydrophobic coating is the physical type. This type of hydrophobic coating has a surface consists of micro-scale hierarchical structure that contains protrusion and trough which provides micro-voids for air. This decreases the effective contact area of the surface with water. Many plants that repel water possess such surface (Ensikat et al. 2011). One of the well-known plants is lotus leaves (see Figure 3.16 for the mirco-structure on lotus leaves). Recent advance in nanotechnology has made the production of such surface possible via surface engineering. Once the air voids between the micro-structure are filled, physical hydrophobic coating will lose its hydrophobicity.
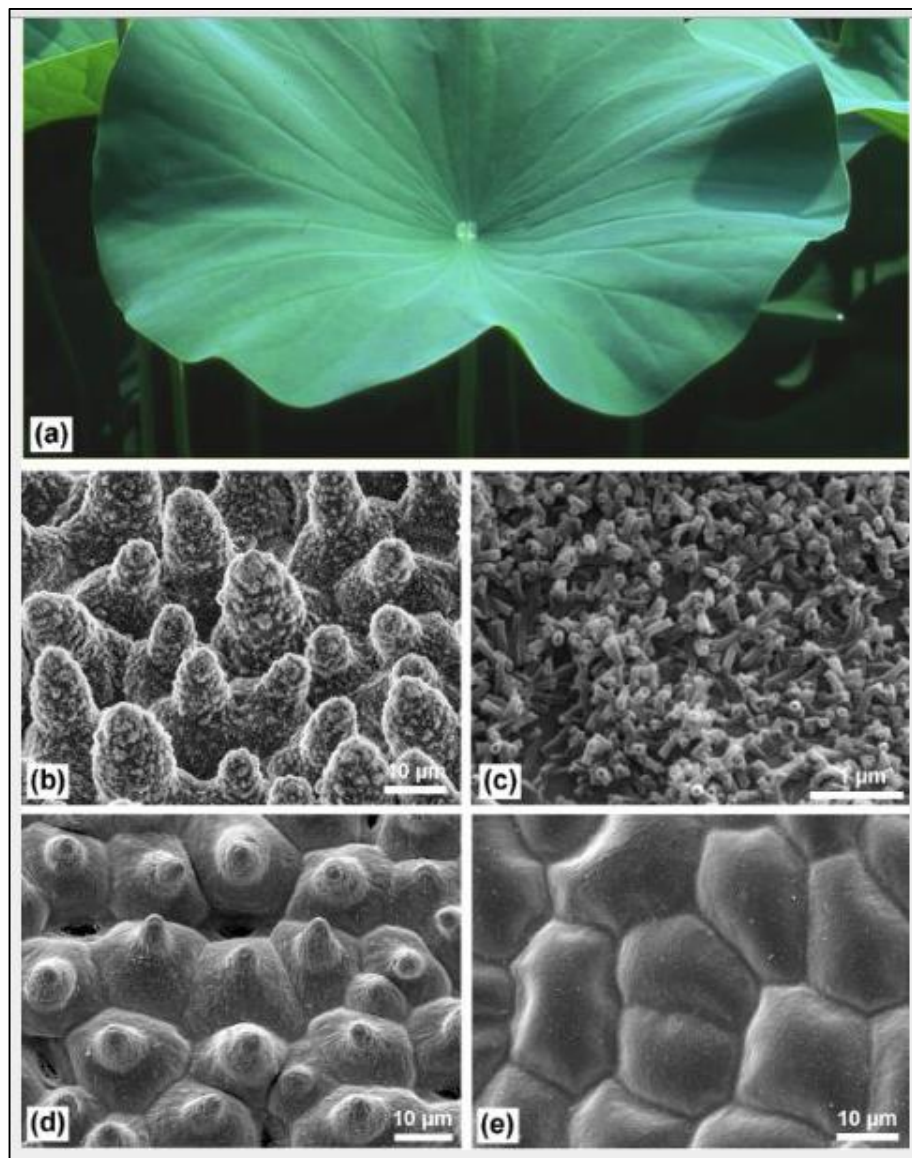
Figure 3.16: Micro-structure of lotus leaf at different scale (Ensikat et al. 2011).

Physically, as the contact area between a liquid and a solid is reduced, the friction between the two substances can be reduced. Hence, the discovery of physical hydrophobic surface is of great interest to researchers and engineers working in tribology. Hydrophobic coating could potentially provide many added values to a system that needs to operate or move under water. One of them is the friction drag reduction for ship hull to save petrol consumption. For HATCT, friction reduction on turbine blade suggests two possibilities. Firstly, a direct reduction in friction drag is positive for L/D ratio. Secondly, low friction drag could possibly lead to faster flow over a surface and result in improved lift forces.

The effects of hydrophobic coating in reducing friction drag reduction have been confirmed by many researchers (Rothstein, 2010; Jiang et al., 2011; Aljallis et al., 2013; Daniello, 2013). Generally, it was found that with higher contact angle, a higher friction drag reduction can be achieved. In fact, most of them used super-hydrophobic surfaces with contact angle more than 150° to achieve high friction drag reduction. But, super-hydrophobic surfaces have a downside. The air-voids in super-hydrophobic surfaces are increased to achieve high contact angle. This allows the surface to entrap thicker air-layers between the liquid/surface interfaces. Unfortunately, the sustainability of these thick air-layers is poor, especially when subjected to high speed flow. Once these air-layers are flushed out by incoming flow, the micro-structures on the surface can no longer provide lubricating effects for friction drag reduction. Contrarily, it will increase surface roughness and exert higher friction drag between the liquid/solid interfaces.

As a result, it seems to be that there is a trade-off between maximum achievable friction drag reduction and sustainability of the air-layers for the application of hydrophobic coating on HATCT turbine blades has Therefore, a hydrophobic coating

with mild contact angle between $90^{\circ} \sim 110^{\circ}$ would be ideal for the current study. Surprisingly, there is anti-fouling coating currently available in the market come with these properties. Since HATCT itself already required anti-fouling coating for protection, utilising hydrophobic anti-fouling coating is highly preferable as it does not only provide protection, but might also help in enhancing performance of a HATCT.

In the current study, no synthesis of hydrophobic coating was involved. Two hydrophobic coatings available in the market have been purchased and directly used. The first hydrophobic coating is the Biocyl, a product produced by a Belgium company called Nanocyl (www.nanocyl.com). It is a hydrophobic anti-fouling coating designed for ship-hulls. Details on this product can be found in their official website. Figure 3.17 shows the contact angles of Biocyl when in contact with water. The measured contact angles were slightly higher than 90°. The second hydrophobic coating is the Always Dry, a product which is also produced by a Belgium company called Nanex (nanexcompany.eu). It is a hydrophobic spray that can be applied on wood, fabric, leather and others. Figure 3.18 shows the contact angles of Always Dry when in contact with water. Overall, water form a higher contact angle with Always Dry, compared with Biocyl. Details on this product can be found in their official website. Both the measurement of contact angles for Biocyl and Always Dry was made by using Techgear Eaglescope TG220.
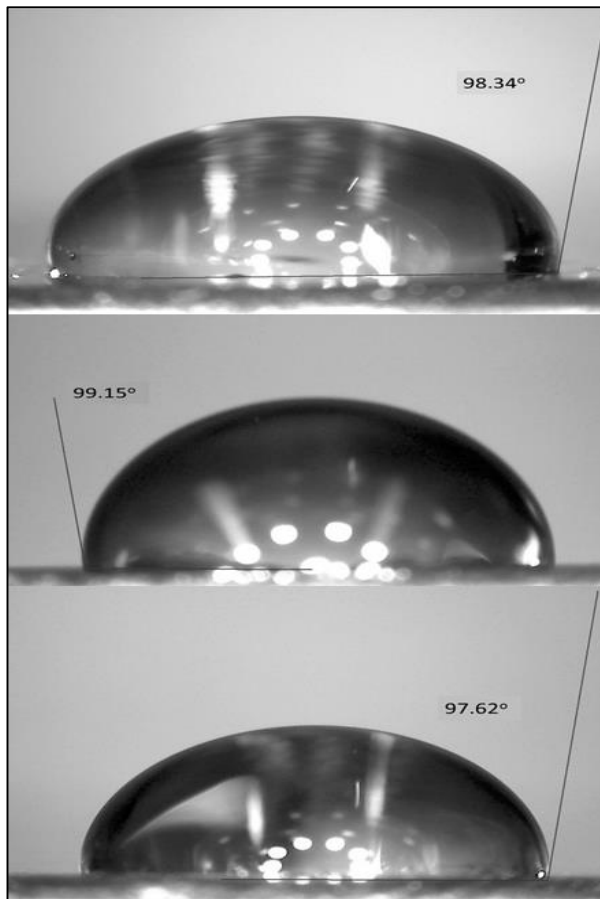
Figure 3.17: Contact angles for Biocyl.
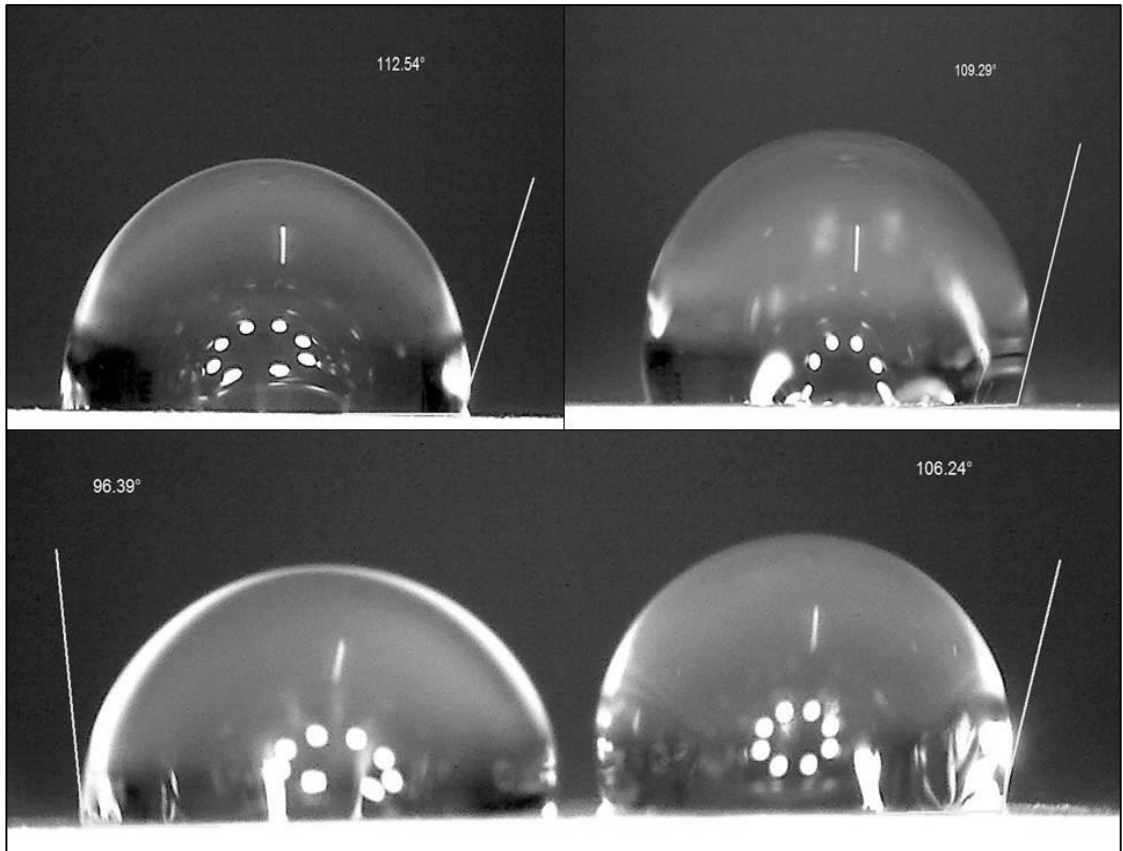
Figure 3.18: Contact angles for Always Dry.

3.3.2.1.1 Analytical Analysis

Before applying the coating, it is important to understand the behaviour of friction drag reduction over a hydrophobic coating. Identifying the points where significant friction drag reduction occurs has advantage in coating method. For instance, coating can be concentrated on points where higher drag reduction occurs to minimise the cost of coating. A two-dimensional model was used to derive a formula to predict the trend of friction drag reduction over a flat plate. The formula will be derived based on the classic Navier's slip model and local wall shear stress formula. The full derivation and validation are discussed in results and discussion sections.

3.3.2.1.2 Numerical Analysis

Numerical analysis on application of hydrophobic coating for performance enhancement was conducted for two parts. First is the effect on hydrofoils' lift and drag forces, and second is the effect on the performance of a lab-scale three-bladed turbine. Pinon et al. (2012) conducted a test on a three-bladed turbine made from NACA 63418. They have provided detailed on blade section configuration and is suitable to be adopted for comparison. Hence, the hydrofoil sections and the lab-scale three-bladed turbine used for both the numerical analysis and lab-scale experiment will be similar to Pinon et al. (2012).

3.3.2.1.2.1 Hydrofoils

The analysis for hydrofoil was done by using the commercial code ANSYS Fluent. ANSYS Fluent is a widely used software in CFD field. It is also commonly used for wind turbines and HATCTs performance analysis. Readers, who are new to ANSYS Fluent, are referred to Fluent User's Guide for details (*Fluent User's Guide*). The reason for using ANSYS Fluent is as mentioned in section 2.3.2.4. Based on the accessible

literature, ANSYS Fluent has never been used in modelling hydrophobic hydrofoils too. Here, the capability of ANSYS Fluent to model the changes of C_L and C_D for hydrophobic hydrofoil was also examined.

The one-equation Spalart Allmaras turbulent model was used. This model is designed for wall-bounded flows and has been proven to model boundary layers, subjected to adverse pressure gradients, considerably well. This model only requires low computational time to provide good prediction. Nonetheless, Spalart Allmaras tends to over predict C_D for 2D airfoils (Basha & Ghaly, 2007; Eleni et al., 2012). This is due to the fact that boundary layers attach to hydrofoils only changes from laminar to turbulent after a certain distance away from leading edge. This limitation can be overcome by introducing user-defined function that covers transition regime (Basha & Ghaly, 2007) or separate domains to model mixed laminar and turbulent flow (Eleni et al., 2012). However, such modifications were not implemented for the current study.

The profile of a 2D NACA 63418 was created using JavaFoil (Martin, 2014). Coordinates generated from JavaFoil was imported to Gambit for meshing. The generated mesh was put into ANSYS Fluent for modelling. Mesh independence test was done, prior to the actual modelling (see Appendix C). It was found that 40,000 mesh cells and above is sufficient for the purpose of current study. All modelling was done under steady state flow and the default settings of Spalart Allmaras Strain/Vorticity-based production were used. Value of 1 x 10^{-6} was set for all residuals to ensure good convergence.

Figure 3.19 illustrates the domain and generated mesh. The boundary conditions for the domain are as follows. AD, AB and CD were set as velocity inlets. BC was set as pressure outlet. The distance of far field AD was set to be 10 chord length from hydrofoil, and far field BC was set at 20 chord length The hydrofoil was divided into upper face and lower face. When modelling uncoated hydrofoil, both faces were set to be no-slip wall. When modelling hydrophobic hydrofoil, both faces were set to be slip wall by changing the specified shear in the boundary conditions. The input for specified shear will be based on the friction drag reduction measured from lab-scale experiment. The C_L and C_D for a range of AoA, based on the lab-scale experiment, were simulated.
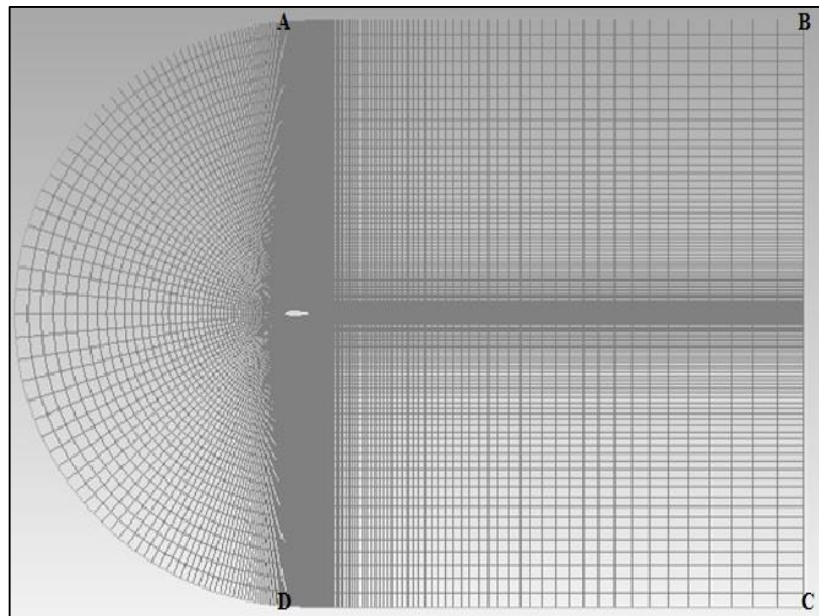
Figure 3.19: Domain for NACA 63418 (shown in ANSYS Fluent).

3.3.2.1.2.2 Three-bladed Turbine

The analysis on performance of lab-scale three-bladed turbine (hereinafter known as TBT) with and without hydrophobic coating was done by using WT_Perf. The developer of WT_Perf is the National Renewable Energy Laboratory (NREL) in U.S.A. This numerical software is freely available at the NREL's website. It uses BEM theory to do analysis and prediction on the performance of wind turbines. The original version of WT_Perf is known as PROP. PROP code has been developed by Oregon State University more than 20 years ago (National Wind Technology Center). The code gets

constant upgrade from National Wind Technology Center, each time comes with new algorithms and functionality. Correction factors like hub losses, swirl effects, tip losses and even skewed wake are included in its algorithm. Therefore, WT_Perf is capable of giving good prediction on a turbine's performance.

WT_Perf is user-friendly. It will compute the relevant outputs based on the input data. The required inputs include the following,

i. The value of C_L and C_D of hydrofoil for AoA -180°~180°;

ii. The total number of hydrofoil elements along a blade section;

iii. The pitch angle of each hydrofoil element;

iv. Numbers of blade;

v. Hub diameter and turbine diameter; and

vi. Distance of hub centreline to seabed.

The outputs include the rotor power in kW, power coefficient in C_p, shaft torque in kN-m, flap bending moment in kN-m, and rotor thrust in kN. These outputs for a series of pre-set TSR will be calculated by WT_Perf. For the current analysis, the desired output is the value of C_P for the TBT with and without hydrophobic coating.

For turbine without coating, the value of C_L and C_D of NACA 63418 for AoA -180°~180° was directly used. For turbine with hydrophobic coating, the value of C_L and C_D of NACA 63418 for AoA -180°~180° were adjusted based on the C_L and C_D obtained from lab-scale experiment on hydrophobic hydrofoil. Table 3.1 tabulates the configuration of the TBT. r/R is the ratio between perpendicular radius of the hydrofoil section from hub centreline and turbine diameter. c/R is the ratio between chord length of the hydrofoil section and turbine diameter. t/c is the thickness ratio for each hydrofoil section. The turbine blade is divided into a total of 23 hydrofoil sections.

3.3.2.1.2.3 Lab-scale Experiment

Lab-scale experiment includes measurement of C_L and C_D for NACA 63418 and measurement of C_P for the TBT. Five identical 3D-printed NACA 63418 with chord length of 135mm, span of 30mm and maximum thickness of 7mm were prepared. The coordinate of hydrofoil follows those generated by JavaFoil. Similarly, three identical 350mm 3D-printed TBT based on the configuration in Table 3.1 were prepared. The drawing of coordinate for the TBT was done by using Salomé. Salomé platform is open-source software for pre and post-processing of numerical simulation.

Table 3.1: Configuration of TBT turbine by Pinon et al. (2012).

r/R	c/R	Pitch (deg)	t/c (%)
0.13	0.06	29.57	80
0.15	0.06	29.57	100
0.16	0.06	29.57	100
0.20	0.15	25.63	36
0.24	0.25	22.15	21
0.29	0.24	19.3	21
0.33	0.23	16.97	22
0/37	0.21	15.05	22
0.42	0.2	13.46	22
0.46	0.19	12.12	22
0.50	0.18	10.98	23
0.55	0.17	10.01	23
0.59	0.17	9.18	22
0.63	0.16	8.45	22
0.68	0.15	7.82	22
0.72	0.15	7.26	21
0.76	0.14	6.77	21
0.81	0.14	6.34	20
0.85	0.13	5.95	19
0.89	0.13	5.61	19
0.94	0.12	5.29	18
0.98	0.12	5.01	18
1.00	0.07	4.87	25

The hydrofoil experiment was carried out at the Center for Advanced Materials and Green Technology in Multimedia University. A circulating water channel with an area of 300mm x 400mm and a length of 3.5m was used. The water flow speed of the channel can vary from 0.2m/s to 0.8m/s. For the hydrofoil experiment, a flow speed of

0.6m/s was used. To minimize 3D effects from trailing edge, the hydrofoil (NACA 63418) was placed vertically in the channel with one end connected to the bottom of the channel and the other end connected to a load cell. The blockage ratio of the NACA 63418 inside the circulating water channel is about 1.8% and hence no blockage correction is required.

The water flow was allowed to flow until it reaches steady state before the measurement starts. Then, the uncoated NACA 63418 was adjusted accordingly to obtain the AoA with zero lift. Once the zero lift AoA was confirmed, it was marked as the 0° AoA. Next, the AoA was increased by 1° and the corresponding C_L and C_D for that AoA were measured and recorded. The measurement was made by reading the digital display connected to the load cell. For each measurement, 10 readings were recorded for both the C_L and C_D. After readings were taken, the AoA was increased to 2° and measurement on C_L and C_D were taken. These steps were repeated until AoA reach 11°. This procedure was repeated for fully coated NACA 63418 and NACA 63418 with hydrophobic coating on its upper surface, with no coating on its lower surface.

The experiment on TBT was carried out at the Hydraulic Lab in University of Malaya. A circulating water channel with an area of 1000mm x 1000mm and a length of 20m was used. There is a limit on water level for this channel. It is not allowed to exceed 600mm. Once this water level is breached, the water pump will shut down automatically. After water level retrace to a lower level, the water pump will start functioning again. The water flow speed can be adjusted by controlling the pump's frequency and the discharge sluice gate. Throughout the experiment the water level was

maintained at a level of approximately 550mm. This provided a 100mm allowance for the TBT's tip from water surface and from channel bottom.

The 350mm TBT was connected to a shaft fixed on a support. A timing belt made of 5mm diameter rope was used to connect the shaft to the generator. A PMSG generator, similar to the one used for the FBT in the field test, was used for this lab-scale experiment. A digital multi-meter was connected to the generator to read voltage output. Rheostat was also connected to the generator to adjust the resistance and control the RPM of TBT. The whole system was supported by a frame that was fixed on the water channel. Water flow was allowed to reach steady state before taking the measurement. Figure 3.20 shows the schematic diagram for the set up.
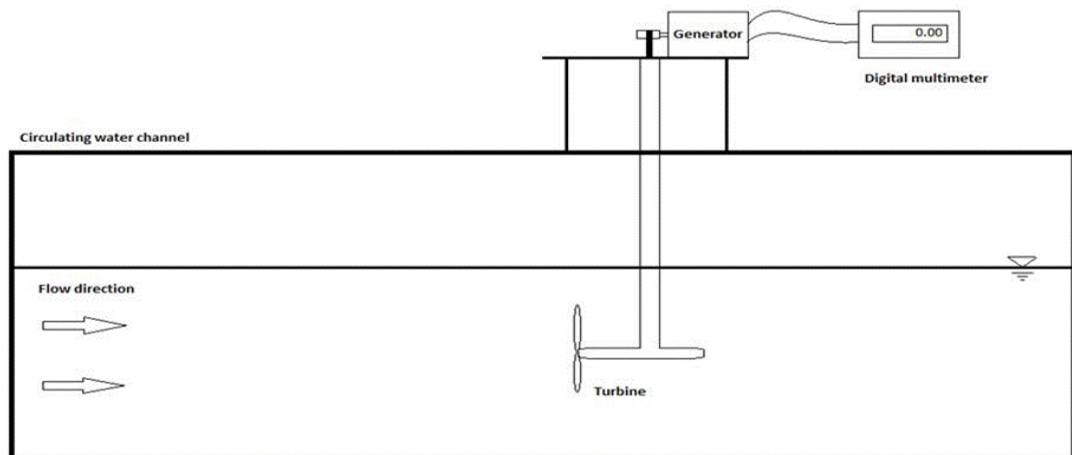
Figure 3.20: Schematic diagram for the TBT test.

Two tests were conducted under this set up. For the first test, performance of TBT with coating and without coating was measured. The targeted output was C_P. The water flow was maintained at 0.35m/s and the voltage outputs of the TBT at different TSR were measured. The control of TSR was done by adjusting the resistance of rheostat. Similar to the hydrofoil test, this test was conducted for TBT without coating, TBT with full coating and TBT with coating on suction side. For the second test, RPM of TBT with coating and without coating, subjected to different water flow, was

measured. Measurement was done by using Tachometer. For the measurement of RPM, the TBT was allowed to rotate without the need to run the generator. Similarly, TBT without coating, TBT with full coating and TBT with coating on suction side were tested.

3.4 Marine Bio-fouling

As discussed in section 2.3.3, marine bio-fouling on HATCT blades can be deteriorating. Malaysia located near the Equator and the temperature of sea water is suitable for marine bio-fouling activities. It is certain that any deployment of HATCT in Malaysia will face this problem. Therefore, it is an issue that needs to be addressed. The focus of the current study put more weightage on the performance and workability of the designed FBT. This aim warrants a study to test the effectiveness of anti-fouling paint in protecting the FBT. It is not the aim of the current study to identify the stressor level, in other words, the fouling species and fouling rate throughout a whole year. Instead, the current study aims to investigate proper measures that could help ensuring the performance of the FBT by protecting it from undesired marine bio-fouling.

3.4.1 Anti-fouling Paints

Two paints with anti-fouling properties were used in the current study. One is the Biocyl mentioned in section 3.3.2.1, and another one is called Palccoat. Biocyl is a hydrophobic coating, but Palccoat is a hydrophilic coating. Palccoat is a product produced by a Japan-based Company called SOUMA. Palccoat consists of Titanium Oxide (TiO_2), which is a photo-catalyst that possesses outstanding self-cleaning effects. Its self-cleaning ability is related to its hydrophilicity that makes water easily attached to it. The effectiveness of self-cleaning can be further enhanced with sufficient presence of visible light.

3.4.2 Field Test Platform

The marine bio-fouling test was divided into two parts. In the first part, the effectiveness of the selected anti-fouling paint was first examined. Three stainless steel plates were prepared. One without coating, one coated with Biocyl and one coated with Palccoat. The field test platform the same at the fishing platform at Pangkor Island. Each plate was fixed to a rope and was allowed to hang freely under the sea water. The distance from sea surface was maintained at about 500mm.

Before putting these plates into the sea water, their initial weight was measured. For the first seven days, these plates were recovered every day and their respective weight was measured. Then, these plates were left in the sea for 3 months (24th April 2015 – 17th July 2015). After three months, these plates were recovered and their respective weights were taken. Next, all the bio-fouling attached on the plates were cleaned to find out the effectiveness of the anti-fouling paint.

In the second part, the anti-fouling paint with better effects from the first part was selected to be coated on the FBT. Similarly, the FBT was submerged under the sea water for 3months (18th Aug 2015 – 18th Nov 2015). In addition, two more dummy FBT, one with coating and one without coating, with a diameter of 500mm were also hung on the field test platform for comparison purpose. The position of dummy turbines is set to be 300mm away from the 800mm FBT. After three months, the three turbines were recovered and bio-fouling condition on turbine blades was observed and recorded. As a gentle reminder, all the coating applied for the lab-scale experiment and field test were done by using sprayer. All coatings were directly sprayed on the stainless-steel plates, the TBT and the FBT without involving any special technique.

CHAPTER 4: RESULTS AND DICUSSION

4.1 Overview

This chapter presents and discusses the results obtained for the tests and experiments discussed in Chapter III. In order to present the results in a smoother sequence, firstly, the test on hydrophobic coating on the TBT is discussed. Next, the FBT's field test is presented and finally, the marine bio-fouling test.

4.2 Hydrophobic Coating

4.2.1 Analytical Analysis

This section presents the derivation of the formula to predict the friction drag reduction pattern over a hydrophobic coating. From physics point of view, the lower friction drag reduction is a result of slip flow, as against the classic no-slip flow. Researchers using the term, slip length Based on the classic Navier's slip model (Figure 4.1) (Rothstein, 2010), the slip velocity (u_s) immediately next to the wall is proportional to the shear rate at the wall, $(\partial u / \partial y)_w$. The formula defined by Navier to relate the slip velocity and the shear rate is $u_s = b(\partial u / \partial y)_w$, where b is known as the slip length. This slip length is widely used by researchers to define the ability of a surface to induce slip flow. The value of slip length is said to be a constant for a given hydrophobic surface. A higher value of slip length will induce a higher slip flow, which means a larger friction drag reduction.

The presence of slip length for hydrophobic surfaces depends on a several factors. Considering a hydrophobic surface created using micro-grates aligned to the fluid flow direction, for laminar flows, it is likely that only stream-wise slip length will presence (Ou & Rothstein, 2005; Park et al., 2013). This is a result of separated

entrapped air-layers and the relatively steady nature of laminar flows. If turbulent flow is considered, span-wise slip length is also likely to presence. If a hydrophobic surface is created using micro-ridges or micro-posts, both stream-wise and span-wise slip length may presence even in laminar flows. This is because the entrapped air-layers are interconnected. Nevertheless, the effects from span-wise slip length might be negligible if the Reynolds number is not high. For a hydrophobic surface created using uneven or random micro-structure, both stream-wise and span-wise slip length should presence even in laminar flows, although the effects of stream-wise slip may easily outrun span-wise slip (Busse et al., 2013).
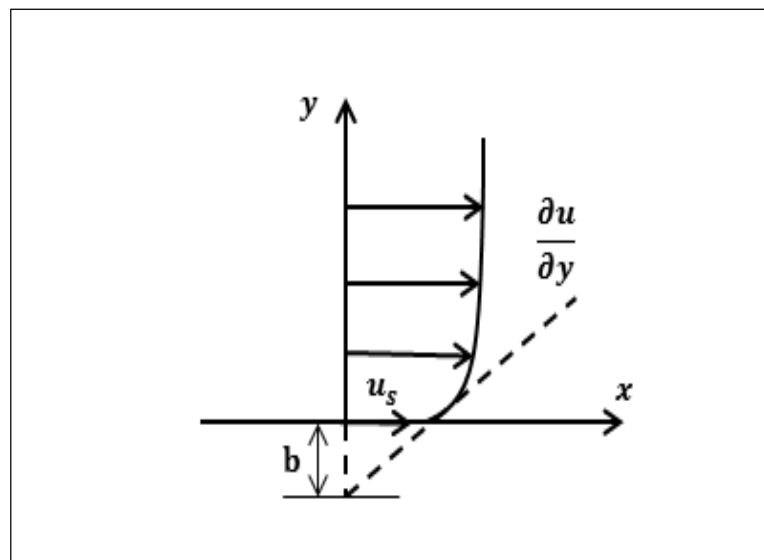
Figure 4.1: Navier's slip model.

For the current derivation of formula, a few assumptions are made to simplify the condition. The first assumption is that the hydrophobic surface is created using parallel micro-grates and is subjected to fluid flows in laminar regime. The second assumption is that there is no depletion of entrapped air-layers for the hydrophobic surface. As the following derivation uses shear stress formula based on boundary layer approximation, the slip length estimated by the formula refers to the effective slip length at a local point. Hence, the formula only needs to consider stream-wise slip

length and the slip length is assumed to be constant for any specific point on the hydrophobic surface.

Consider Figure 4.1, recall that the shear stress at the wall for no-slip flow is defined as $\tau_w = \mu(\partial u / \partial y)_w$, where τ_w is the shear stress for no-slip flow at the wall and μ is the viscosity of fluids. The shear stress for a slip flow in the laminar regime should follow the same pattern as no-slip flow. Theoretically, viscosity should remain the same as there will be no alteration towards fluid's properties. Substituting shear rate at the wall for slip flow, the shear stress equation becomes

$$\tau_{ws} = \mu \left. \frac{\partial u}{\partial y} \right|_w , \qquad (4.1)$$

where τ_{ws} is the shear stress at the wall for slip flow. Substituting $u_s = b(\partial u / \partial y)_w$ into equation (1) gives

$$\tau_{ws} = \mu \frac{u_s}{b} . \qquad (4.2)$$

The τ_{ws} can be related to τ_w and the friction drag reduction rate as $R_D = 1 - (\tau_{ws} / \tau_w)$ or $\tau_{ws} = \tau_w(1 - R_D)$. Substituting this into equation (4.2) gives

$$u_s = b \frac{\tau_w}{\mu}(1 - R_D) . \qquad (4.3)$$

According to the established knowledge in fluid mechanics, the local wall shear stress for laminar flow over a flat plate (Çengel & Cimbala, 2010) can be expressed as

$$\tau_w = 0.332 \frac{\rho U_\infty^2}{\sqrt{Re_x}} , \qquad (4.4)$$

where ρ is the density of fluids, U_∞ is the free stream velocity and Re_x is the local Reynolds number. Substituting equation (4.4) into equation (4.3) gives

$$u_s = 0.332 \frac{U_\infty^2}{v\sqrt{\mathrm{Re}_x}} b(1 - R_D),$$ (4.5)

where $v = (\mu / \rho)$ is the kinematic viscosity of fluids. Next, consider the shear stress in the no-slip condition and the slip condition with same incoming flow speed as illustrated in Figure 4.2.
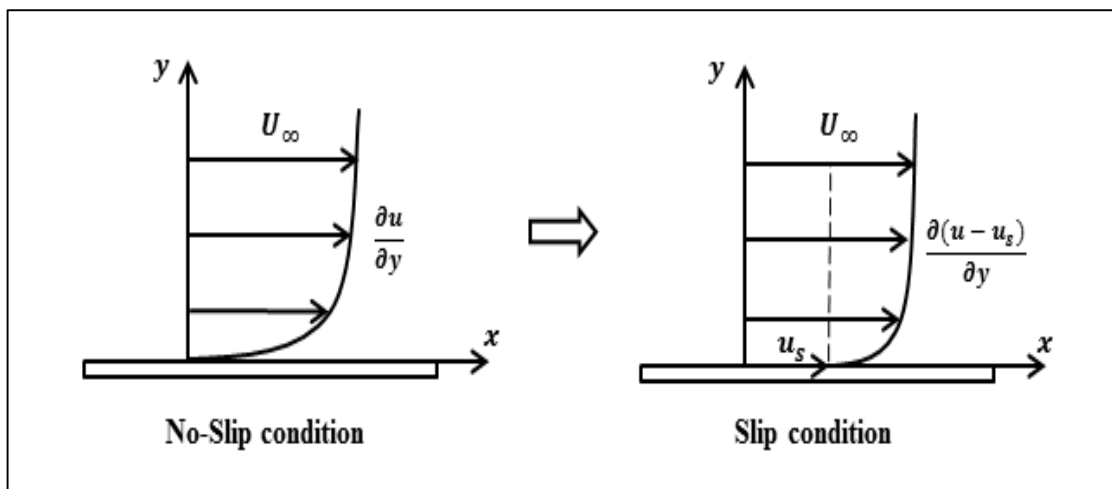
Figure 4.2: Illustration of shear rate for no-slip flow and slip flow.

For no-slip condition, the shear stress at a given point is $\tau_w = \mu(\partial u / \partial y)$. Whereas for the slip condition, the shear stress at a given point can be expressed similarly as $\tau_{ws} = \mu[\partial(u - u_s) / \partial y]$. When $u = U_\infty$, it can be showed that (Gogte et al., 2005)

$$\frac{u_s}{U_\infty} = 1 - \frac{\tau_{ws}}{\tau_w}.$$ (4.6)

Recall that $R_D = 1 - (\tau_{ws} / \tau_w)$. This suggests that $R_D = u_s / U_\infty$. Substituting this into equation (4.5) and some algebra yields

$$R_D = \frac{0.332 U_\infty \text{b}}{\nu \sqrt{\text{Re}_x} + 0.332 U_\infty \text{b}} \, . \tag{4.7}$$

or

$$b \approx \frac{\nu R_D (\text{Re}_L)^{1/5}}{0.0295 U_\infty (1 - R_D)} \, . \tag{4.8}$$

Equation (4.7) is the formula that can be used to predict the friction drag reduction rate over a flat plate. Equation (4.8) is just a re-arrangement of equation (4.7). With a known R_D, equation (4.8) can be used to predict the slip length. A gentle reminder is that the slip length in the formula only refers to the stream-wise slip. This simple formula is useful in understanding the friction drag reduction pattern over a hydrophobic surface subjected to laminar flows.

In order to validate the formula, experimental result reported by Jiang et al. (2011) was used. Jiang et al. (2011) used parallel hydrophobic wires in their experiment. This matches with the assumption 1 made in the derivation. Jiang et al. (2011) measured and compared the drag changes between a miniature flat plate boat and a hydrophobic grille bottomed miniature boat subjected to laminar flows. They have tested the effect of drag reduction from a free stream velocity of 4.12cm/s to 12.47cm/s. The results are shown in figure 4.3. There are eight data points in total. The Reynolds number for each data point was calculated by them using a mid-chord length of 16cm. As the Reynolds number and mid-chord length are known, free-stream velocity for each data point can be determined from Figure 4.3 by using Reynolds number formula $\text{Re}_L = U_\infty x / \nu$, where x is the mid-chord length. Equation (4.8) will be used alongside the first data point to estimate the slip length. Next, equation (4.7) will be used to estimate the friction drag reduction rate for the rest of the data points by using the slip length estimated by equation (4.8).
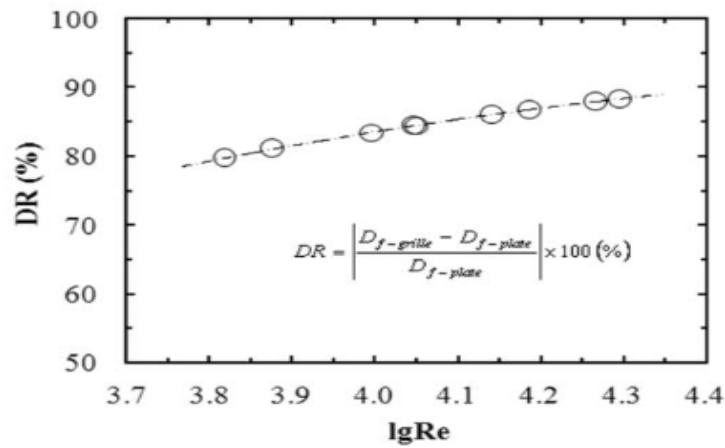
Figure 4.3: The friction drag reduction rate reported by Jiang et al. (2011).

Results are shown in Table 4.1. Generally, the prediction of the derived formula shows good agreement with the results from Jiang et al. (2011). This comparison shows that the derived formula is capable of estimating friction drag reduction reasonably, at least, from engineering point of view. Now, the friction drag reduction pattern over a surface can be predicted by using the derived formula. Consider a 1m long flat plate which has a constant 50µm stream-wise slip length over the surface. With a constant U_∞ of 1m/s, the R_D at different distance from the leading edge can be estimated using equation (4.7). Results are shown in Figure 4.4.

Table 4.1: Comparison of friction drag reduction rate reported by Jiang et al. and friction drag reduction rate predicted by equation (4.7)

Reynolds number obtained from Figure 4.3	Free stream velocity calculated based on the estimated Reynolds number	Experimental drag reduction rate from Figure 4.3	Slip length estimated by equation (4.8)	Friction drag reduction rate predicted by equation (4.7)
6606.9	4.12cm/s	80%	2.38cm	-
7498.9	4.69cm/s	81%	-	81.05%
10232.9	6.40cm/s	83%	-	83.33%
11220.2	7.01cm/s	84%	-	83.95%
14125.4	8.83cm/s	85%	-	85.44%
15135.6	9.46cm/s	86%	-	85.87%
18836.5	11.77cm/s	87%	-	87.14%
19952.6	12.47cm/s	87.5%	-	87.46%
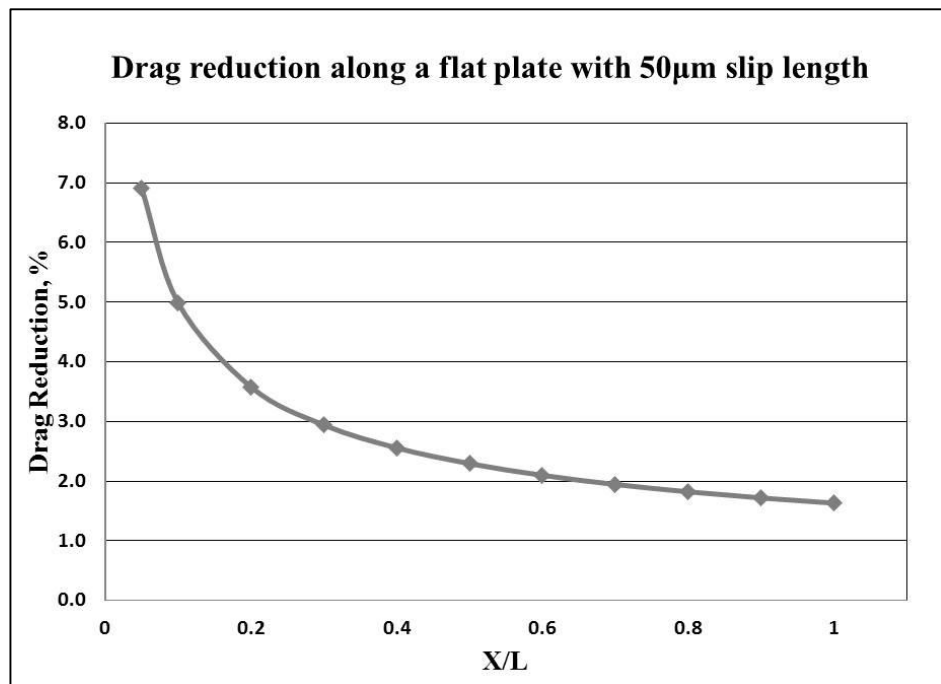
Figure 4.4: Friction drag reduction pattern over a hydrophobic surface predicted by eqn. 4.7.

As can be seen from Figure 4.4, higher friction drag reduction concentrates at the front half of a surface. After X/L=0.5, percentage in friction drag reduction gradually becomes flat. This implies that for the hydrophobic coating, coating the front half of a turbine blade's surface may be sufficient to achieve desirable effects in improving the performance. On the other hand, this result suggests that it is important to ensure the effectiveness of the front half of a hydrophobic coating, in order to benefit from the friction drag reduction. This results essentially provides insights on how should a hydrophobic coating be applied over a turbine blade's surface prior to the actual lab-scale test.

As a gentle reminder, although similar derivation steps can be applied to obtain another formula for turbulent flows, this is not done in the current study. This is because the aim of the analytical analysis is to obtain a general idea on the friction drag reduction pattern over a hydrophobic surface. Any further detail study will deviate from the objectives of the current work.

4.2.2 Lab-scale Test on Hydrophobic Hydrofoils

Figure 4.5 and Figure 4.6 shows the measured C_L and C_D for NACA 63418 with and without upper face coated with BioCyl. Figure 4.7 and Figure 4.8 shows the measured C_L and C_D for NACA 63418 with and without both faces coated with Biocyl. As can be seen from Figure 4.5 and Figure 4.6, there is no noticeable changes in C_L, but there is reduction in C_D for the AoA range tested. An average reduction of 3% for C_D is achieved with the use of Biocyl coating on upper surface. The percentage of reduction is at its highest at low AoA and gradually decreases as AoA increases. When Biocyl is coated on both surfaces, a similar trend is obtained with higher reduction occurs at low AoA (Figure 4.7). A higher average reduction of 3.5% is achieved when NACA 63418 is fully coated with Biocyl. For C_L, there is a slight reduction of not more than 1% at high AoA, especially at $10^{\circ}\sim11^{\circ}$.

This results shows that Biocyl, being a hydrophobic coating with a mild contact angle, does reduce drag. The reason for diminishing effects in reducing drag at higher AoA can be attribute to the fact that there are two types of drag over a hydrofoil. One is the friction drag, and the other one is pressure drag (also known as form drag). At low AoA, friction drag is the dominant drag. As AoA increases, pressure drag gradually becomes more dominant and the effect from friction drag becomes less. Once flow separation occurs, the friction drag will become negligible as flow detaches from surface.

For lift, the reason for the reduction at high AoA is believed to be attributed to the coating at lower surface. As pointed out by Daniello (2013), a super-hydrophobic coating that directly facing towards incoming flow has tendency to lose its lubricating effects and results in increased friction. Although Biocyl for the current study is a

normal hydrophobic coating, a similar condition may take place when it is directly facing towards incoming flow. This occurs as AoA increases. But the overall effect is minimal as the reduction only takes place between AoA 10º-11º. When averaged, the reduction is not as significant as reduction in drag.

Figure 4.9 shows Daniello (2013) C_L and C_D results. Daniello used a superhydrophobic coating specifically designed with high contact angle of more than 150º in his study. This high contact angle superhydrophobic coating achieved a high drag reduction of about 13% at angle of AoA between 0º~8º. However, the coating started to cause increase in drag beyond AoA 10º. In addition, the coating has caused an averaged reduction in lift of about 10% for all AoA considered. Comparison of current study with Daniello (2013) results implies that a high contact angle superhydrophobic coating does not necessarily provide better L/D ratio.
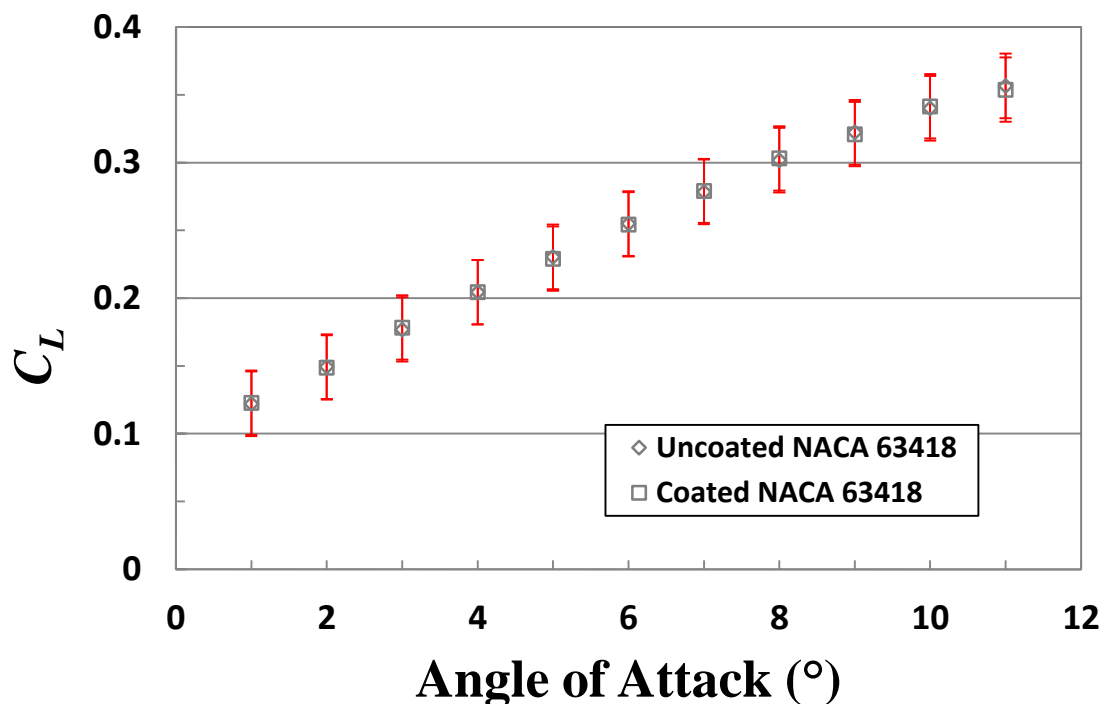
Figure 4.5: Comparison of C_L between NACA 63418
with and without Biocyl on upper surface.
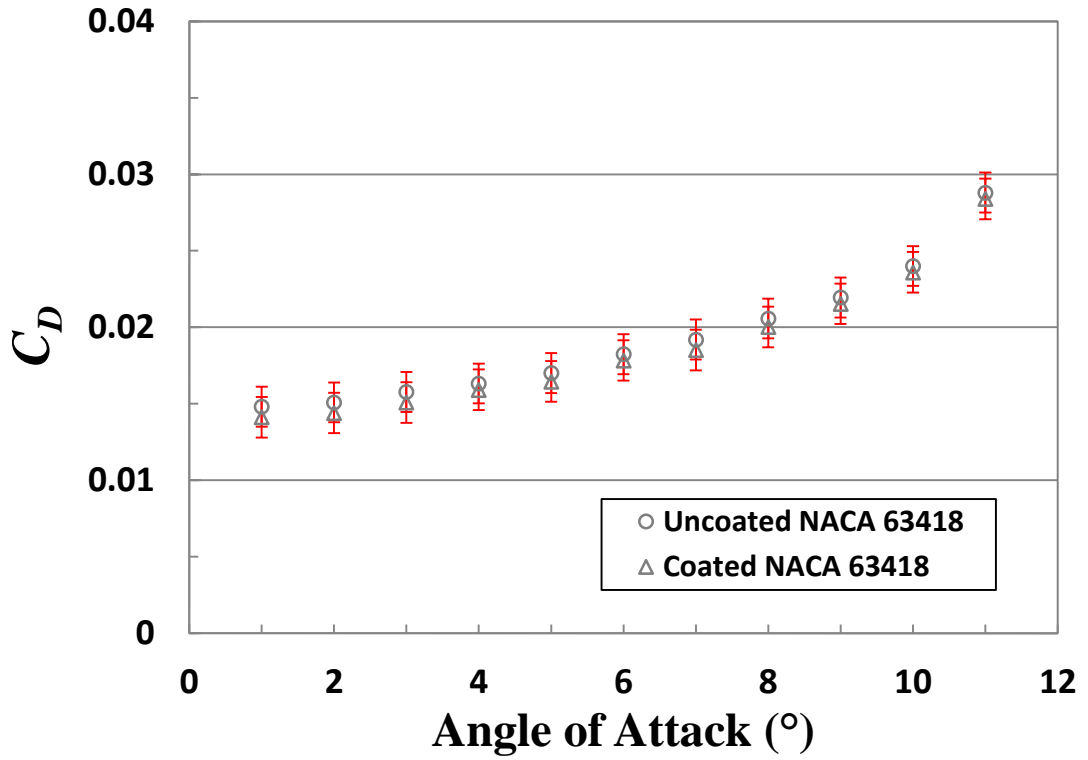
Figure 4.6: Comparison of C_D between NACA 63418 with and without Biocyl on upper surface.
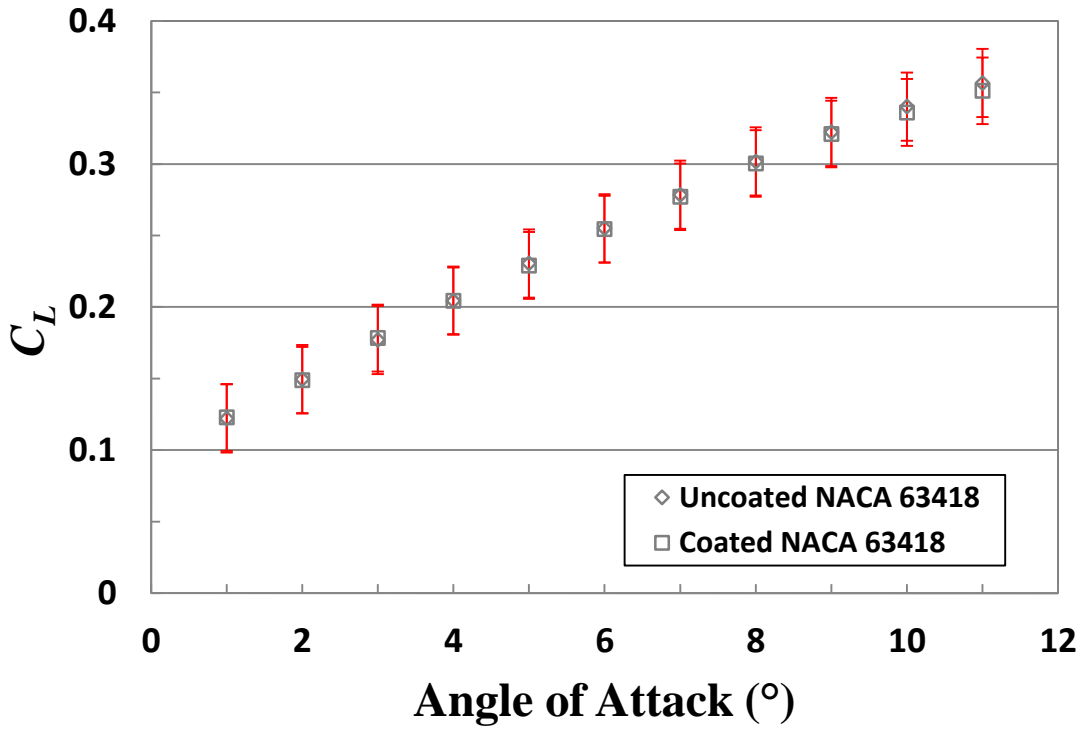
Figure 4.7: Comparison of C_L between NACA 63418 with and without Biocyl on both surfaces.
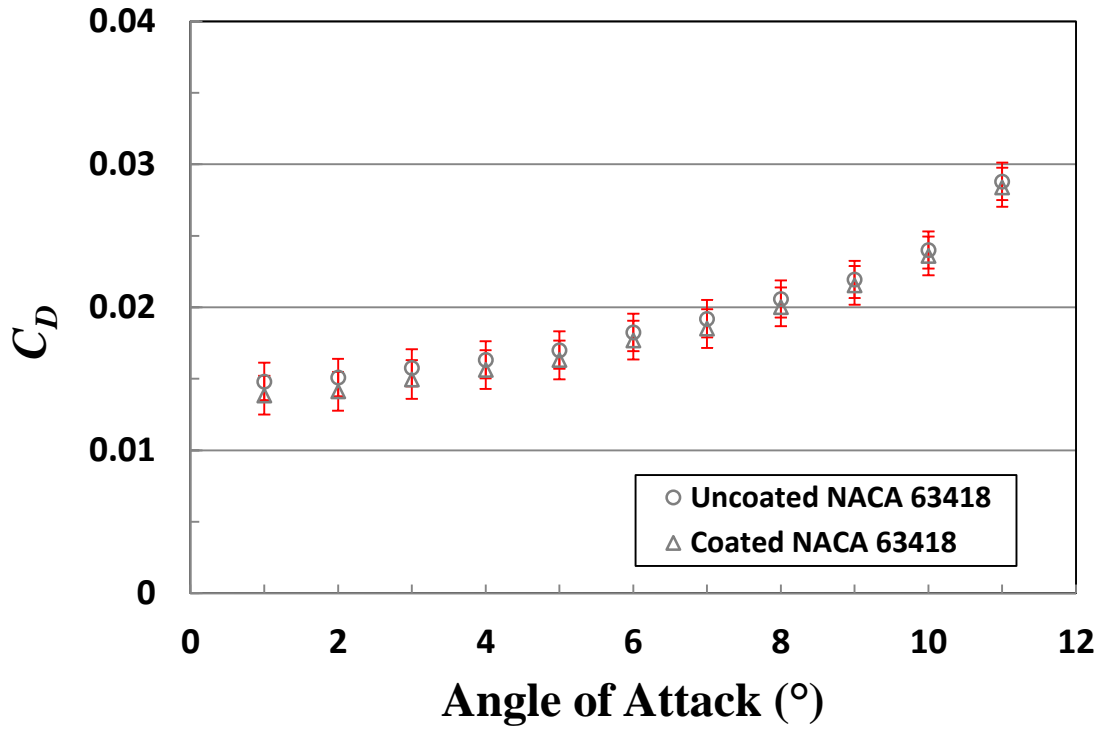
Figure 4.8: Comparison of C_D between NACA 63418
with and without Biocyl on both surfaces.
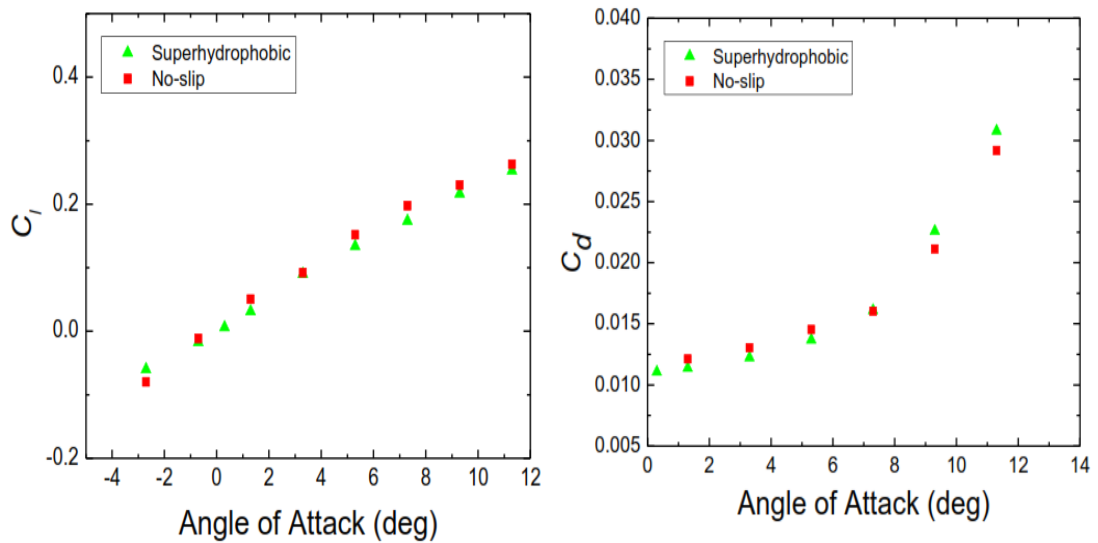
Figure 4.9: C_L and C_D of superhydrophobic hydrofoils by Daniello (2013).

Figure 4.10 and Figure 4.11 shows the measured C_L and C_D for NACA63418 with upper face coated with Always Dry. Figure 4.12 and Figure 4.13 shows the measured C_L and C_D for NACA63418 with both faces coated with Always Dry. As can be seen from Figure 4.10 and Figure 4.11, there is also no noticeable changes in C_L, but Always Dry achieved a slightly higher reduction rate. An average reduction of 3.5% for

C_D is achieved with the use of Always Dry coating on upper surface. Similarly, the percentage of reduction is at its highest at low AoA and gradually decreases as AoA increases. When Always Dry is coated on both surfaces, a similar trend is obtained with higher reduction occurs at low AoA (Figure 4.12). A higher average reduction of 4% is achieved when NACA 63418 is fully coated with Always Dry. Likewise, reduced C_L was noticed at high AoA, especially at $10^\circ \sim 11^\circ$.
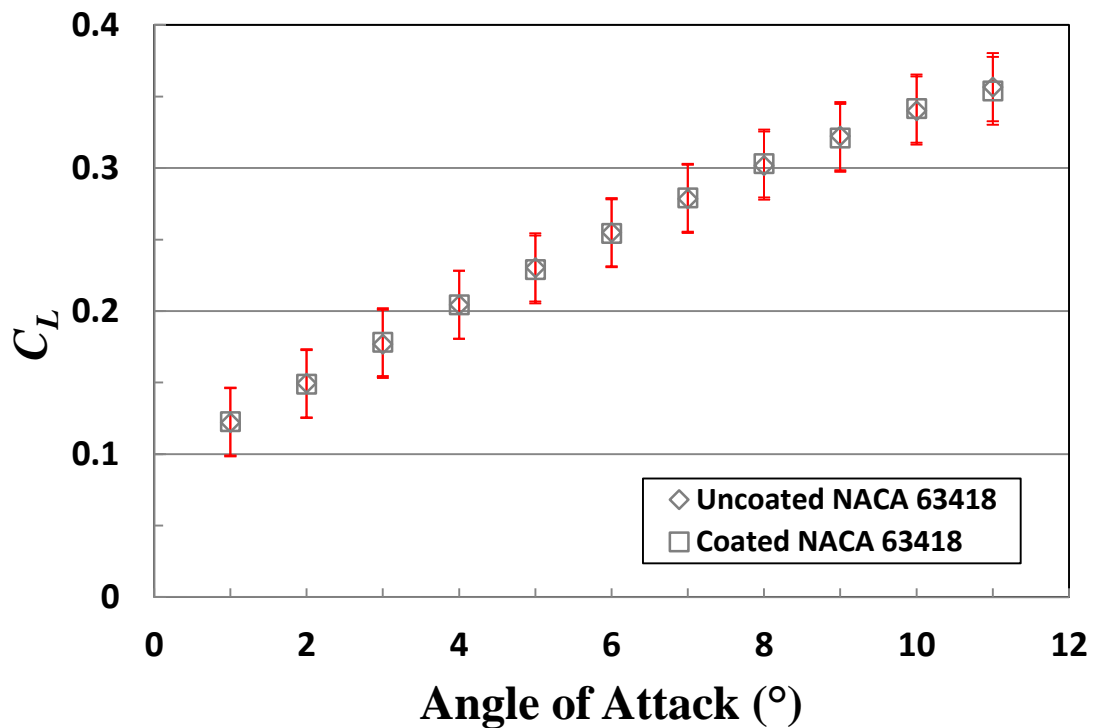
Figure 4.10: Comparison of C_L between NACA 63418
with and without Always Dry on upper surface.
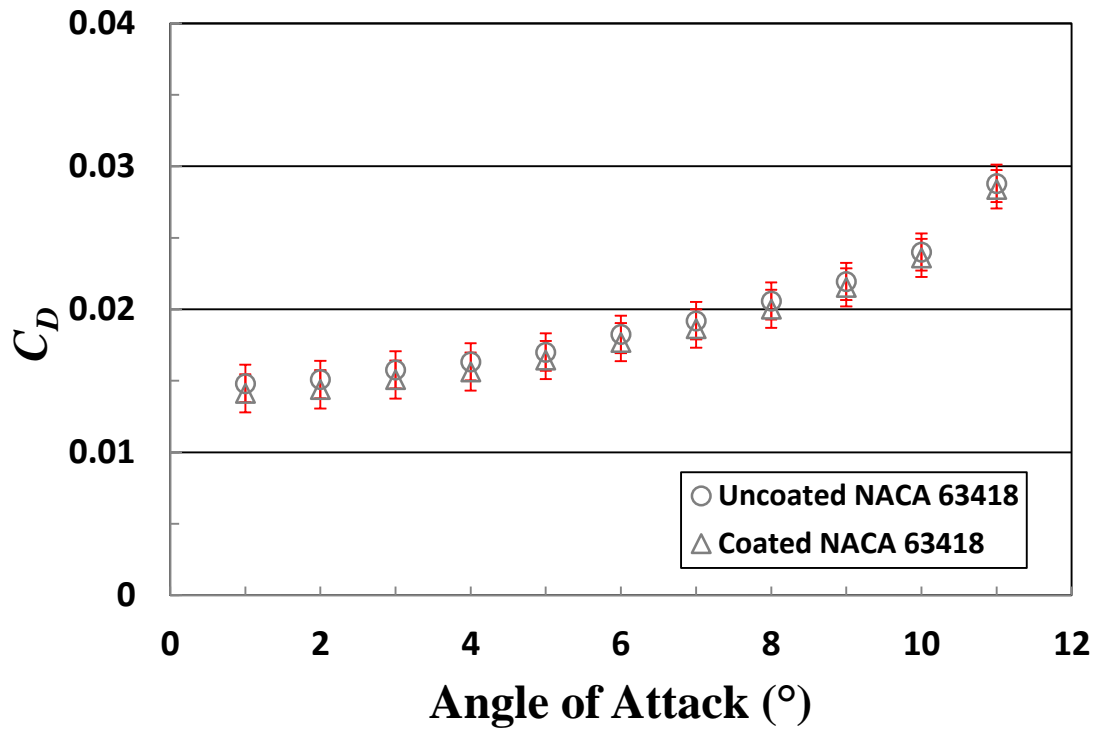
Figure 4.11: Comparison of C_D between NACA 63418 with and without Always Dry on upper surface.
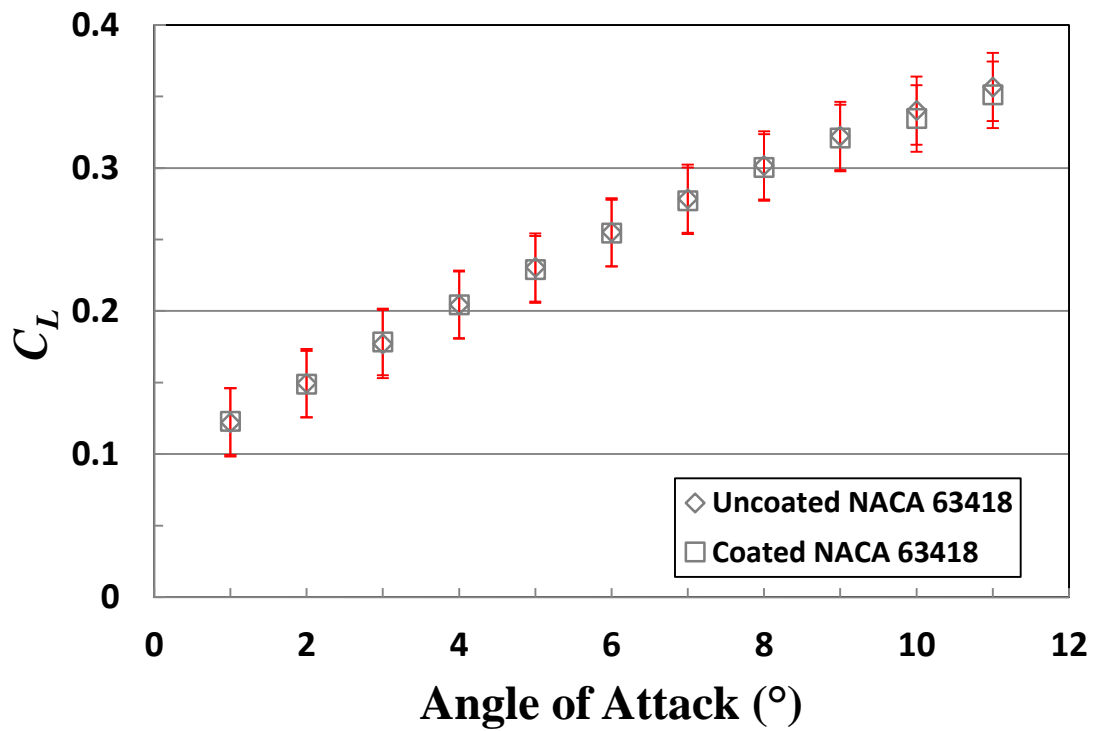
Figure 4.12: Comparison of C_L between NACA 63418 with and without Always Dry on both surfaces.
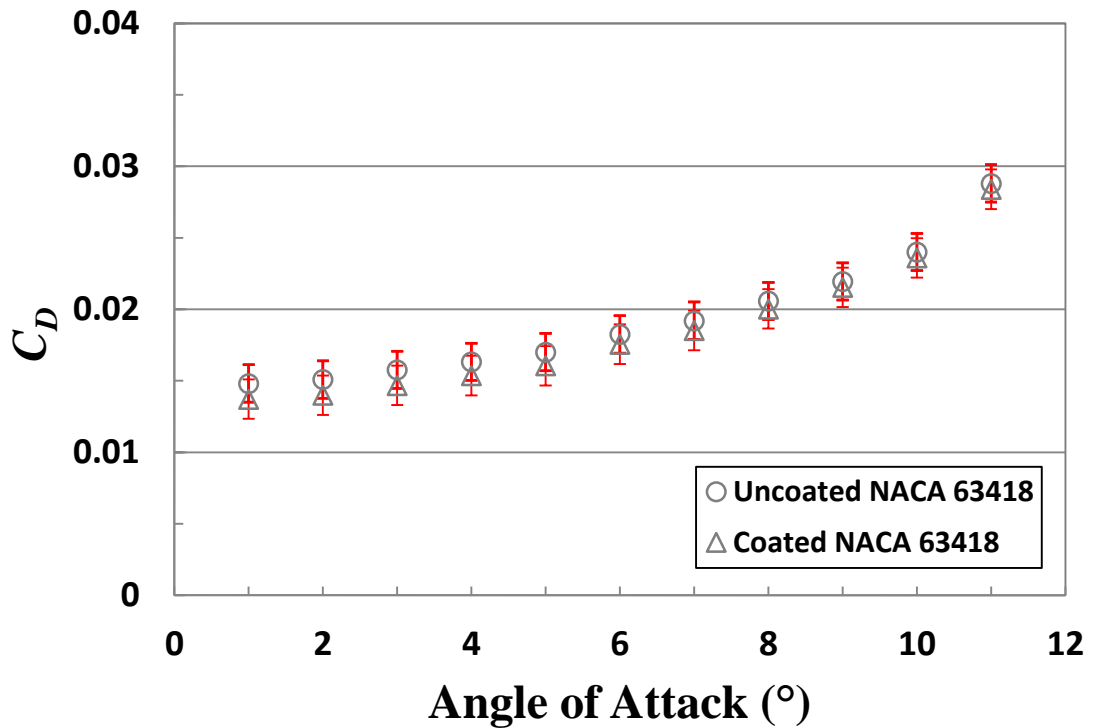
Figure 4.13: Comparison of C_D between NACA 63418
with and without Always Dry on both surfaces.

The current study on hydrophobic hydrofoil is encouraging, as it shows the present of such surface affects C_L and C_D positively. Both Biocyl and Always Dry are capable of reducing drag. Meanwhile, the analytical results in section 4.2.1 have also been tested. The measured C_L and C_D for a hydrofoil coated with Biocyl and Always Dry at the front half of upper surface are similar to the hydrofoil that has its upper surface fully coated (see Appendix C). But, as the overall reduction in drag is only about 3~3.5%, the results are less convincing. The difference may not be clearly seen with this small percentage. Hence, it is believed that a load cell with higher accuracy is required to justify whether a upper front half coated hydrofoil does provide good drag reduction similar to a hydrofoil with its upper surface fully coated.

4.2.3 Numerical Analysis

Figure 4.14 and Figure 4.15 show the comparison of C_L and C_D between experimental data and ANSYS Fluent for NACA 63418 without coating. Simulation of ANSYS Fluent on C_L is in good agreement with experimental data. But, simulation on C_D under predicts at low AoA and gradually over predicts at high AoA. This is rather surprising as one would expect when simulation of C_L is in agreement, C_D should obtain agreement as well. The difference may be a result of error in defining the domain to fit the Reynolds number used in the lab-scale test.

Figure 4.16 and Figure 4.17 show the comparison of C_L and C_D between experimental data and ANSYS Fluent for NACA 63418 having hydrophobic coating on upper face. The percentage reduction in specified shear was set to be 3%, which is the average friction drag reduction obtained from the lab-scale test. ANSYS Fluent has predicted an averaged lift increment of 0.8% C_L and an averaged drag reduction of 2.8% for C_D.

Although the current numerical analysis does not show agreement in C_D value, it is still acceptable to be used to determine whether ANSYS Fluent can simulate the changes in drag accurately with the presence of hydrophobic coating. As can be seen from Figure 4.17, the average 2.8% reduction is close to the results in Figure 4.6, which is an average of 3% (hydrophobic coating on upper face). This shows that ANSYS Fluent is capable of capturing the changes in drag induced by hydrophobic coating by adjusting the input of specified shear.
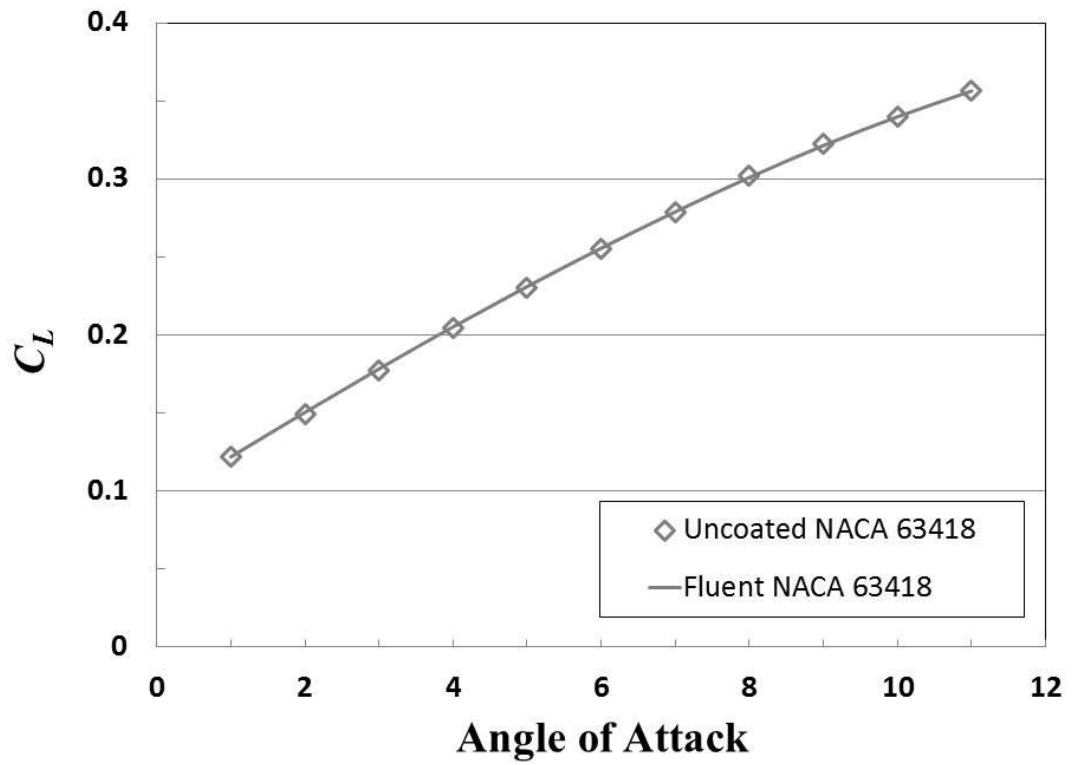
Figure 4.14: Comparison of C_L between experimental data and ANSYS Fluent for NACA 63418 without hydrophobic coating.
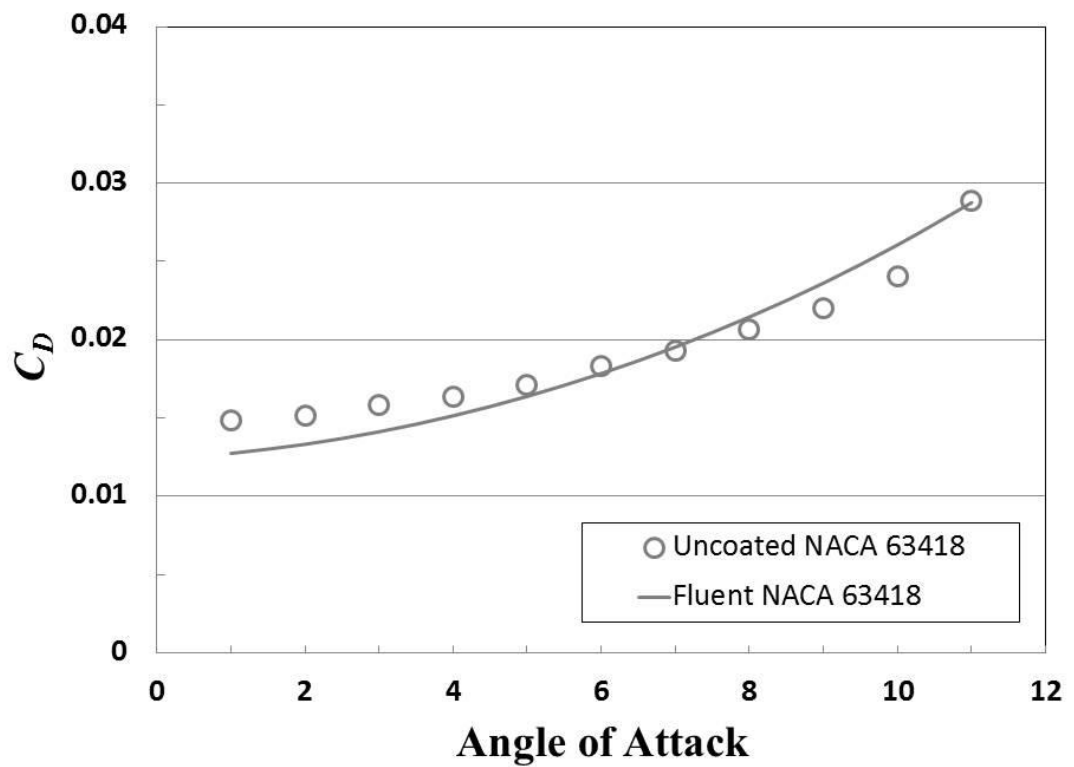
Figure 4.15: Comparison of C_D between experimental data and ANSYS Fluent for NACA 63418 without hydrophobic coating.
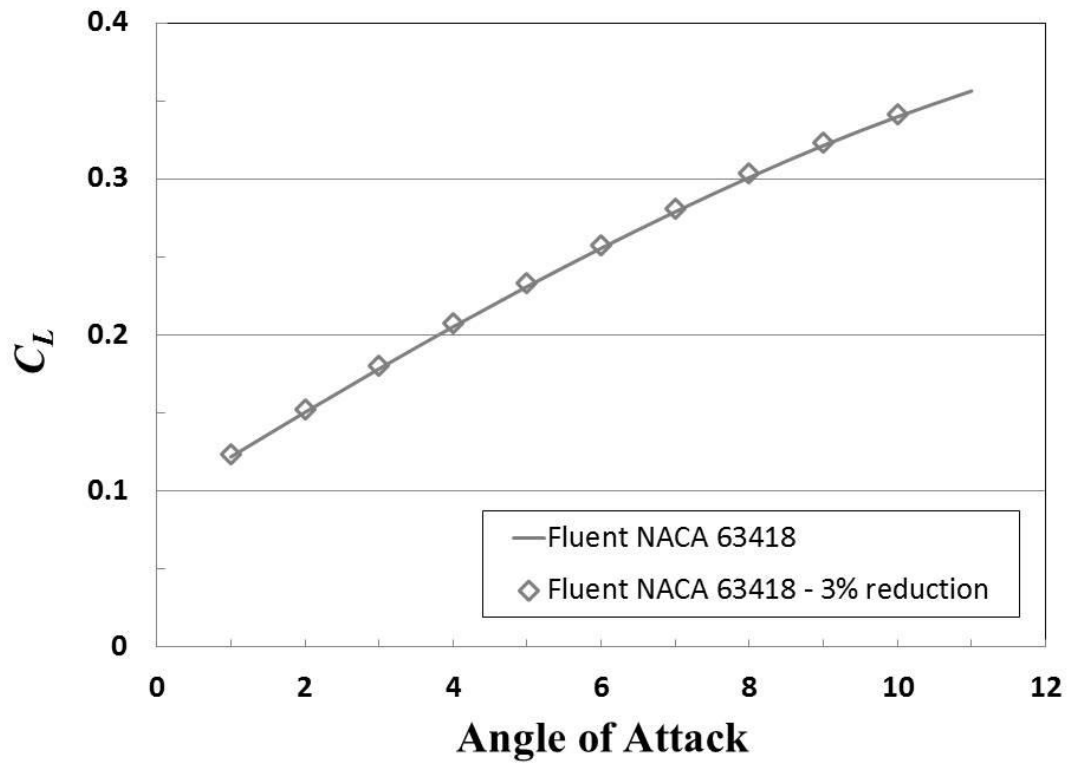
Figure 4.16: Comparison of C_L simulated by ANSYS Fluent for NACA 63418 with and without hydrophobic coating on upper surface.
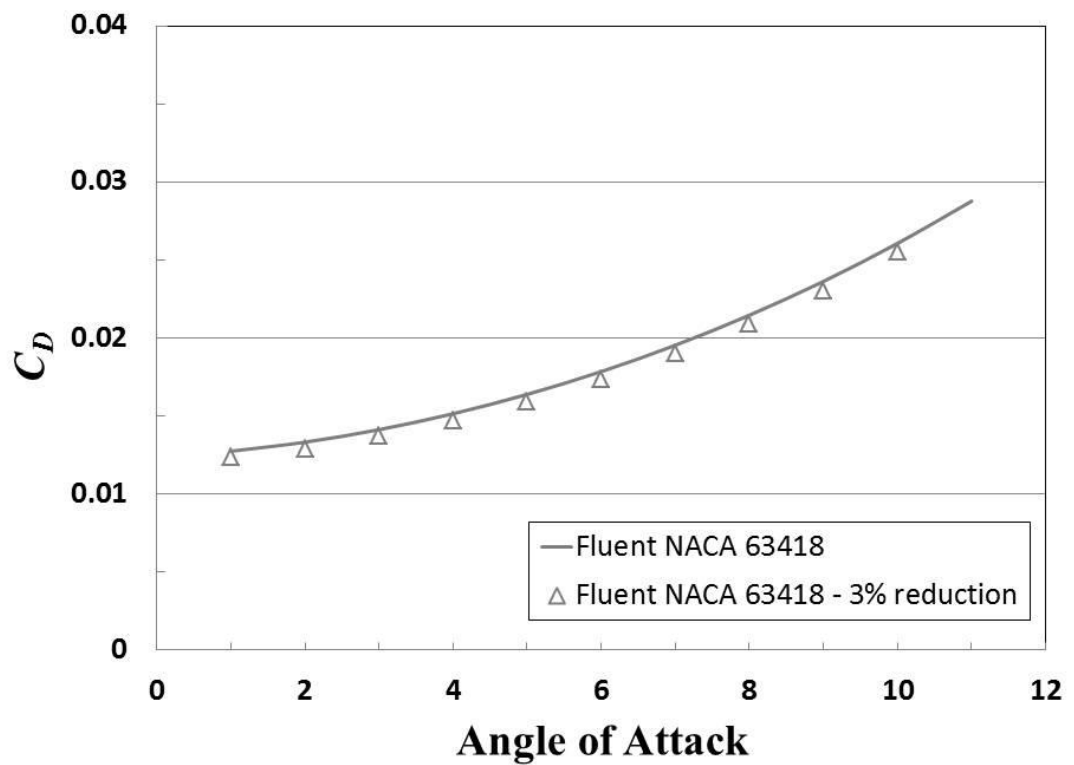
Figure 4.17: Comparison of C_D simulated by ANSYS Fluent for NACA 63418 with and without hydrophobic coating on upper surface.

However, ANSYS Fluent predicted an increment in C_L, which is in contrast to the experimental results. This is attributed to the nature of the CFD code where it derives lift forces based on the shear stresses along boundary layer. As a result, with lower specified shear, the simulation will yield higher lift. The current numerical analysis shows that ANSYS Fluent can be readily used to simulate changes in lift associate with hydrophobic coating, but it is not suitable to be used to simulate changes in lift. Note that simulation on both surfaces coated with hydrophobic coating has not been carried out as the results should be similar to the upper surface coated with hydrophobic coating.

4.2.4 Lab-scale Test on Hydrophobic Three-bladed Turbine

Figure 4.18 shows the comparison of C_p value between the TBT with and without Biocyl coating. As can be seen from the figure, the C_p value trend is in reasonable agreement with Pinon et al. (2012) results. The difference between TSR 3-5 is believed to be attributed to the fact that the TBT used in the current study has a flat hub, while the one used by Pinon et al. (2012) has a streamlined smooth hub. The measured C_p values for the TBT with and without Biocyl show little difference. Note that the coated turbine in Figure 4.18 refers to a fully coated TBT. When turbine with only coating on suction side was tested, a similar result was obtained. No noticeable difference between coated and uncoated TBT. Likewise, similar results have been obtained for Always Dry. It is difficult to determine whether hydrophobic coating has any effect on turbine based on these data.
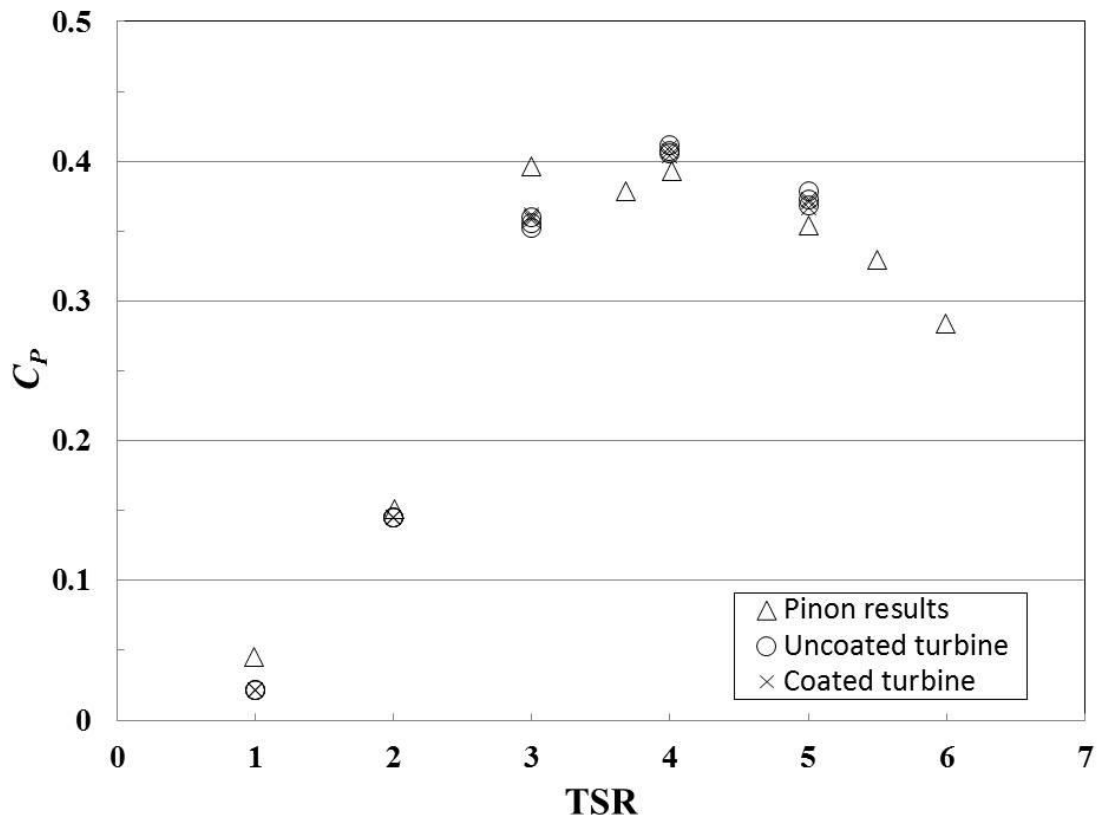
Figure 4.18: C_p comparison for the TBT with and without Biocyl.

Figure 4.19 and Figure 4.20 show the RPM of turbine with coating on suction side and full coating of Biocyl at different velocity. The RPM shown in both figures are averaged data from 10 readings at each velocity. Surprisingly, a constant improvement in RPM was observed at all velocity, although small in magnitude. Unexpectedly, turbine with coating on suction side has better RPM than turbine with full coating. RPM for turbine with coating on suction side improved by an average of 2.0%, but RPM for turbine with full coating only improved by an average of 1.0%.

Figure 4.21 and Figure 4.22 show the RPM of turbine with coating on suction side and full coating of Always Dry at different velocity. Similar to Biocyl, a constant improvement in RPM was also observed at all velocity. However, the improvement is slightly higher than Biocyl. Coating on suction side recorded an increase of approximately 2.5% in RPM, while full coating recorded an increase of approximately

1.3%. These results show that both Biocyl and Always Dry have positive effects on rotational speed of the TBT. The reason for Always Dry to record a higher improvement is self-explanatory based on the results in section 4.2.2. Always Dry helps a hydrofoil to achieve higher drag reduction compared to Biocyl.

Two observations can be drawn from these results. Firstly, it seems to be that the improvement on RPM is constant for a specific coating and does not get affected by velocity. This suggests that the effects may be more significant at lower velocity range. Secondly, although fully coated hydrofoil can achieve better drag reduction as shown in section 4.2.2, this benefit is not seen for a fully coated turbine blade. The slight reduction in C_L at high AoA ranges may be one of the reasons that lead to lower improvement in RPM. Therefore, coating on suction side alone appears to be a more favourable method to achieve better enhancement for a turbine.
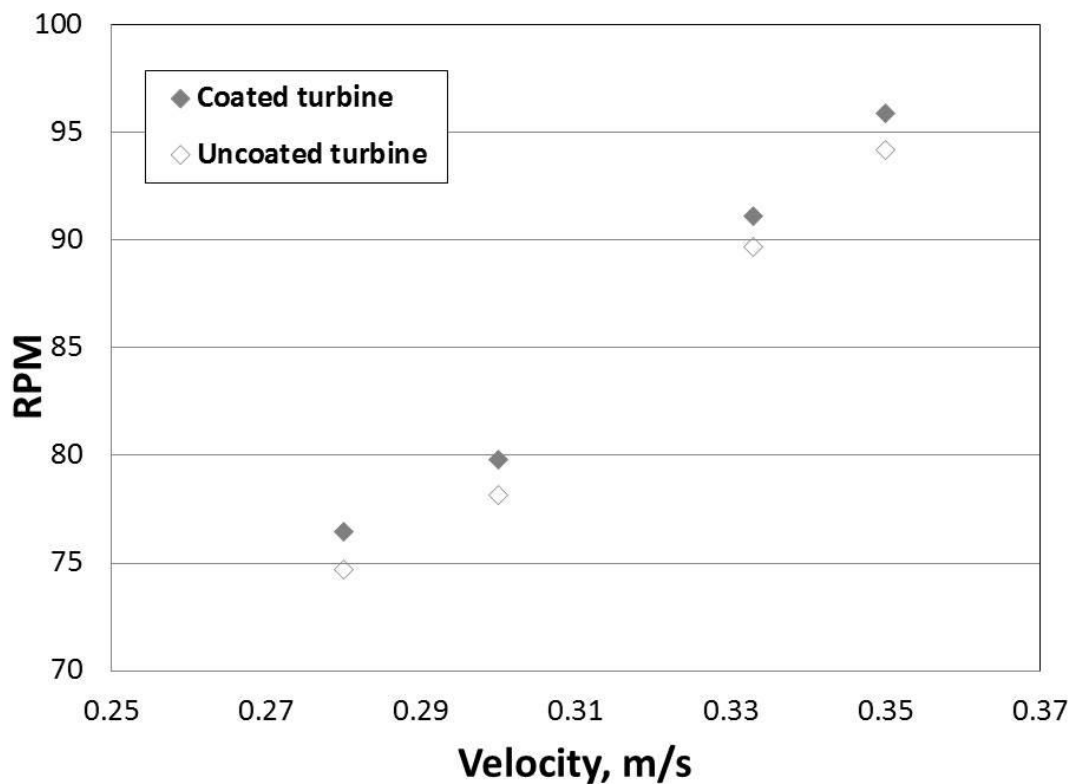
Figure 4.19: RPM of the TBT coated with Biocyl on suction side.
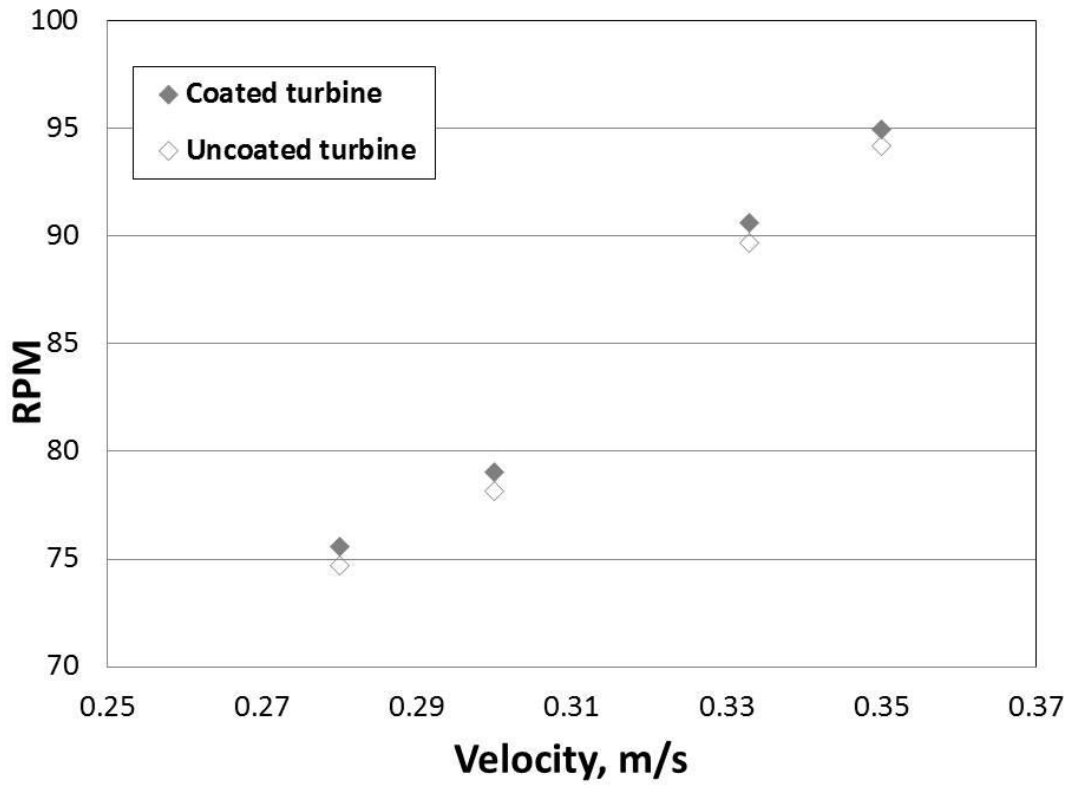
Figure 4.20: RPM of the TBT fully coated with Biocyl.
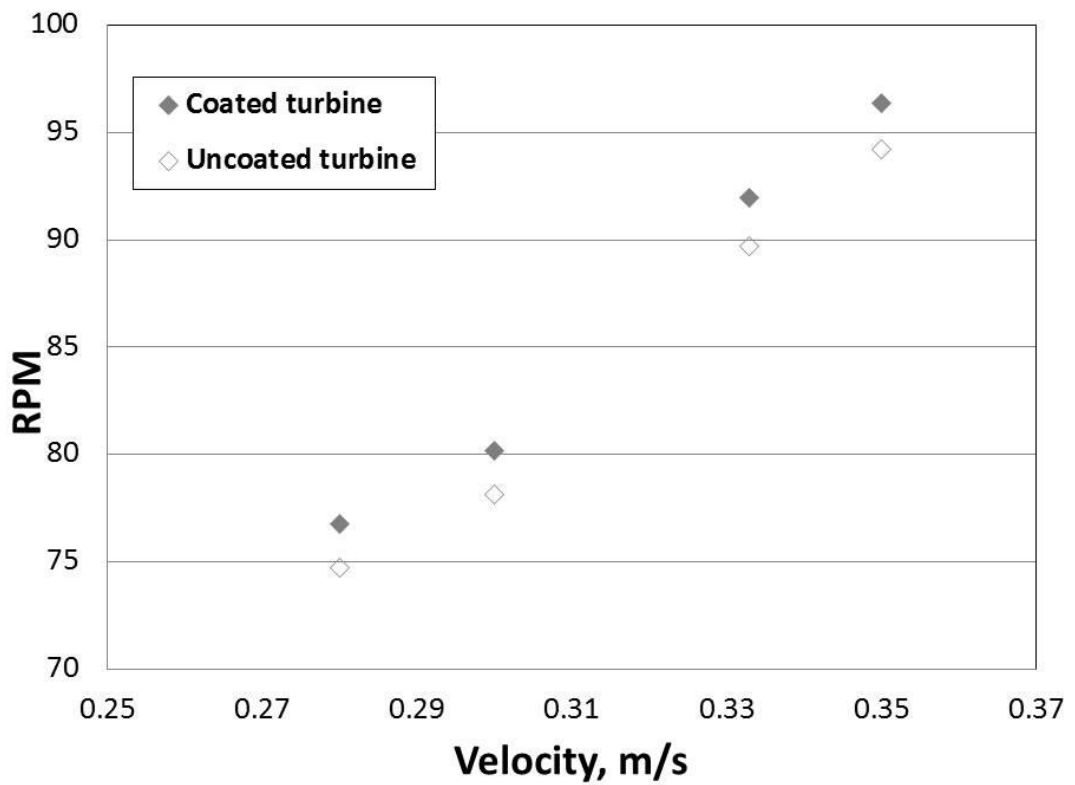
Figure 4.21: RPM of the TBT coated with Always Dry on suction side.
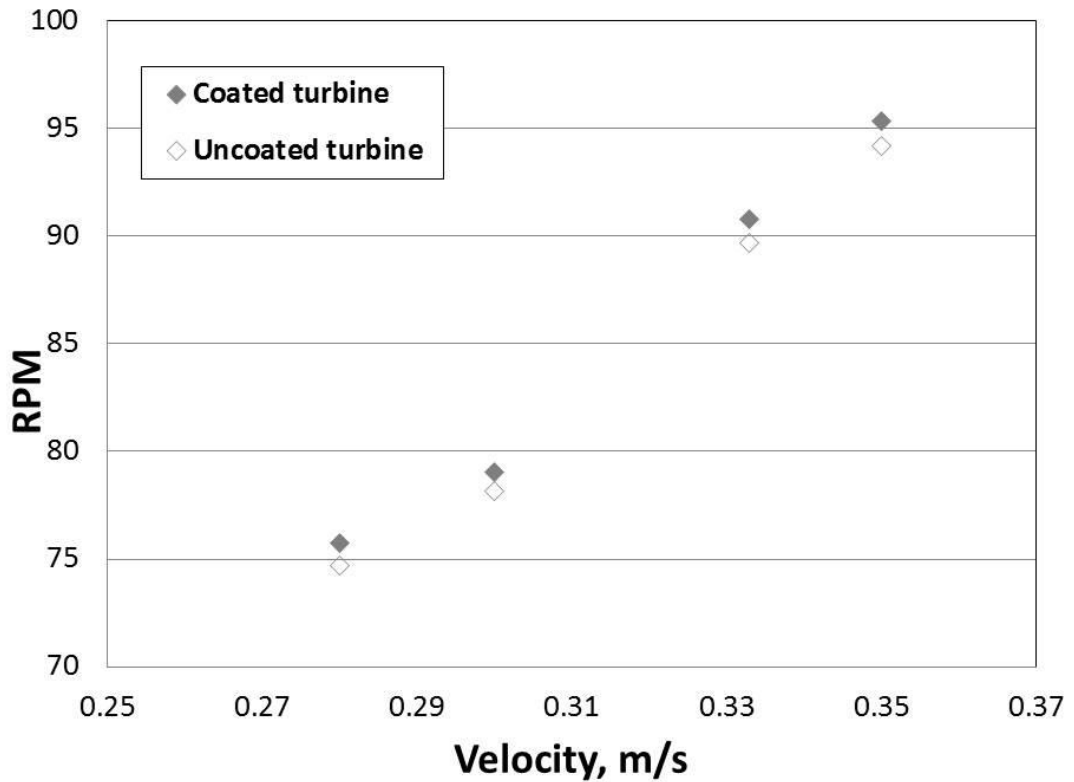
Figure 4.22: RPM of the TBT fully coated with Always Dry.

The low magnitude of improvement in RPM explains why there is no noticeable change in the C_P value for a turbine with hydrophobic coating. A clearer picture can be seen from Figure 4.23. Figure 4.23 shows the results of WT_Perf on prediction of C_P value. Based on the results from section 4.2.2, the input of C_L for hydrofoil of coated turbine blade was set to be same with uncoated hydrofoil, whereas the input of C_D for hydrofoil of coated turbine blade was set to be lower than the uncoated hydrofoil. Two sets of simulation were tested, namely 10% drag reduction and 30% drag reduction.

As can be seen from Figure 4.23, the simulation of WT_Perf is in good agreement with experimental results for TSR 2-3. Beyond TSR 4, it over-predicted the value of C_p. Since the optimum TSR based on experimental data is around 3, the prediction by WT_Perf for TSR 2-3 should be reliable. Based on the simulation, with a drag reduction of 10%, it is possible to improve C_p by about 3% at TSR=2 and less than

1% at TSR=3. With a drag reduction of 30%, C_p at TSR=2 can have an improvement of 10% and C_p at TSR=3 can have an improvement of approximately 3%.
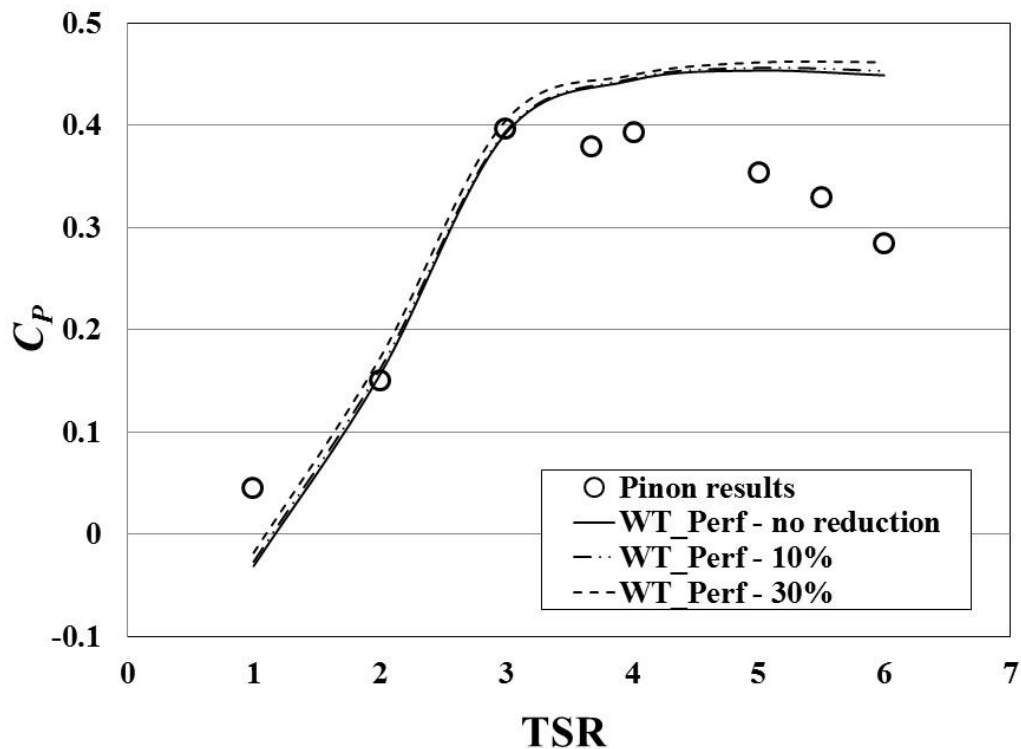
Figure 4.23: C_p comparison for the TBT simulated using WT_Perf.

Apparently, Biocyl and Always Dry cannot provide such enhancement to the TBT as the drag reduction achieved by them is only about 3.5%. This explains the results in Figure 4.18. The effects on L/D ratio from Biocyl and Always Dry are simply not enough to achieve a noticeable change on C_p. furthermore, the measurement of C_L and C_D for NACA 63418 in the current study are of 2D. Consider the fact that a rotating turbine will definitely subject to 3D effects, especially near the tips, the effectiveness of friction drag reduction from hydrophobic coating is going to be affected.

Likewise, the reason for having better C_p improvement at low TSR is due to the fact that at low TSR, the rotation of a HATCT is relatively slow and most of the drag forces acting upon turbine blades are of friction nature. At high TSR, the swirling drag

and pressure drag gradually increase. This causes the effects from friction drag reduction to become smaller. The WT_Perf simulation is in agreement with the observation made from RPM study, where the improvement in RPM is higher at low RPM. This suggests that when a hydrophobic coating can provide measurable changes on C_p, it will allow a HATCT to harness more energy at low current velocity.

The current study on hydrophobic coating as a measure to enhance performance of a HATCT reveals that the idea is workable. However, a normal hydrophobic coating available in the market appears to be not the right candidate for this purpose. Hence, a study on specially designed hydrophobic surface is necessary to further realise the potential of hydrophobic surface, or more specific, the drag reduction phenomenon for HATCTs. In fact, any measure that can reduce friction drag over turbine surface can be a potential alternative to hydrophobic coating, for example, the air injection method which has already been studied intensively in the field of ship hull.

Since the lab results reveal that, at the current stage, application of hydrophobic coating for performance enhancement is insignificant even under steady flow condition, testing of this measure in field test was not carried out.

4.3 Field Test of Small Scale HATCT

The full assembly of the FBT is shown in Appendix. A problem was encountered after the full assemblage. The stuffing box was not well aligned to the shaft's support. This caused additional friction to the rotation. Fortunately, during the field test, tidal current was sufficient to overcome this unexpected additional friction. Nevertheless, this minor defect is still going to have impact on the power output of the FBT.

The field test was conducted for 5 days after the Full moon on August 2015. The average tidal current velocity was ranging from 0.06m/s to 0.3m/s during the field test period. The calibration of the FBT before submerging it fully under the water was done one day before the Full moon. It was found that tidal current speed above 0.27m/s during the period only occurred for less than half an hour and the flow was unstable. On the other hand, below 0.1m/s, the FBT hardly rotates. Hence the power output recorded only covers the range between 0.1m/s to 0.25m/s.

The initial scale between the pulley at shaft and pulley at generator was set to be 2x. Under this setting, it was found that the rotation of turbine blade was not able to provide constant and sufficient rotation for generator to generate steady output. The power output only started to become stable when tidal current velocity was above 0.22m/s. After that, the 80mm small pulley was replaced by 40mm small pulley to increase the scale to 4x. Under this setting, the power output became steady when tidal current velocity was above 0.15m/s. When the scale was further increased to 8x by replacing the 40mm small pulley with 20mm small pulley, a steadier power output was obtained when tidal current velocity stayed above 0.12m/s.

Figure 4.24 and Figure 4.25 show the power output at different tidal current velocity for 4x scale and 8x scale. As can be seen from Figure 4.21, the small scale FBT fabricated for the current study can produce a power output of approximately 1.3W at a velocity of 0.25m/s. This is equivalent to a C_P of 0.32, which is considerably good. This is an encouraging outcome as the FBT was a modification from axial ventilation fan. This shows that with proper modification, the FBT can operate considerably well. Additionally, this result also shows that harnessing tidal current energy from a potential

site with low tidal current flow is workable, even though the initial know-how can only

harness a small fraction of the energy from it.
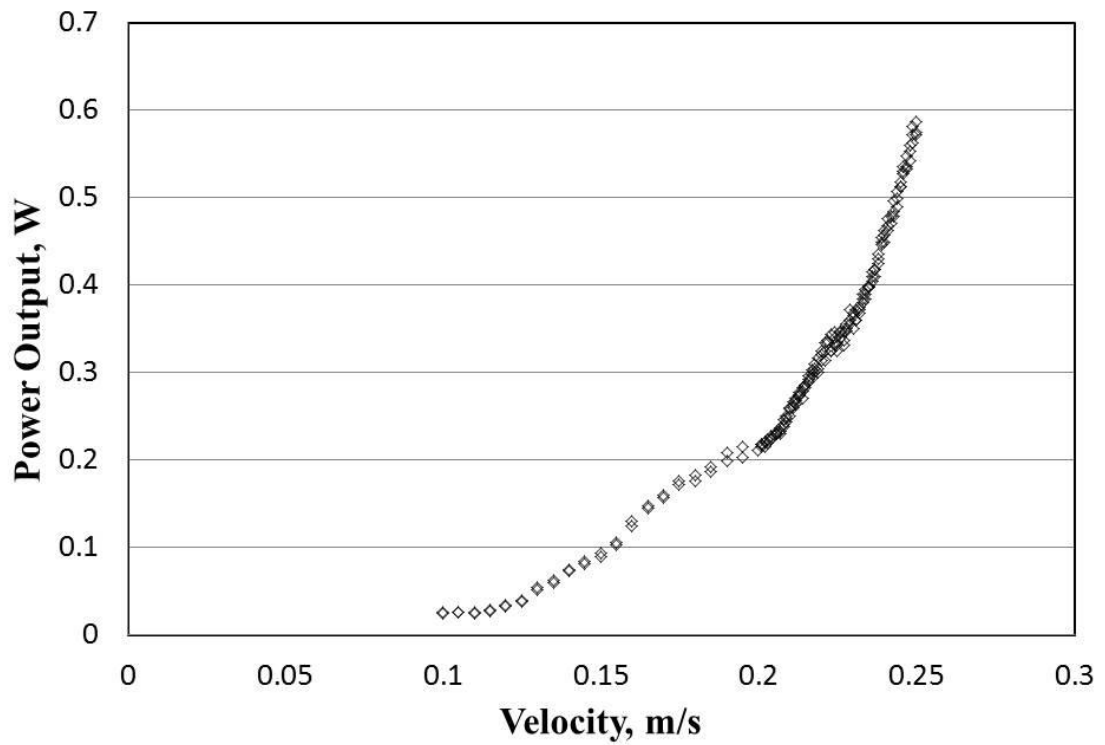
Figure 4.24: Power output curve of the FBT for 4x scale.
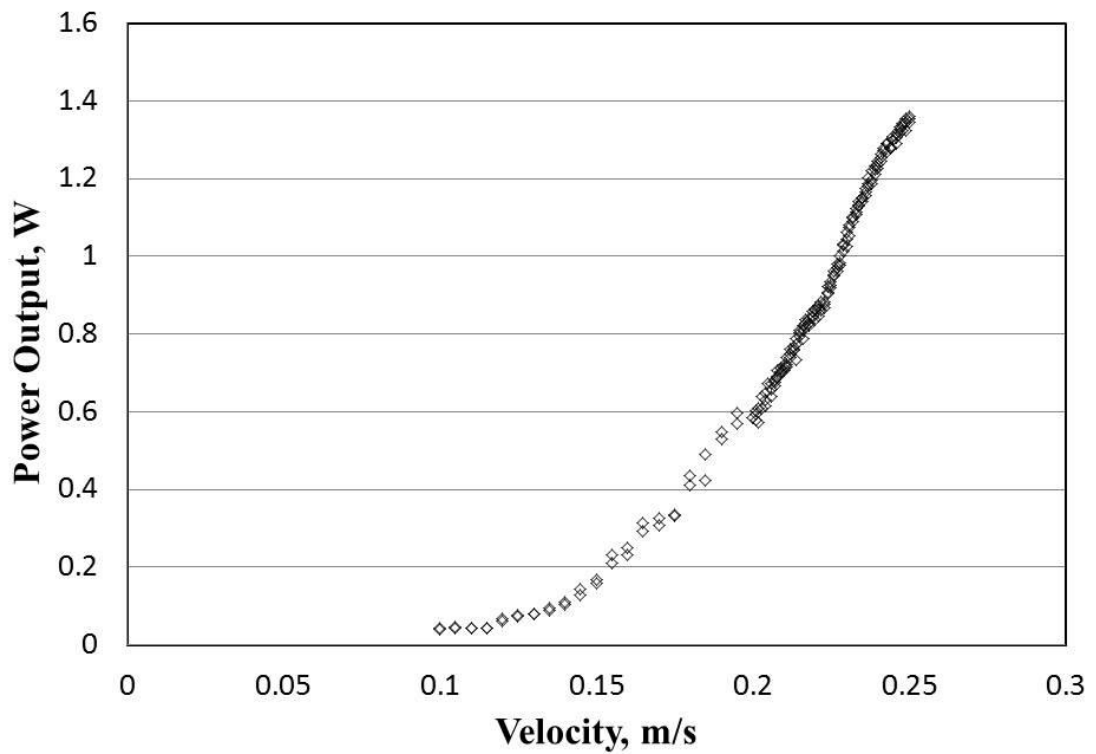
Figure 4.25: Power output curve of the FBT for 8x scale.

Throughout the test, the mechanical seal placed at the stuffing box was able to prevent water from leaking into the casing. This shows that mechanical seal with a stuffing box is sufficient to prevent water leaking at a depth of approximately 0.9m from sea surface. On the other hand, the timing belt used for the FBT appeared to be exerting considerably high friction to the shaft. When the velocity of tidal current is between 0.05-0.8m/s, the FBT rotates steadily, though very slow, when timing belt is loosen. Contrarily, when timing belt is tightened, the FBT only starts rotating when velocity is above 0.1m/s.

The results obtained from the current field test are site specific. There are many factors that are uncontrollable and the FBT constantly receive disturbance from external forces. Some of the external forces include the vertical motion of the floating platform and the turbulence nature of the tidal current itself. Hence, the accuracy of the measured power output in the current study is only limited to this site.

During the field test, it is observed that deployment of HATCTs near to Pangkor Island need to overcome one challenge, which is ocean garbage. There were huge broken tree branches, big plastic sheet and big dead fish body approached to the FBT. Although dead fish body floats on the sea surface and is less likely to hit directly on to turbine, but as far as the FBT is concerned, the impact from the dead fish body can affect the operation of the FBT when it hits the casing. As for the huge broken tree branches, the long branches can easily hit the turbine blade's tip which is about 500mm below sea surface. Collision of tree branches happened three times during the field test. For small scale HATCT, the presence of such ocean garbage can disturb the rotating turbine blade. For large scale HATCT, ocean garbage may slip into some mechanical

parts and cause undesired maintenance issues. In fact, ocean garbage has affected the marine bio-fouling test, which will be discussed in the next section.

4.4 Marine Bio-fouling Test

This section presents the results on marine biofouling study conducted in Pangkor Island. Figure 4.26 shows the stainless-steel plates with Biocyl, Palccoat and without coating after been putting into water for one day. Figure 4.27 shows these plates after being submerged under seawater for 90 days. The impact of the marine bio-fouling is obvious. It can be seen that for Biocyl, the biofouling activity remains at the soft fouling stage where thin film growing on the surface. For Palccoat, although surface is mostly covered by soft fouling, hard fouling has also taken place such as at the middle part and lower right corner. For plain plate, it has been fully covered by hard fouling.

Hard fouling means the growing of marine organisms with hard shell such as barnacles. If a surface is under soft fouling, it still can be cleaned manually to remove the soft thin bio film without damaging the surface. But, once a barnacle attached on it, it is unlikely to remove the barnacle completely without causing a certain damage on the surface. As a barnacle grows larger, it gets more difficult to remove it. Figure 4.28 shows the cleaned stainless-steel plates. Surprisingly, some minor hard fouling have already attacked the plate coated with Biocyl. For Palccoat, although there are a few barnacles cannot be removed, the remaining surface is generally cleaner than Biocyl. For plain plate, the barnacles were unable to be removed through brushing.

Apart from visual observation, the weight difference before and after marine biofouling for each plate was also measured. It was found that the weight for plate with Biocyl increased by 10% due to fouling and the weight for plate with Palccoat increased

by 16% due to fouling. For the plain plate, the increment was a shocking 100% of the plate's original weight, which is 250g. These results show that an uncoated HATCT is unlikely to serve its designed lifespan if no anti-fouling coating is applied to protect it.

For the FBT and the two dummies, the selected coating was Biocyl due to its low weight difference and relatively low hard fouling compared to Palccoat. Figure 4.29 shows the picture of the dummies before putting into seawater. The purpose of the two dummies is to find out the growing pattern of marine bio-fouling over a turbine, for instance, which parts will have higher bio-fouling. Unfortunately, after 3 months, it was found that a net has covered both the dummies (as they are placed in close proximity to each other), as shown in Figure 4.30. Hence the bio-fouling rate has been affected by the presence of the net. Nevertheless, the bio-fouling over the turbines still can provide some clues.

Figure 4.26: Stainless steel plates for marine bio-fouling test after 1 day,
left (Biocyl), centre (Palccoat) and right (plain).

Figure 4.27: Stainless steel plates for marine bio-fouling after 90 days,
left (Biocyl), centre (Palccoat) and right (plain).

Figure 4.28: Cleaned stainless steel plates for marine bio-fouling,
left (Biocyl), centre (Palccoat) and right (plain).

Figure 4.29: Dummies turbine before the marine bio-fouling test,
left (coated), right (uncoated).

Figure 4.30: Dummies turbine after the the marine bio-fouling test,
left (coated), right (uncoated).

Figure 4.30 has clearly shown how ocean garbage can be trapped by turbine blades. This observation also suggests that provision of ducts or diffusers are not a favourable option for enhancement of power output. Figure 4.31 and Figure 4.32 show the dummies turbine after removing the net. Surprisingly, the uncoated dummy turbine was not fully covered with hard fouling, which is different from what was observed for plain stainless-steel plate. This may be due to the nature of different materials. But,

according to local fishermen, plastic resin has higher degree of getting fouled compared to steel. For the coated dummy, there were more barnacles attached to it.

Based on the observation from figure 4.31 and figure 4.32, it can be seen that along a blade, bio-fouling occur randomly at different position. But, close to the hub area, it was found that the presence of hard fouling is higher. This finding is quite similar to that of Kyozuka et al. (2014a), where they reported that the parts around hub has high tendency to have hard fouling even when anti-fouling coating has been applied. Figure 4.33 shows a close look to the hub area of coated dummy turbine.

Figure 4.31: Coated dummy turbine after the marine bio-fouling test, left (front), right (back).

On the other hand, for the 800mm FBT, the outcome is shown in Figure 4.34. For unknown reason, the coating on the turbine was washed away and left with minor soft fouling and hard fouling. It is believed that there may be some collision with ocean garbage during the period that causes scratches over turbine blade. The low occurrence of bio-fouling might be a result of the presence of the dummy turbines and the net, which serve as a sacrifice that provides better condition for marine bio-fouling activity. Additionally, the constant rotating motion may also have positive effects in minimizing the chance of getting fouled. Nevertheless, as the coating was obviously been disturbed

by unknown reason, the outcome of the 800mm FBT can only be taken as a reference. Unfortunately, no useful conclusion can be made from the bio-fouling study on the 800mm FBT.

Figure 4.32: Uncoated dummy turbine after the marine bio-fouling test, left (front), right (back).

Figure 4.33: Hub area of coated dummy, up (front), down (back).

The current bio-fouling study shows that a commercial anti-fouling coating may need a frequent cleaning to ensure a HATCT is free from marine bio-fouling, if a HATCT is to be deployed near to Pangkor Island. Judging from the 3 months period, a routine cleaning of one to one and a half month may be required. Such a frequent cleaning is apparently tedious. For a small scale HATCT, the recovery of HATCT is still considerably easy. For a large scale HATCT that is bigger than 2m, the maintenance work can be even tiring. This suggests a need for more effective anti-fouling coating or other measures to protect the performance of a HATCT.

Figure 4.34: The FBT after marine fouling test, left (front), right (back).

CHAPTER 5: CONCLUSION AND FUTURE REMARK

5.1 Conclusion for First Objective

The first objective of the current study is to run field test for a HATCT. The utilisation of a 800mm diameter five-bladed turbine modified from industrial axial ventilation fan as the turbine for the small scale HATCT in the current study has been proven to be successful. The FBT has been tested at Pangkor Island. It was observed that the FBT starts rotating when tidal current velocity is above 0.05m/s, but it only starts to rotate steadily when tidal current velocity is above 0.1m/s.

With the help of proper gearing between the shaft and generator, the small scale FBT can harness energy from a tidal current velocity ranges between 0.1m/s to 0.25m/s with an average efficiency of 30%. This is considerably good considering the turbine blade was initially an industrial axial ventilation fan. Hence, it is concluded that the current study has succeeded in achieving the first objective by succeeded in running field test for an operational small-scale five-bladed HATCT. Additionally, relevant information on the operation of a tidal current turbine in Malaysian water has been obtained.

5.2 Conclusion for Second Objective

The second objective of the current study is to study performance enhancement methods to improve the efficiency of HATCT. Two design modifications have been studied for this objective, which are the use of different gearing between shaft and generator and the use of hydrophobic coating.

The gearing of shaft and generator has been proven to be useful for the small scale five-bladed HATCT. However, the use of hydrophobic coating has shown limited impact. Although both the two hydrophobic coatings, namely Biocyl and Always Dry, used in the current study have shown positive effects on the L/D ratio of a hydrofoil, the magnitude was not big enough to give observable changes in the performance of turbine. The lab test on a 350mm diameter with hydrophobic coating on turbine blades showed improvement in RPM, but no noticeable changes in power coefficient. The reason was investigated by using numerical tools. It was found that to have a noticeable change on power coefficient, a drag reduction of 30% is required. As a result, hydrophobic coating has not been applied to the small-scale five-bladed HATCT.

Therefore, it is concluded that two potential methods have been tested to modify the performance of a small-scale five-bladed HATCTs. The scaling method has improved the power output of the small-scale FBT significantly. The hydrophobic coating method has also shown its positive effects on the performance of turbine. With the current state-of-the-art, more studies are required to establish better understanding on how to utilise the potential of hydrophobic coating on HATCT.

5.3 Conclusion for Third Objective

The third objective of the current study is to study and understands marine bio-fouling activity in Pangkor Island. The bio-fouling activity in Pangkor Island has been studied by using stainless steel plate and turbines. Stainless steel plates with/without anti-fouling coating have been put under water for 3 months to study bio-fouling activity on these plates. It was found that stainless steel plate without anti-fouling was fully covered by barnacles and its weight has doubled. For stainless steel plates coated with

anti-fouling coating, namely Biocyl and Palccoat, there were only a few barnacles attach on them while the rest of soft fouling can be removed by manual cleaning.

This observation is rather worrying as it shows standard commercial anti-fouling coatings currently available in the market could not provide sufficient protection for turbine blade for a period of more than 3 months. The current study also shows that the parts near to blade roots and hub have a higher tendency of getting fouled. Although fouling of those parts may not directly affect the hydrodynamic performance of turbine blades, it is still undesired. Hence, protection near to blade root is also required.

Viewing that a HATCT will surely stay under seawater much longer than 3 months, studies on other measures are required to address this bio-fouling issue. The prevention of hard fouling, growth of barnacles, is crucial as once barnacles grow, it is difficult to remove them without leaving physical damage on turbine blades. This study has confirmed that marine bio-fouling is a challenge for the operation of HATCTs in Malaysia. In order for an performance enhancement for HATCT to be effective, the pre-requisite is to provide the basic need for protection against bio-fouling. Without proper protection and maintenance measures, it is unlikely for an on-site tidal current turbine to maintain its performance.

5.4 Recommendation

The current study has shown that utilising HATCT to harness tidal current energy is workable in Malaysian water. Although tidal current velocity of the selected site in the current study is far lower than the desired 0.5m/s, the fabricated FBT still operates well and manage to generate power. Moving forward, there are many things that can be done to further improve the operation of the prototype FBT fabricated in the current study.

In future works, it is recommended to fabricate a specially designed turbine blade. This is particularly useful to improve the efficiency of turbine blade. Note that the FBT used in the current study is a modified from an industrial axial ventilation fan. A five-bladed turbine is till the preferable configuration for sites with tidal current velocity lower than 0.5m/s. For site with higher tidal current velocity, a three-bladed turbine is recommended. In order to harness more energy for Pangkor Island, a larger turbine blade can be used, for instance, a diameter of 1.0m or 1.5m. Otherwise, it would require more unit of the FBT to harness sufficient energy to generate usable electricity.

For the study on performance enhancement of a HATCT, although the use of hydrophobic coating has shown positive results, there is a need to identify methods to improve its effects. It is recommended to study and create a hydrophobic coating specifically designed for HATCT turbine blade. This would require knowledge on material synthesis and essentially can be another PhD study. Similar methods, which utilise friction drag reduction, can also be studied. For example, the use of air injection method to provide air layers to turbine blades' surface is a potential method.

Last but not least, continuous study on marine bio-fouling activity is required. This include identify the stress level on a particular site and identify better measure to protect turbine blade from getting fouled. Note that regular cleaning of turbine blade is labour intensive. Hence, a turbine blade that is free from marine bio-fouling is more desirable. As the current study shows that commercial anti-fouling paint may not be effective in providing protection, future study on making a special anti-fouling paint for HATCT and best measure to apply such coating is warrant.

References

Abundo, M. L. S., Nerves, A. C., Ang, M. R. C. O., Paringit, E. C., & Bernado, L. P. C. (2011). Energy Potential Metric for Rapid Macro-Level Resources Assessment of Tidal In-stream Energy in the Philippines. *Paper presented in the 10th International Conference on Environmental and Electrical Engineering (EEEIC), Rome, Italy, 8-11 May 2011.*

Adcock, T. A. A. (2012). On The Garrett & Cummins Limit. *Paper presented at Oxford Tidal Energy Workshop*, 29-30 March 2012 Oxford, UK. (Retrieved from: www.eng.ox.ac.uk.)

Adcock, T. A. A., Draper, S., Houlsby, G. T., Borthwick, A. G. L., & Serhadlioglu, S. (2013). The Available Power From Tidal Stream turbines in The Pentland Firth. *Proceedings of The Royal Society A*, *469*(2157).

Aljallis, E., Sarshar, M. A., Datla, R., Sikka, V., Jones V., & Choi, C. H. (2013). Experimental Study of Skin Friction Drag Reduction on Superhydrophobic Flat Plates in High Reynolds Number Boundary Layer Flow. *Physics of Fluids*, 25: 025103.

Avery, W. H., & Wu C. (1994). *Renewable Energy from The Ocean – A Guide to OTEC*. New York, NY: Oxford Univ. Press.

Bahaj, A. S., Batten, W. M. J., & McCann, G. (2007). Experimental Verifications of Numerical Predictions for the Hydrodynamic Performance of Horizontal Axis Marine Current Turbines. *Renewable Energy*, *32*(15): 2479-2490.

Bahaj, A. S., Molland, A. F., Chaplin, J. R., & Batten, W. M. J. (2007). Power and Thrust Measurements of Marine Current Turbines in a Cavitation Tunnel and a Towing Tank. *Renewable Energy*, *32*(3): 407-426.

Bahaj, A. S., Myers, L. E., & Thompson, G. (2007). Characterizing the Wake of Horizontal Axis Marine Currnet Turbines. *Paper presented in the 7th European Wave and Tidal Energy Conference, Porto, Portugal, 11-14 September   2007.* (Retrieved from www.gl-garradhassan.com).

Barltop, N., Varyani, K. S., Clelland, D., & Pham, X. P. (2007). Investigations Into Wave-Current Interactions in Marine Current Turbines. *Proceedings of The Institutions of Mechanical Engineer. Part A: Journal of Power and Energy, 221*(2): 233-242.

Basha, W. A., & Ghaly, W. S., (2007). Drag Prediction in Transitional Flow Over Airfoil. *Journal of Aircraft*, *44*(3): 824-832.

Batten, W. M. J., Bahaj, A. S., Molland, A. F., & Chaplin, J. R. (2007). Experimentally Validated Numerical Method for the Hydrodynamic Design of Horizontal Axis Tidal Turbines. *Ocean Engineering*, *34*(7): 1013-1020.

Bedard, R., Jacobson, P. T., Previsic, M., Musial, W., & Varley, R. (2010). An Overview of Ocean Renewable Energy Technologies. *Oceanography, 23*(2): 22-23.

Ben Elghali, S. E., Balme, R., Le Saux, K., Benbouzid, M. E. H, Charpentier, J. F., & Hauville, F. (2007). A Simulation Model for The Evaluation of The Electrical Power Potential Harnessed By A Marine Current Turbine. *IEEE Journal of Ocean Engineering, 32*(4): 786-797.

Ben Elghali, S. E., Benbouzid, M. E. H., Ahmed-Ali, T., & Charpentier, J. F. (2010). High-order Sliding Mode Control of a Marine Current Turbine Driven Doubly-fed Induction Generator. *IEEE Journal of Ocean Engineering*, *35*(2): 402-411.

Ben Elghali, S. E., Benbouzid, M. E. H., Ahmed-Ali, T., Charpentier, J. F., & Makri, F. (2008). High-Order Sliding Mode Control of DFIG-Based Marine Current Turbine. *Paper presented in the 34th Annual Conference of IEEE Industrial Electronics. Orlando, FL, USA, 10-13 November 2008*. 1228-1233. (Retrieved from hal.archives-ouvertes.fr).

Ben Elghali, S. E., Benbouzid, M. E. H., & Charpentier, J. F. (2009). Modelling and Control of A Marine Current Turbine-Driven Doubly Fed Induction Generator. *IET Renewable Power Generation*, *4*(1): 1-11.

Ben Elghali, S. E., Benbouzid, M. E. H., & Charpentier, J. F. (2010). Comparison of PMSG and DFIG for Marine Current Turbine Applications. *Paper presented in the XIX International Conference on Electrical Machines, Roma, Italy, 6-8 September 2010.*

Ben Elghali, S. E., Benbouzid, M. E. H., & Charpentier, J. F. (2011). Performance Comparison of Three- and Five-phase Permanent Magnet Generators for Marine Current Turbine Applications under Open-Circuit Faults. *Paper presented in the International Conference on Power Engineering Energy and Electrical Drivers (POWERENG), Istanbul, Turkey, 13-17 May 2011.*

Ben Elghali, S. E., Benbouzid, M. E. H., & Charpentier, J. F. (2012). Generator Systems for Marine Current Turbine Applications: A Comparative Study. *IEEE Journal of Ocean Engineering*, *37*(3):

Ben Elghali, S. E., Benbouzid, M. E. H., Charpentier, J. F., Ahmed-Ali, T., Gahery, J. M., & Denis, A. (2008). Modelling and MPPT Sensorless Control of a DFIG-Based Marine Current Turbine. *Paper presented in the 18th International Conference on Electrical Machines, Vilamoura, Portugal, 6-9 September 2008.* (Retrieved from hal.archives-ouvertes.fr).

Ben Elghali, S. E., Benbouzid, M. E. H., Charpentier, J. F., Ahmed-Ali, T., & Munteanu, I. (2011). Experimental Validation of a Marine Current Turbine Simulator: Application to a Permanent Magnet Synchronous Generator-based System Second-order Sliding Mode Control. *IEEE Transactions of Industrial Electronics, 58*(1): 118-126.

Blanchfield, J., Garrett, C., Rowe, A., & Wild, P. (2008). Tidal Stream Power Resource Assesment for Masset Sound, Haida Gwaii. *Proceedings of The Institutions of Mechanical Engineer. Part A: Journal of Power and Energy*, *222*(5): 485-492.

Blanchfield, J., Garrett C., Wild, P., & Rowe, A. (2008). The Extractable Power from A Channel Linking A Bay to The Open Ocean. *Proceedings of The Institutions of Mechanical Engineer. Part A: Journal of Power and Energy, 222*(3): 289-297.

Blunden, L. S., & Bahaj, A. S. (2006). Initial Evaluation of Tidal Stream Energy Resources at Portland Bill, UK. *Renewable Energy*, *31*(2): 121-132.

Blunden, L. S., & Bahaj, A. S. (2007). Tidal Energy Resources Assessment for Tidal Generators. *Proceedings of The Institutions of Mechanical Engineer. Part A: Journal of Power and Energy*, *221*(2): 137-146.

Blunden, L. S., Batten, W. M. J., Harrison, M. E., & Bahaj, A. S. (2009). Comparison of Boundary-Layer and Field Models for Simulation of Flow through Multiple Row Tidal Fences. *Paper presented in the 8th European Wave and Tidal Energy Conference, Uppsala, Sweden, 7-10 September 2009.* (Retrieved from eprints.soton.ac.uk)

Bonjean, F., & Lagerloef, G. S. E. (2002). Diagnostic Model and Analysis of the Surface Currents in the Tropical Pacific Ocean. *Journal of Physical Oceanography.*(Retrieved from http://oceanmotion.org/html/resources/oscar.htm 25 April 2015).

Bryden, I. G., & Couch, S. J. (2006). ME1-Marine Energy Extraction: Tidal Resource Analysis. *Renewable Energy*, *31*(2). 133-139.

Bryden, I. G. & Couch S. J. (2007). How Much Energy Can Be Extracted from Moving Water with A Free Surface: A Question of Importance In the Field of Tidal Current Energy? *Renewable Energy*, *32*(11): 1961-1966.

Bryden, I. G., Couch, S. J., Owen, A., & Melville, G. (2007). Tidal Current Resource Assessment. *Proceedings of The Institutions of Mechanical Engineer. Part A: Journal of Power and Energy, 221*(2): 125-135.

Bryden, I. G., Grinsted, T., & Melville, G. T. (2004). Assessing the Potential of A Simple Tidal Channel to Deliver Useful Energy. *Applied Ocean Research*, *26*(5): 198-204.

Bryden, I. G., & Melville, G. T. (2004). Choosing and Evaluating Sites for Tidal Current Development. *Proceedings of The Institutions of Mechanical Engineer. Part A: Journal of Power and Energy*, *218*(8): 567-577.

Busse, A., Sandham, N. D., McHale, G., & Newton, M. I. (2013). Change in drag, apparent slip and optimum air layer thickness for laminar flow over an idealised superhydrophobic surface. *Journal of Fluid Mechanics*, *727*: 488-508.

Carballo, R., Iglesias, G., & Castro, A. (2009). Numerical Model Evaluation of Tidal Stream Energy Resources in the Ria de Muros (NW Spain). *Renewable Energy*, *34*(6): 1517-1524.

Çengel, Y.A., & Cimbala, J.M. (2010). *Fluid Mechanics: Fundamentals and Applications*. *2nd Ed.* New York: McGraw-Hill.

Chen, H., Ait-Ahmed, N., Zaim, E. H., & Machmoum, M. (2012). Tidal Current systems: State of The Art. *Paper presented in the 2012 IEEE International Symposium on Industrial Electronics (ISIE), Hanzhou, China, 28-31 May 2012.* Pp.1431-1437.

Clarke, J. A., Connor, G., Grant, A. D., & Johnstone C. M. (2007). Design and Testing of a Contra-rotating Tidal Current Turbine. *Proceedings of The Institutions of Mechanical Engineer. Part A: Journal of Power and Energy*, *221*(2): 171-179.

Clarke, J. A., Connor, G., Grant, A. D., Johnstone, C. M., & Mackenzie D. (2007). Development of a Contra-Rotating Tidal Current Turbine and Analysis of Performance. *Paper presented in the 7th European Wave and Tidal Energy Conference, Porto, Portugal, 11-14 September 2007.* (Retrieved from strathprints.strath.ac.uk/6688/)

Clarke, J. A., Connor, G., Grant, A. D., Johnstone, C. M., & Ordenez-Sanchez, S. (2008). Contra-Rotating Marine Current Turbines: Performance in Field Trials and Power Train Developments. *Paper presented in the 10th World Renewable Energy Congress, Glasglow, UK, 19-25 July 2008.* (Retrieved from: strathprints.strath.ac.uk/8054/)

Clarke, J. A., Connor, G., Grant, A. D., Johnstone, C. M., & Ordenez-Sanchez, S. (2010). Analysis of a Single Pont Tensioned Mooring System for Station Keeping of a Contra-Rotating Marine Current Turbines. *IET Renewable Power Generation*, *4*(6): 473-487.

Coiro, D. P., Masito, U., Scherillo, F., Melone, S., & Grasso, F. (2006). Horizontal Axis Tidal Current Turbine: Numerical and Experimental Investigations. *Paper presented in the Offshore Wind and Other Marine Renewable Energies in Mediteranean and European Seas, European Seminar*, Rome, Italy, April 2006. (Retrieved from http://192.107.92.31/test/owemes/33.pdf).

Couch, S. J., & Bryden, I. G. (2004). The Impact of Energy Extraction on Tidal Flow Development. *Paper presented in the 3rd International Conference on Marine Renewable Energy,* Blyth, UK, 7-9 July 2004. (Retrieved from http:// tethys.pnnl.gov/sites/default/files/publications/Impact_Tidal_Energy_Extraction. pdf).

Couch, S. J., & Bryden, I. G. (2006). Tidal Current Energy Extraction: Hydrodynamic Resource Characteristics. *Proceedings of The Institutions of Mechanical Engineer. Part M: Journal of Engineering for the Maritime Environment, 220*(4): 185-194.

Couch, S. J., & Bryden, I. G. (2007). Large-Scale Physical Response of the Tidal System to Energy Extraction and Its Significance for Informing Environmental and Ecological Impact Assessment. *OCEANS 2007-Europe.*

Cresswll, N. W., Ingram, G. L., & Dominy, R. G. (2015). The Impact of Diffuser Augmentation on a Tidal Stream Turbine. *Ocean Engineering*, *108*: 155-163.

Daniello, R. J. (2013) *Experimental studies of superhydrophobic surfaces in flow*. Doctoral Dissertations Available from Proquest. (Retrieved from: http://scholarworks.umass.edu/dissertations/AAI3603073)

Defne, Z., Haas, K. A., & Fritz, H. M. (2011). Numerical Modelling of Tidal Currents and the Effects of Power Extraction on Estuarine Hydrodynamics along the Georgia Coast, USA. *Renewable Energy*, *36*(12): 3461-3471.

Draper, S., Adcock, T. A. A., Borthwick, A. G. L., & Houlsby, G. T. (2014). A Note on The Power Potential of Tidal Currents in Channels. *International Journal of Marine Energy*, *6*: 1-17.

Drew, B., Plummer, A. R., & Sahinkaya, M. N. (2009). A Review of Wave Energy Converter Technology. *Proceedings of The Institutions of Mechanical Engineer. Part A: Journal of Power and Energy, 223*(8): 887-902.

Drouen, L., Charpentier, J. F., Semail, E., & Clent, S. (2007). Study of an Innovative Electrical Machines Fitted to Marine Current Turbines. *Paper Presented in the OCEANS 2007-EUROPE, Aberdeen, UK, 18-21 June 2007.*

Eleni, D. C., Athanasios, T. I., & Dionissios, M. P. (2012). Evaluation of The Turbulence Models for The Simulation of The Flow Over a National Advisory Committee for Aeronautics (NACA) 0012 Airfoil. *Journal of Mechanical Engineering Research, 4*(3): 100-111.

Ensikat, H. J., Ditsche-Kuru, Neinhuis, C., & Barthlott, W. (2011). Superhydrophobicity in Perfection: The Outstanding Properties of The Lotus Lead. *Journal of Nanotechnology*, *2*(19): 152-161.

Fraenkel, P. L. (2002). Power from Marine Currents. *Proceedings of the Institution of Mechanical Engineers Part A: Journal of Power and Energy, 216*(1): 1-14.

Fluent User's Guide. Available from (Retrieved from http://148.204.81.206/Ansys/150/ANSYS%20Fluent%20Users%20Guide. pdf.).

Galloway, P. W., Myers, L. M., & Bahaj, A. S. (2014). Quantifying Wave and Yaw Effects on A Scale Tidal Stream Turbine. *Renewable Energy*, *63*: 297-307.

Garrett, C., & Cummins, P. (2004). Generating Power from Tidal Current. *Journal of Waterway, Port, Coastal, Ocean Engineering, 130*(3): 114-118.

Garrett, C., & Cummins, P. (2005). The Power Potential of Tidal Currents in Channels. *Proceedings of The Royal Society A*, *461*(2060): 2563-2572.

Garrett, C., & Cummins, P. (2007). The Efficiency of A Turbine In A Tidal Channel. *Journal of Fluids Mechanics, 588*: 243-251.

Garrett, C., & Cummins, P. (2008). Limits to Tidal Current Power. *Renewable Energy*, *33*(11): 2485-2490.

Gogte, S., Vorobieff, R., Truesdell, R., Mammoli, A., Swol, F., Shah, P. & Brinker, C.J., (2005). Effective slip on textured superhydrophobic surfaces. *Physic of Fluids*, *17*: 051701.

Grabbe, M., Lalander, E., Lundin, S., & Leijon, M. (2009). A Review of the Tidal Current Energy Resources in Norway. *Renewable & Sustainable Energy Reviews*, *13*(8): 1898-1909.

Gruber, T., Murray, M. M., & Fredriksson, D. W. (2011). Effect of Humpback Whale Inspired Tubercles on Marine Tidal Turbine Blades. *Paper presented in ASME 2011 International Mechanical Engineering Congress and Exposition. Denver, Colorado, USA, 11-17 November, 2011.*

Hong, G. H., Zhang, B. P., Glabman, S., Uzal, N., Dou, X. M., Zhang, H. G.,… Chen ,Y. S. (2015). Potential Ion Exchange Membranes and System Performance in Reverse Electrodialysis for Power Generation: A Review. *Journal of Membrane Science*, *486*(15): 71-88.

Hou, F., Bao, X., Li, B., & Liu, Q. (2015). The Assessment of Extractable Tidal Energy and the Effect of Tidal Energy Turbine Deployment on the Hydrodynamics in Zhoushan. *Acta Oceanologica Sinica*, *34*(5): 86-91.

Huang, B., & Kanemoto, T. (2015). Multi-objective Numerical Optimization of the Front Blade Pitch Angle Distribution in a Counter-Rotating Type Horizontal-axis Tidal Turbine. *Renewable Energy*, *81*: 837-844.

Jeffcoate, P., Whittaker, T., Boake, C., & Elsaesser, B. (2016). Field Tests of Multiple 1/10 Scale Tidal Turbines in Steady Flows. *Renewable Energy*, *87*: 240-252.

Jiang, G. C., Xin, S. C., & Wu, C. W. (2011). Drag Reduction of A Miniature Boat with Superhydrophobic Grille Bottom. *AIP Advances*, *1*: 032148.

Jo, C. H., Lee, K. H., Lee, J. H., & Nichita, C. (2011). Wake Effect on HAT Tidal Current Power Device Performance. *International Journal of Ocean System Engineering, 1*(3): 144-147.

Jo, C. H., Lee, K. H., Yim, J. Y., & Rho, Y. H. (2011). Interaction Effect Analysis for Tidal Current Power Farm Feasibility Study Applied to Projects in Korea. *Paper presented in the 9th European Wave and Tidal Energy Conference, Southampton, UK, 5-9 September 2011.* (Retrieved from www.see.ed.ac.uk).

Jo, C. H., Yim, J. Y., Lee, K. H., & Rho, Y. H. (2012). Performance of Horizontal Axis Tidal Current Turbine by Blade Configuration. *Renewable Energy*, *42*: 195-206.

Karsten, R. H., McMillan, J. M., Lickley, M. J., & Haynes, R. D. (2008). Assessment of Tidal Current Energy in the Minas Passage, Bay of Fundy. *Proceedings of the Institution of Mechanical Engineers Part A: Journal of Power and Energy, 222*(5): 493-507.

Kyozuka, Y., Ida, M., Katsuyama, I., Kobayashi, S., & Igawa, S. (2014). Study on Marine Biofouling Effects on Tidal Power Generator. *Paper presented in the 24th Ocean Engineering Symposium, Japan, March 13-14, 2014.*

Kyozuka, Y., Kobayashi, S., Katsuyama, I., Ida, M., & Igawa, S. (2014). Study on Biofouling on Test Plates in Strong Tidal Current. *Paper presented in the proceedings of the Japan Spciety of Naval Architects and Ocean Engineers*, Japan, *November 20-21, 2014 .*

Lawn, C. J. (2003). Optimization of the Power Output from Ducted Turbines. *Proceedings of The Institutions of Mechanical Engineer. Part A: Journal of Power and Energy*, *217*(1): 107-117.

Lee, N. J., Kim, I. C., Kim, C. G., Hyun, B. S., & Lee, Y. H. (2015). Performance Study on a Counter-Rotating Tidal Current Turbine by CFD and Model Experimentation. *Renewable Energy*, *79*: 122-126.

Li, H. J., Wu, G. X., Liang, B. C., & Fei, F. (2012). Numerical Assessment of Tidal Stream Energy Resource in Langyatai Strait. *Paper presented in the OCEANS 2012 Yeosu, Korea, 21-24 May 2012.*

Lim, Y. S., & Koh, S. L. (2010). Analytical Assessments on The Potential of Harnessing Tidal Currents for Electricity Generation in Malaysia. *Renewable Energy*, *35*(5): 1024-1032.

Lin, J., Sun, J., Liu, L., Chen, Y., & Lin, B. (2015). Refined Represntation of Turbines Using a 3D SWE model for Predicting Distributions of VelocityDeficit and Tidal Energy Density. *International Journal of Energy Research*, *39*(13): 1828-1842.

MacEnri, J., Reed, M., & Thiringer, T. (2013). Influence of Tidal Parameters on SeaGen Flicker Performance. *Philosophical Transactions of Royal Society A: Mathematical, 371*(1985). 20120247.

MacLeod, A. J., Barnes, S., Rados, K. G., & Bryden, I. G. (2001). Wake Effects in Tidal Current Turbine Farms. *Paper presented in the Marine Renewable Energy Conference, Newcastle, UK, 27-28 March 2001.* (Retrieved from tethys.pnnl.gov).

Maganga, F., Germain, G., King, J., Pinon, G., & Rivoalen, E. (2009). Experimental Study to Determine Flow Characteristic Effects on Marine Current Turbine Behaviour. *Paper presented in the 8th European Wave and Tidal Energy Conference, Uppsala, Sweden, 7-10 September 2009.* (Retrieved from archimer.ifremer.fr).

Maganga, F., Germain, G., King, J., Pinon, G., & Rivoalen, E. (2010). Experimental Characterisation of Flow Effects on Marine Current Turbine Behaviour and on its Wake Properties. *IET Renewable Power Generation, 4*(6): 498-509.

Maganga, F., Gregory, P., Grégory, P., & Elie, R. (2008). Numerical Characterisation of the Wake Generated by Marine Current Turbines Farm. *Paper presented in the*

2nd International Conference on Ocean Energy, Brest, France, 15-17 October 2008. (Retrieved from archimer.ifremer.fr).

Maganga, F., Pinon, G., Germain, G., & Rivoalen, E. (2008). Numerical Simulation of the Wake of Marine Current Turbine with a Particle Method. *Paper presented in the 10th World Renewable Energy Congress, Glasglow, UK, 19-25 July 2008.* (Retrieved from archimer.ifremer.fr).

Manwell, J. F., McGowan, J. G., & Rogers, A. L. (2009). *Wind Energy Explained: Theory, Design and Application. 2nd Ed.* New Jersey :Wiley-Blackwell.

Martin, H. (2014). *JAVAFOIL User's Guide Contents.* (Retrieved from http://www.mh-aerotools.de/airfoils/javafoil.htm).

McCann, G. N. (2007). Tidal Current Turbine Fatigue Loading Sensitivity to Waves and Turbulence- A Parametric Study. *Paper presented in the 7th European Wave and Tidal Energy Conference, Porto, Portugal, 11-14 September 2007.* (Retrieved from www.gl-garradhassan.com).

Mekri, F., Ben Elghali, S. E., Benbouzid, M. E. H., & Charpentier, J. F. (2011). A Fault-Tolerant Multiphase Permanent Magnet Generator for Marone Current Turbine Applications. *Paper Presented in the 20th IEEE International Symposium on Industrial Electronics (ISIE), Gdansk, Poland, 27-30 June 2011.* (Retrieved from: hal.archives-ouvertes.fr)

Milne, I. A., Day, A. H., Sharma, R. N., Flay, R. G. J., & Bickerton, S. (2011). Tidal Turbine Blade Load Experiments for Oscillatory Motion. *Paper presented in the 9th European Wave and Tidal Energy Conference, Southampton, UK, 5-9 September 2011.* (Retrieved from: strathprints.strath.ac.uk/43575).

Mirzaei, A., Tangang, F., & Liew, J. (2014). Wave Energy Potential along the East Coast of Peninsular Malaysia. *Energy*, *68*(15): 722-734.

Mycek, P., Gaurier, B., Germain, G., Pinon, G., & Rivoalen, E. (2013). Numerical Experimental Study of the Interaction between Two Marine Current Turbines. *International Journal of Marine Energy*, *1*: 70-83.

Myers, L. E., & Bahaj, A. S. (2007). Wake Studies of a 1/30th Scale Horizontal Axis Marine Current Turbine. *Ocean Engineering*, *34*(5-6): 758-762.

Myers, L. E., & Bahaj, A. S. (2009). Near Wake Properties of Horizontal Axis Marine Current Turbine. *Paper presented in the 8th European Wave and Tidal Energy Conference, Uppsala, Sweden, 7-10 September 2009.* (Retrieved from eprints.soton.ac.uk)

Myers, L. E., & Bahaj, A. S. (2010). Experimental Analysis of The Flow Field around Horizontal Axis Tidal Turbines by Use of Scale Mesh Disk Rotor Simulators. *Ocean Engineering*, *37*(2-3): 218-227.

Myers, L. E., & Bahaj, A. S. (2012). An Experimental Investigation Simulating Flow Effects in First Generation Marine Current energy Converter Arrays. *Renewable Energy*, *37*(1): 28-36.

Myers, L. E., Keogh, B. & Bahaj, A. S. (2011). Experimental Investigation of Inter-array wake properties in Early Tidal Turbine Arrays. *Paper presented in the OCEANS 2011, Waikoloa, HI, USA, 19-22 September 2011.* (Retrieved from ieeexplore.ieee.org)

Myers, L. E., Bahaj, A. S., & Germain, G. (2008). Flow Boundary Interaction Effects for Marine Current Energy Conversion Devices. *Paper presented in the 10th World Renewable Energy Congress, Glasglow, UK, 19-25 July 2008.* (Retrieved from eprints.soton.ac.uk.

Myers, L. E., Bahaj, A. S., Rawlinson-Smith, R. I., & Thomson, M. (2008). The Effects of Boundary Proximity upon the Wake Structure of Horizontal Axis Marine Current Turbines. *Paper presented in the Proceedings of 27th International Conference on Offshore Mechanics and Arctic Engineering, Estoril, Portugal, 15-20 June 2008.* (Retrieved from archimer.ifremer.fr)

National Geospatial-intelligence Agency. (2005). *Sailing Directions (planning guide) South Atlantic Ocean and Indian Ocean.* Culver City, CA: Prostar Pubns 2005.

Ng, K. W., Lam, W. H., & Ng, K. C. (2013). 2002-2012: 10 Years of Research Progress in Horizontal-Axis Marine Current Turbines. *Energies*, *6*(3): 1497-1526.

Ng, K. W., Lam, W. H. & Saravanan, P. (2013). A Review on Potential Applications of Carbon Nanotubes in Marine Current Turbines. *Renewable and Sustainable Energy Reviews, 28*: 331-339.

O'Rourke, F., Boyle, F., & Reynolds, A. (2010). Tidal Current Energy Resource Assessment in Ireland: Current Status and Future Update. *Renewable & Sustainable Energy Reviews*, *14*(9): 3206-3212.

OES-IA. (2010). Annual Report 2010 Implementing Agreement on Ocean Energy Systems. Retrieved from: www.ocean-energy-systems.org/library/annual_reports/.

OES-IA. (2011). Annual Report 2011 Implementing Agreement on Ocean Energy Systems. Retrieved from: www.ocean-energy-systems.org/library/annual_reports/.

OES-IA. (2012). Annual Report 2012 Implementing Agreement on Ocean Energy Systems. Retrieved from: www.ocean-energy-systems.org/library/annual_reports/.

OES-IA. (2013). Annual Report 2013 Implementing Agreement on Ocean Energy Systems. Retrieved from: www.ocean-energy-systems.org/library/annual_reports/.

Orme, J. A. C., Masters, I. & Griffiths, R. T. (2001). Investigation of the Effect of Biofouling on the Efficiency of the Marine Current Turbines. *Paper presented in*

the Marine Renewable Energy Conference, Newcastle, UK, 27-28 March 2001. (Retrieved from: swanturbines.co.uk).

Ou, J. & Rothstein, J. P. (2005). Direct velocity measurements of the flow past drag-reducing ultrahydrophobic surfaces. *Physic of Fluids*, *17*: 103606.

Park, H. W., Park, H. M., & Kim, J. (2013). A numerical study of the effects of superhydrophobic surface on skin-friction drag in turbulent channel flow. *Physic of Fluids*, *25*: 110815.

Pauly, D., & Martosubroto, P. (1996). *Baseline Studies of Biodiversity: The Fish Resources of Western Indonesia.* Makati City, Philippines: Internaional Center for Living Aquatic Resources Management.

Pinon, G., Mycek, P., Germain, G., & Rivoalen, E. (2012). Numerical Simulation of the Wake of Marine Current Turbines with a Particle Method. *Renewable Energy*, *46*: 111-126.

Polagye, B. Kawase, M., & Malte, P. (2009). In-stream Tidal Energy Potential of Puget Sound, Washinton. *Proceedings of the Institution of Mechanical Engineers Part A: Journal of Power and Energy, 223*(5): 571-587.

Prickett, P., Grosvenor, R., Byrne, C., Jones, A. M., & Morris, C. (2011). Consideration of the Condition Based Maintenance of Marine Tidal Turbines. *Paper presented in the 9th European Wave and Tidal Energy Conference, Southampton, UK, 5-9 September 2011.* (Retrieved from: orca.cf.ac.uk/26111/.

Rocks, L., & Runyon, R. P. (1972). *The Energy Crisis*. New York, NY: Crown Publishers 2009.

Rothstein, J. P. (2010). Slip on Superhydrophobic Surfaces. *Annual Review of Fluid Mechanics*, *42*: 89-109.

Searchinger, T., Heimlich, R., Houghton, R. A., Dong, F. X., Elobeid, A., Fabiosa, J., …Yu, T. H. (2008). Use of U.S. Croplands for Biofuels Increases Greenhouse Gases Through Emissions from Land-use Change. *Science*, *319*(5867): 1238-1240.

Setoguchi, T., Shiomi, N., & Kaneko, K. (2004). Development of Two-way Diffuser for Fluid Energy Conversion System. *Renewable Energy*, *29*(10): 1757-1771.

Shives, M., & Crawford, C. (2010). Overall Efficiency of Ducted Tidal Current Turbines. *Paper presented in the OCEANS 2010, Seattle, WA, USA, 20-23 September 2010.*

Shives, M., & Crawford, C. (2012). Developing an Empirical Model for Ducted Tidal Turbine Performance using Numerical Simulation Results. *Proceedings of The Institutions of Mechanical Engineer. Part A: Journal of Power and Energy*, *226*(1): 112-125.

Slutherland, G., Foreman, M., & Garrett, C. (2007). Tidal Current Energy Assessment for Johnson Strait, Vancouver Island. *Proceedings of The Institutions of Mechanical Engineer. Part A: Journal of Power and Energy, 221*(2): 147-157.

Sousounis, M. C., Shek, J. K. H., Crozier, R. C., & Mueller, M. A. (2015). Comparison of Permanent Magnet and Induction Generator for a Tidal Current Conversion System with Onshore Converters. *Paper presented in the IEEE International Conference on Industrial Technology (ICIT), 17=19 March 2015, Seville, Spain.* 2481-2486.

Stallard, T., Collings, R., Feng, T., & Whelan, J. I. (2013). Interaction Between Tidal Turbine Wakes: Experimental Study of a Group of 3-Bladed Rotors. *Philosophical Transactions of Royal Society A*, *371*(1985):

The Switch. (20 March 2014). *PMG vs DFIG – The Big Generator Technology Debate*. (Retrieved from: http://www.theswitch.com/wp-content/uploads/2014/03/Technology_Point-_PMG_DFIG_06032014.pdf)

Vennell, R. (2010). Tuning Turbines in a Tidal Channel. *Journal of Fluid Mechanics, 663*: 253-267.

Vennell, R. (2011). Estimating The Power of Tidal Currents and The Impact of Power Extraction on Flow Speeds. *Renewable Energy*, *36*(12): 3558-3565.

Vennell, R. (2011). Tuning Tidal turbines In-concert to Maximise Farm Efficiency. *Journal of Fluid Mechanics*, *671*: 587-604.

Vennell, R. (2012). Realizing The Potential of Tidal Currents and The Efficiency of Turbine Farms In A Channel. *Renewable Energy*, *47*: 95-102.

Vennell, R. & Adcock, T. A. A. (2014). Energy Storage Inherent in Large Tidal Turbine Farms. *Philosophical Transactions of the Royal Society A: Mathematical and Physical Sciences, 470*(2166).

Walker, J. M., Flack, K. A., Lust, E. E., Schultz, M. P., & Luznik, L. (2014). Experimental and Numerical Studies of Blade Roughness and Fouling on Marine Current Turbine Performance. *Renewable Energy*, *66*: 2557-267.

Winter, A. I. (2011). Difference in Fundamental Design Drivers for Wind and Tidal Turbines. *Proceedings of the IEEE OCEANS: 2011, June 6-9; Santander, Spain. 1-10*.

Whelan, J. I., & Stallard, T. (2011). Arguments for Modifying the Geometry of A Scale Model Rotor. *Paper presented in the 9th European Wave and Tidal Energy Conference, Southampton, UK, 5-9 September 2011*. (Retrieved from gl-garradhassan.com).

Work, P. A., Haas, K. A., Defna, Z., & Gay, T. (2013). Tidal Stream Energy Site Assessment via Three-dimensional Model and Measurements. *Applied Energy*, *102*: 510-519.

Xia, J., Falconer, R. A., & Lin, B. (2010). Numerical Model Assessment of Tidal Stream Energy Resources in the Severn Estuary, UK. *Proceedings of The Institutions of Mechanical Engineer. Part A: Journal of Power and Energy*, *224*(7): 969-983.

Internet reference:

- (URL-http://www.tgepower.com/), 24/4/2015

- (URL-http://www.mima.gov.my/), 24/4/2015

- (URL-http://www1.american.edu/ted/malacca.htm/), 25/4/2015

- (URL-http://www.nanocyl.com/), 15/6/2015

- (URL-http://nanexcompany.eu/), 7/7/2015

APPENDIX A

ENGINEERGIN DRAWINGS OF SMALL SCALE TURBINE CASING
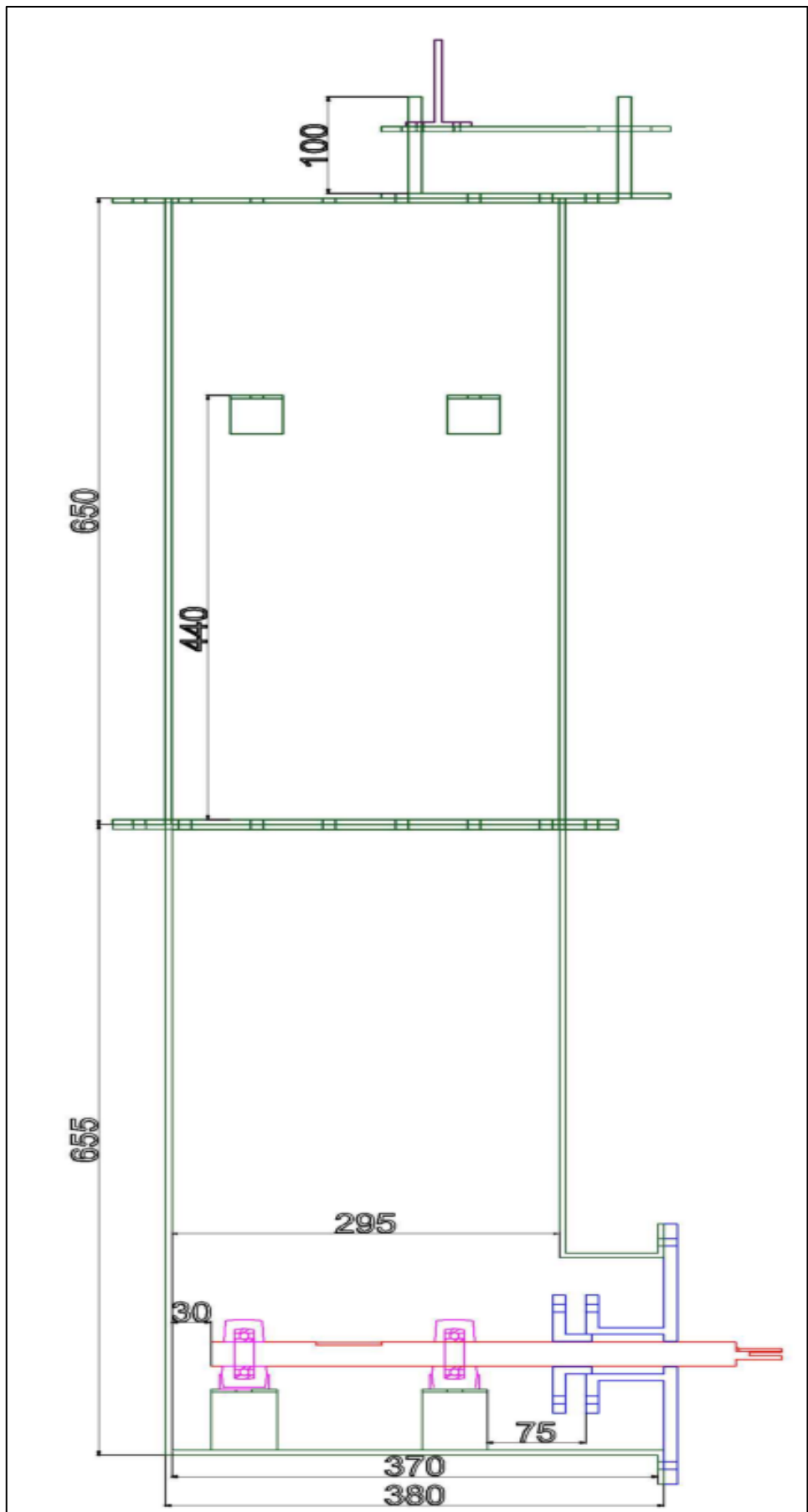
Fig. A1: Full assemble of casing.
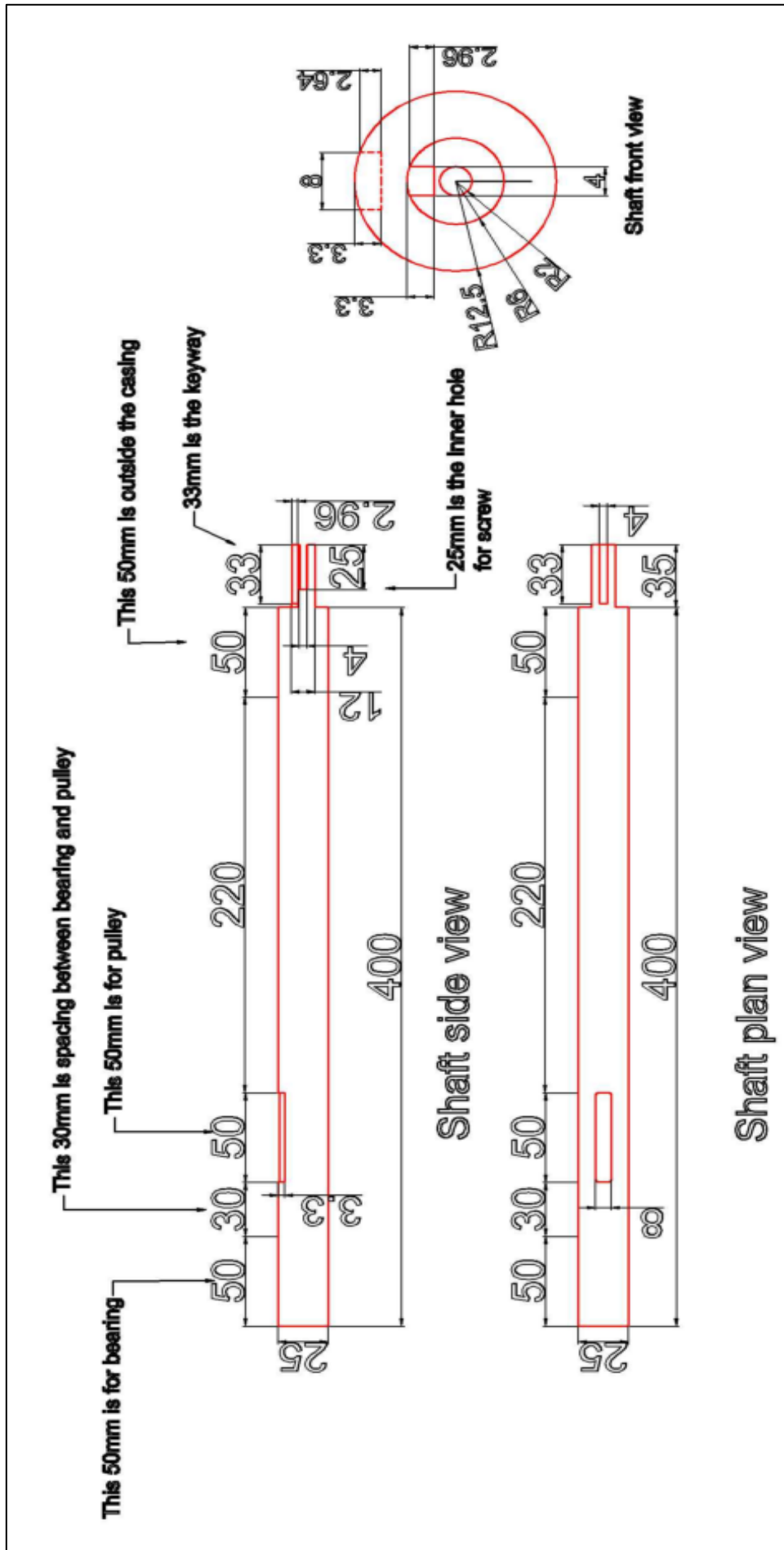
Fig. A2: Shaft.

Fig. A3: Stuffing box.
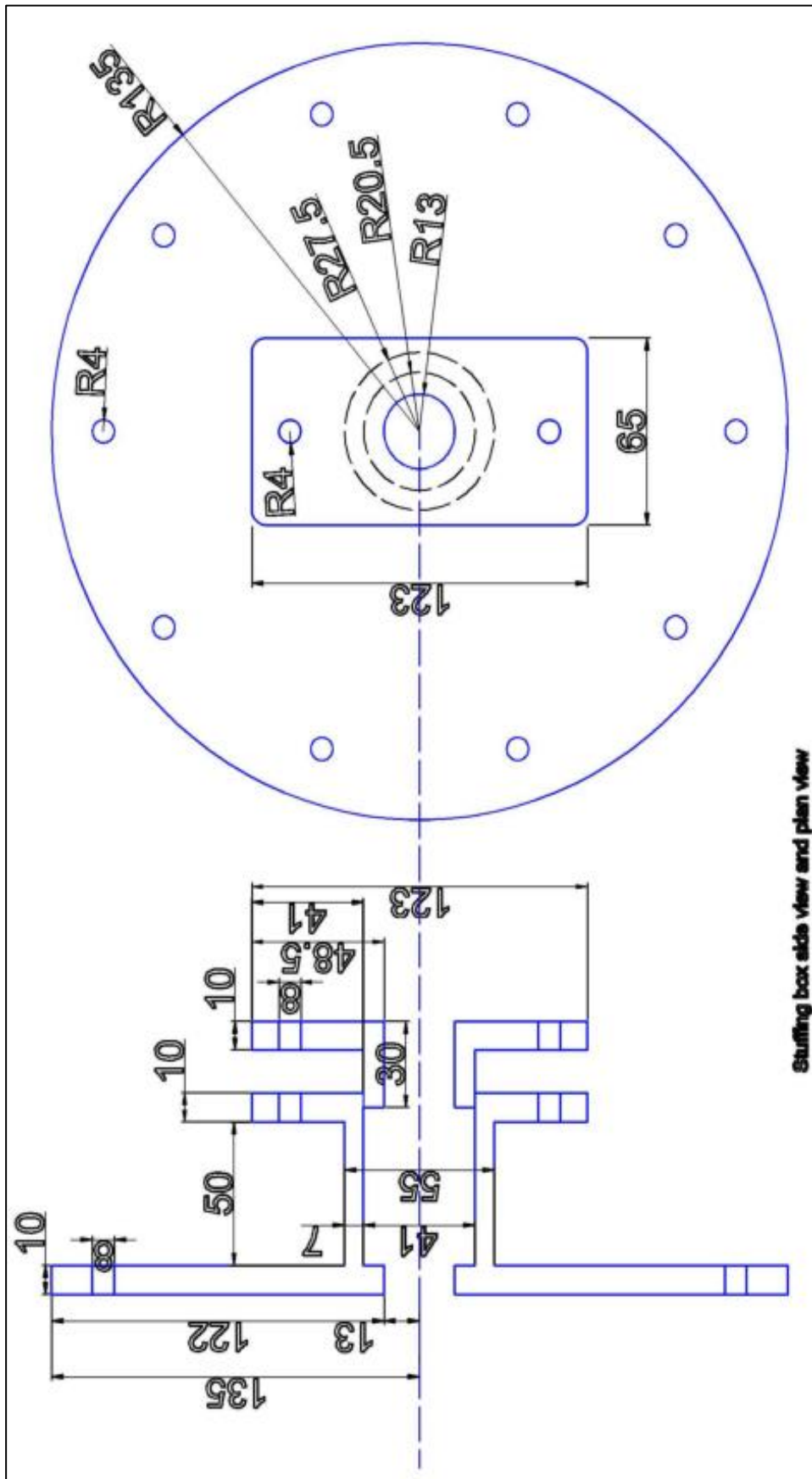
Fig. A4: Side view of bottom casing.
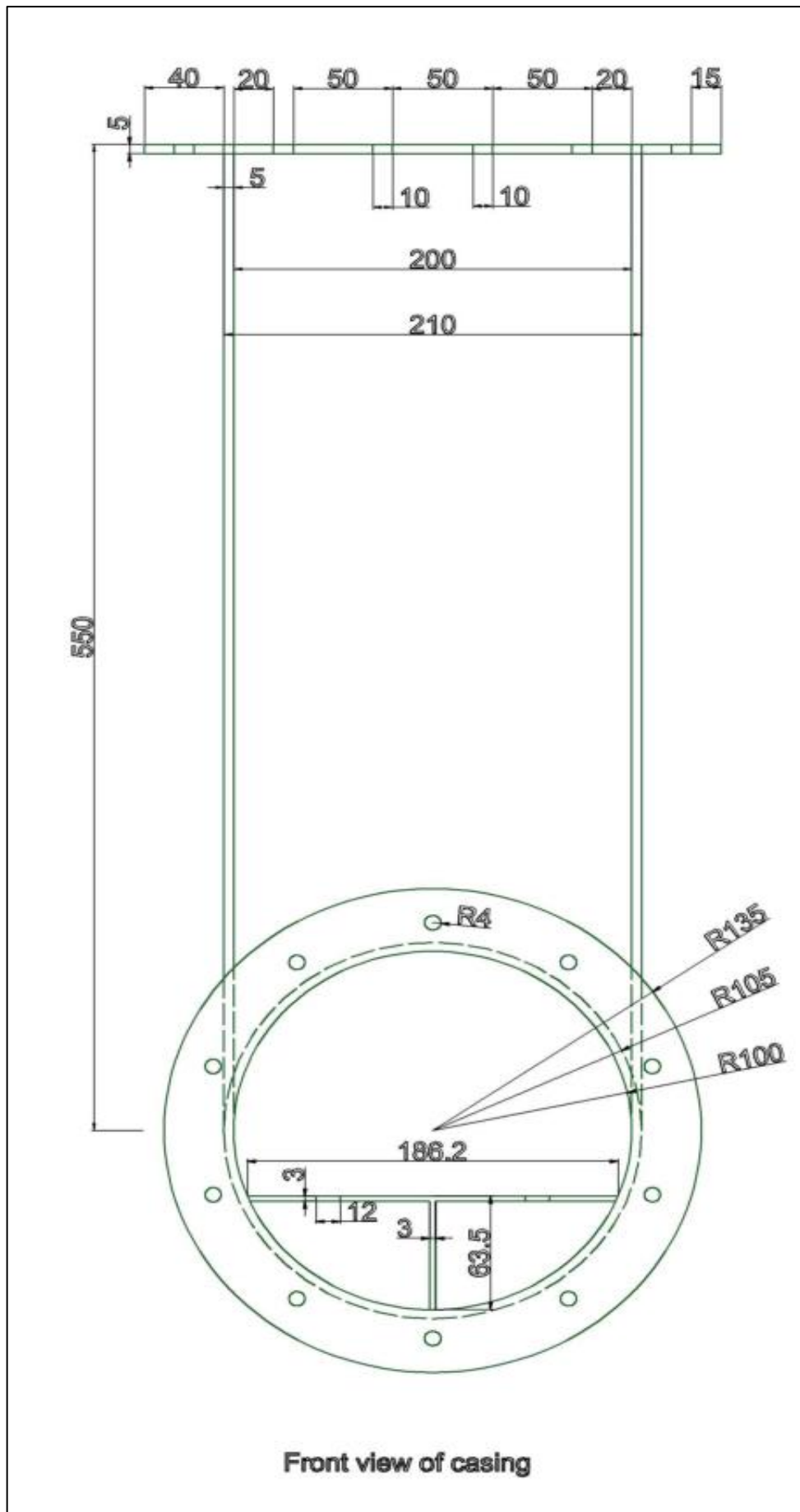
Fig. A5: Front view of bottom casing.
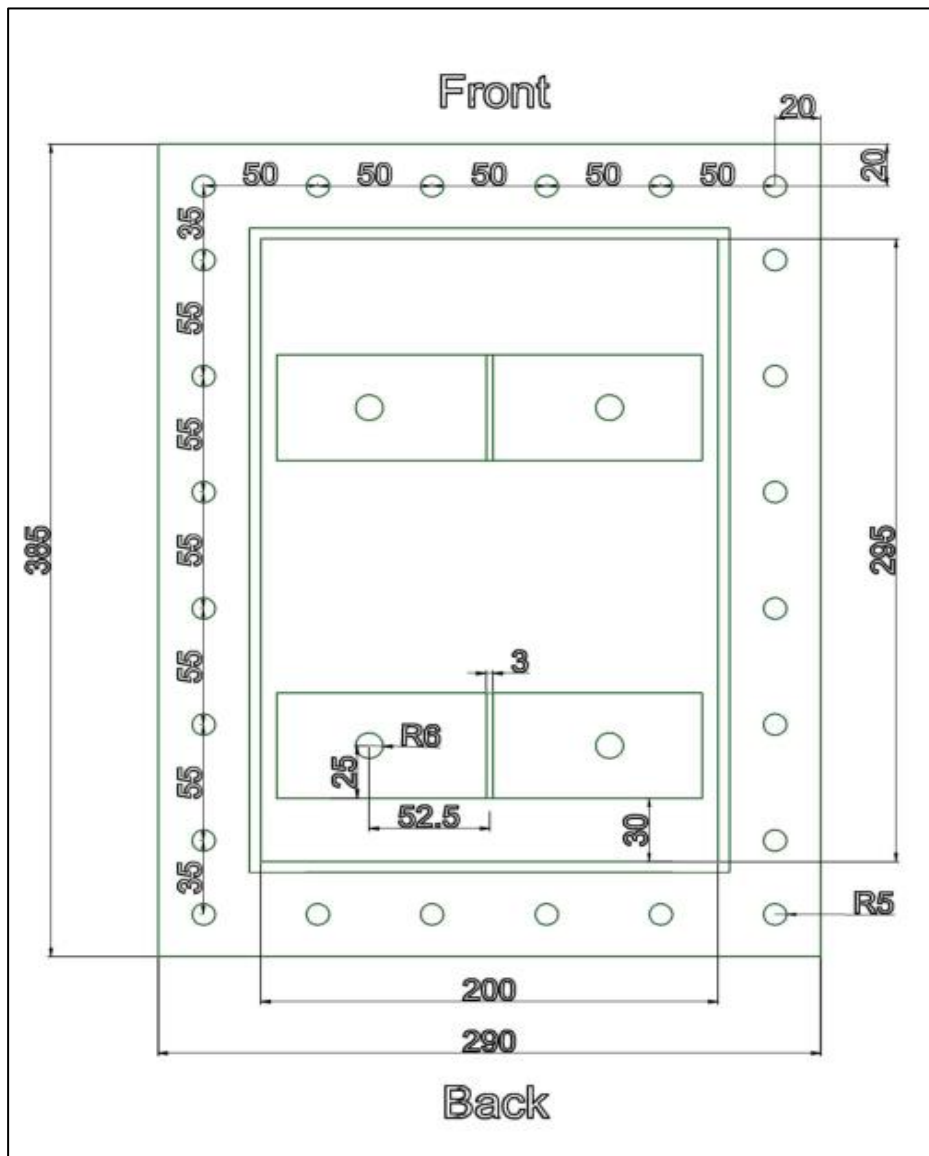
Fig. A6: Plan view of bottom casing.
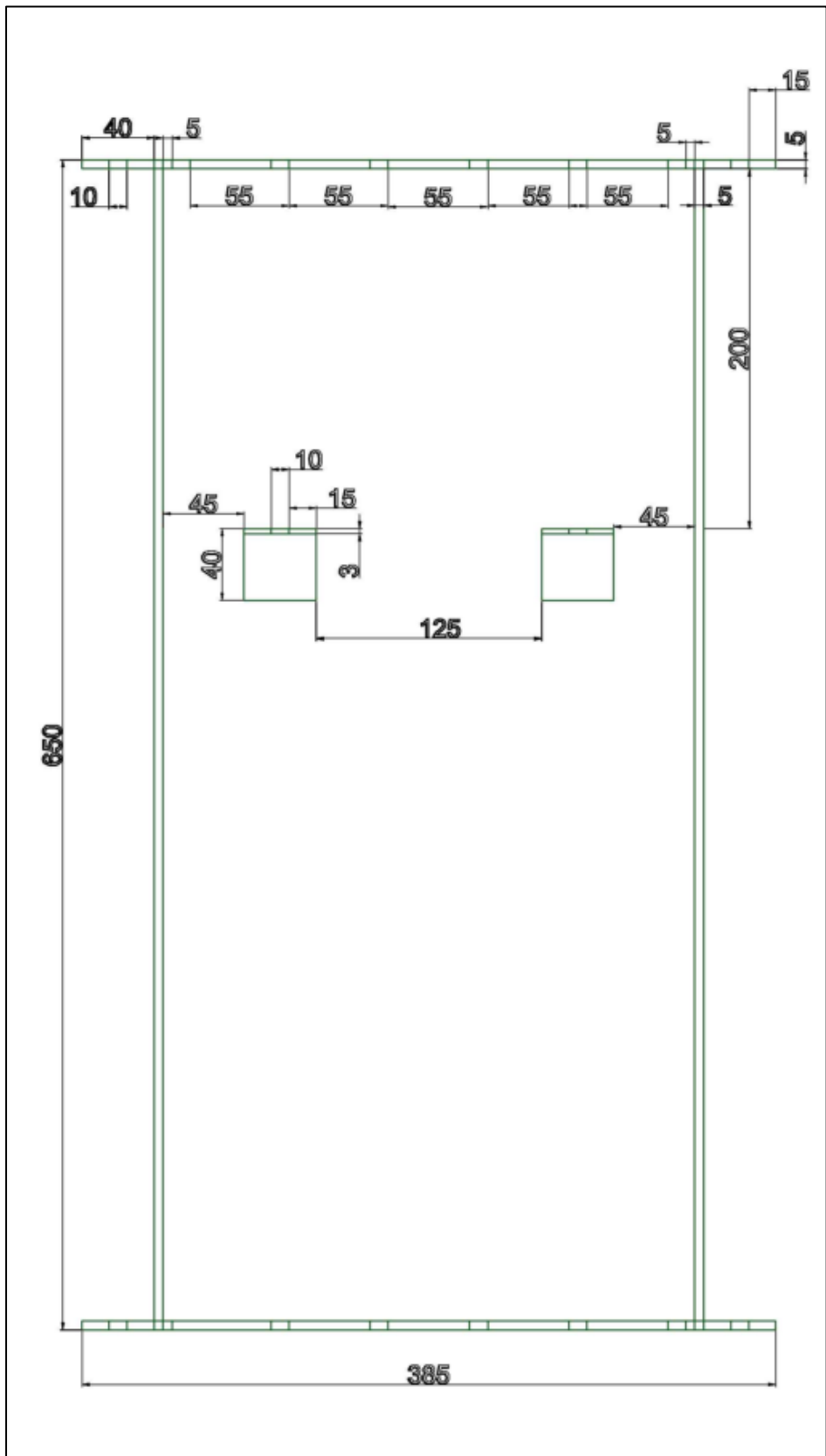
Fig. A7: Side view of top casing.
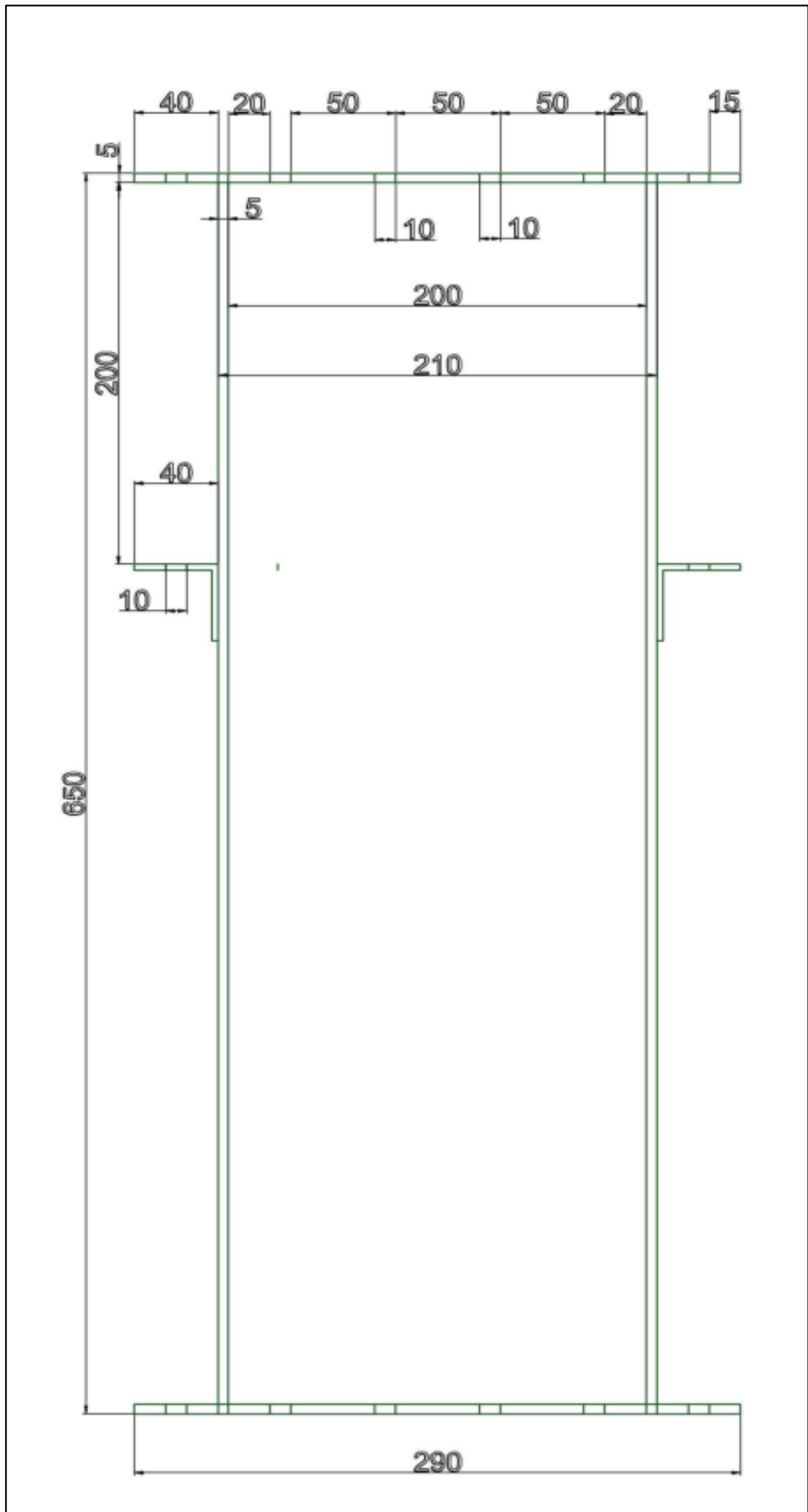
Fig. A8: Front view of top casing.
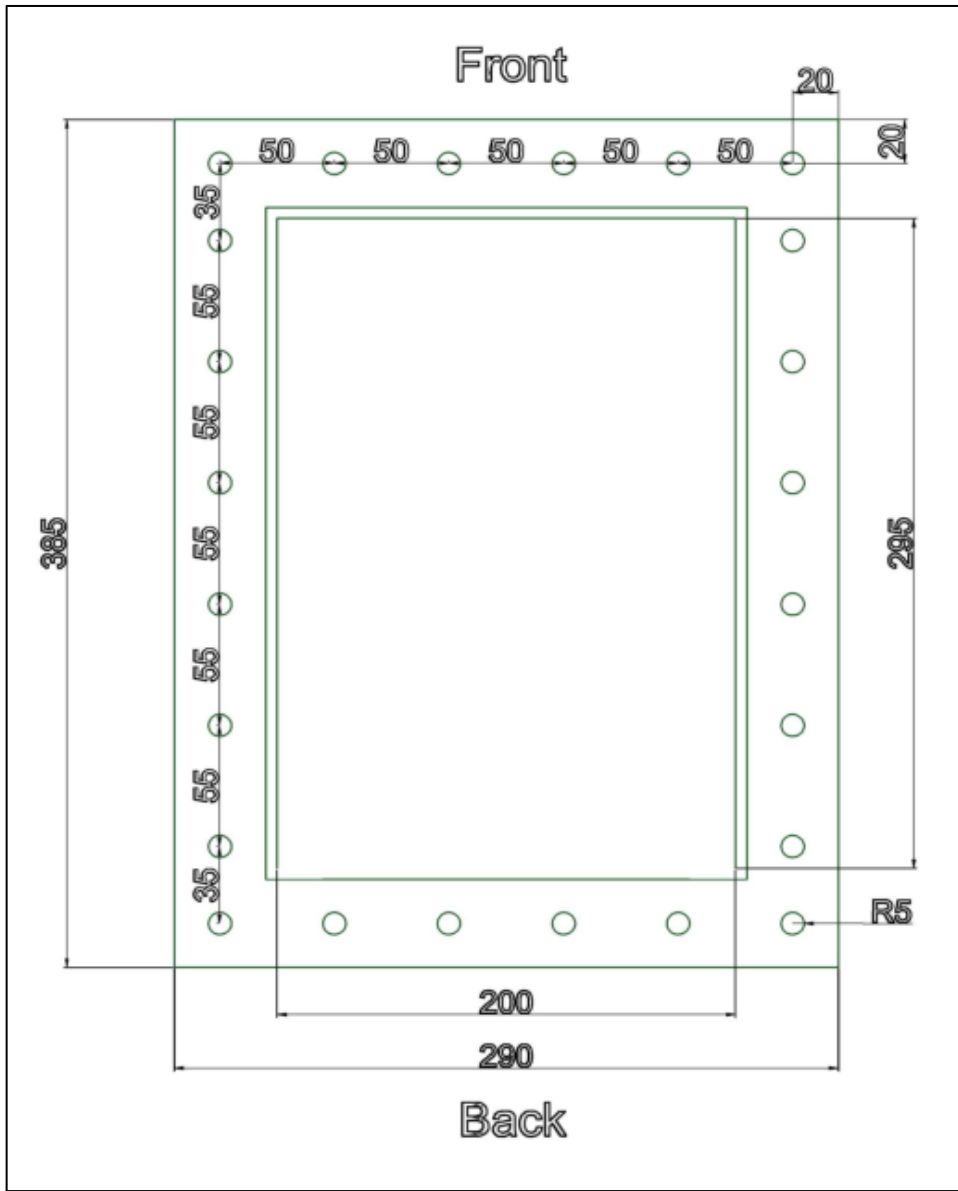
Fig. A9: Plan view of top casing.
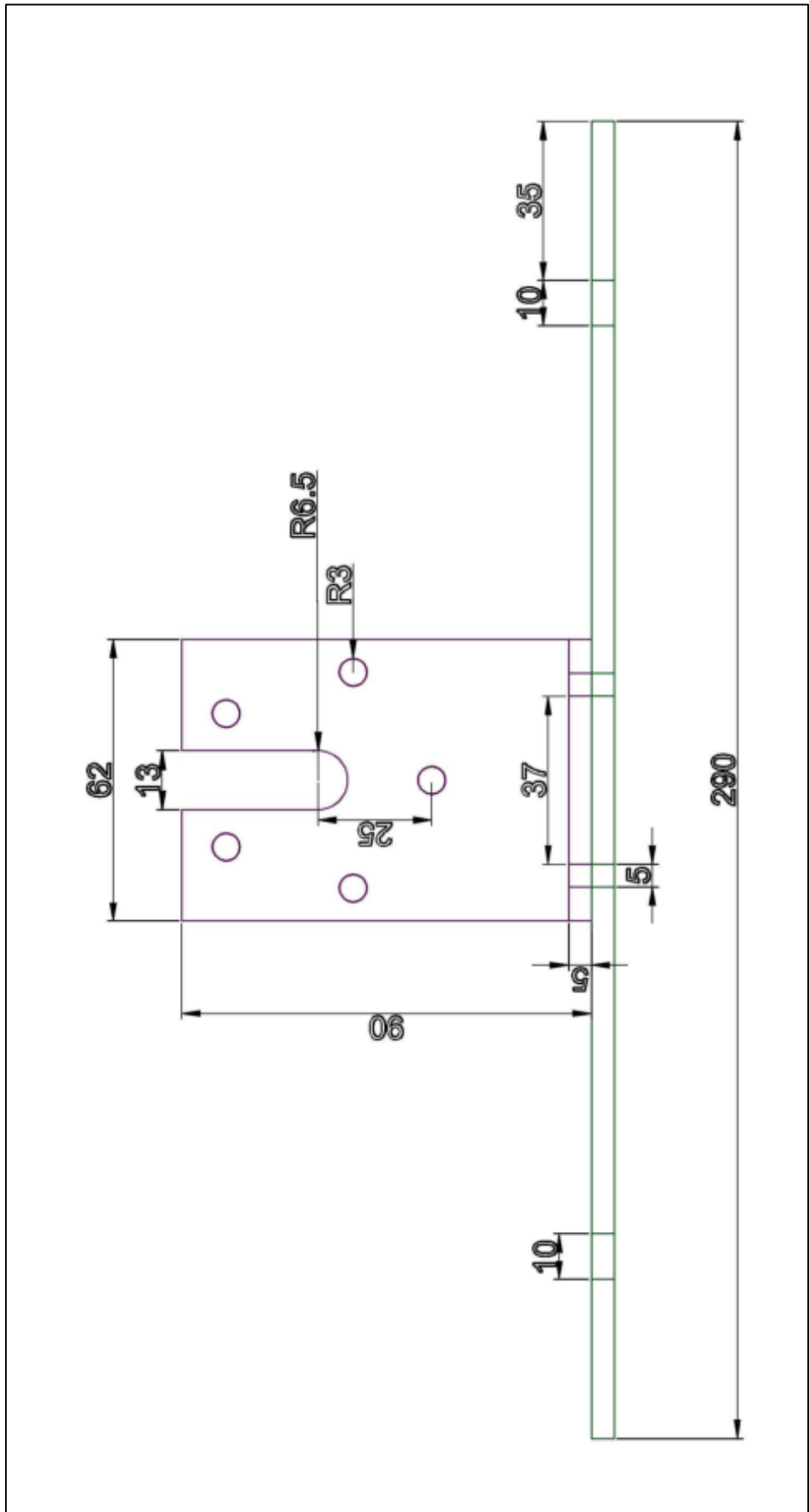
Fig. A10: Front view of generator platform with portable support flange.
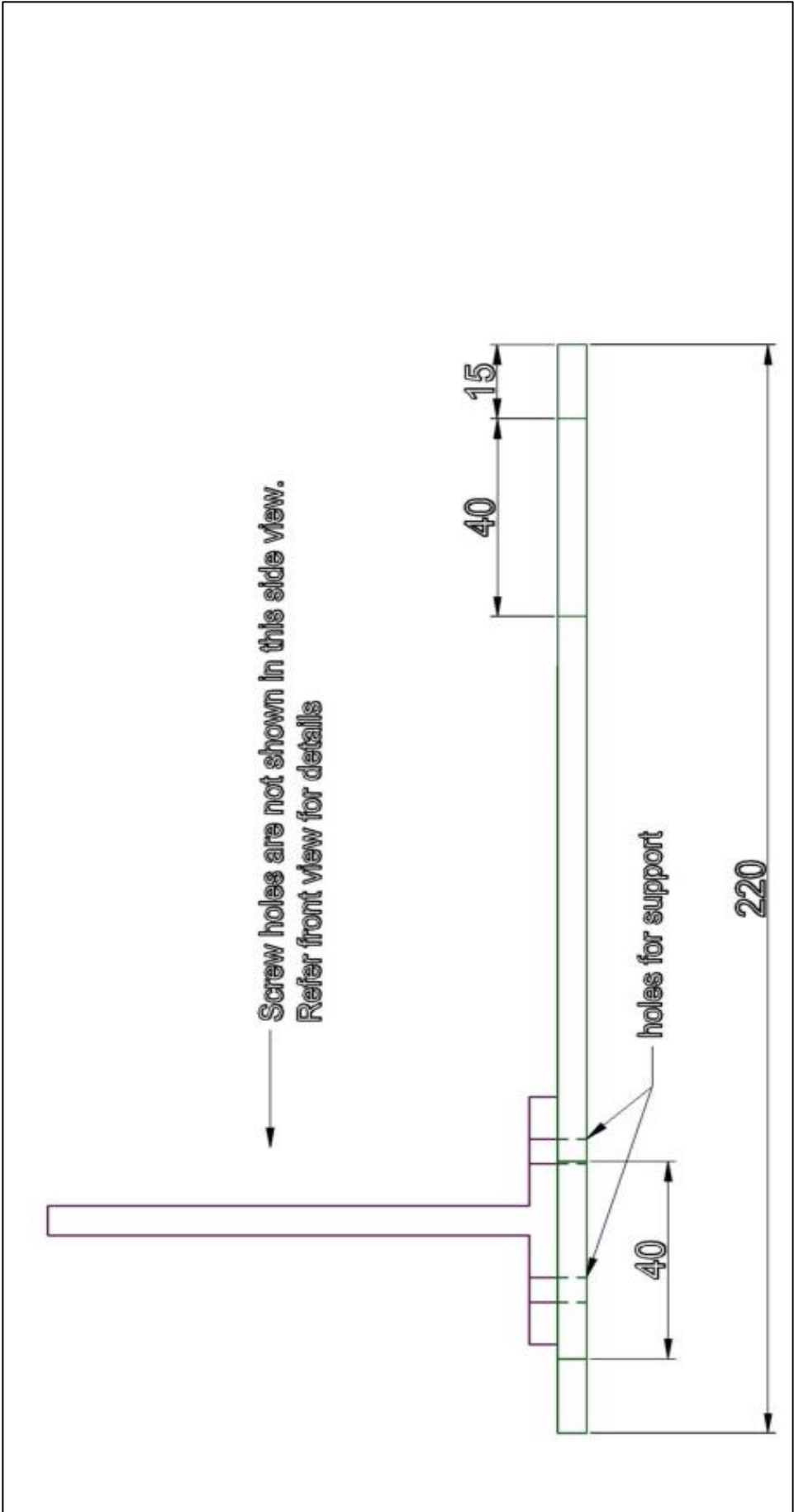
Fig. A11: Side view of generator platform with portable support flange.
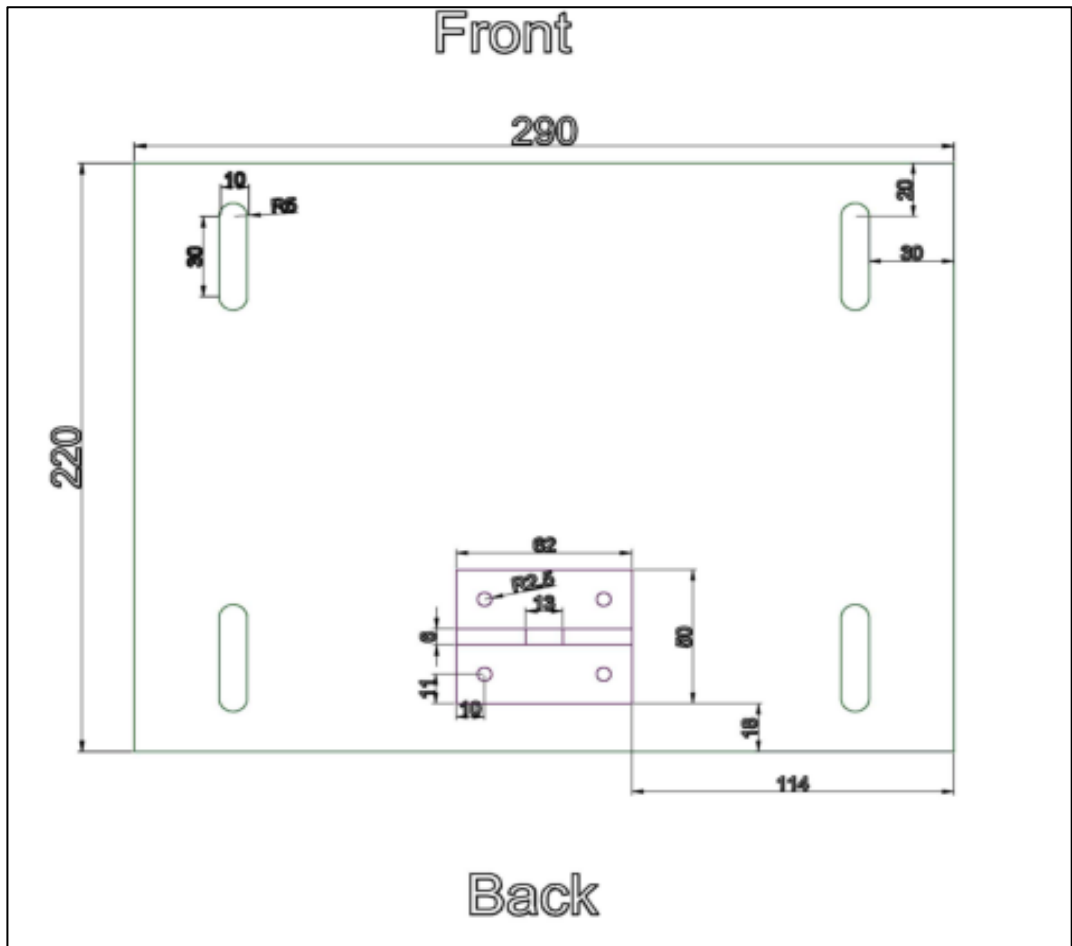
Fig. A12: Plan view of generator platform with portable support flange.
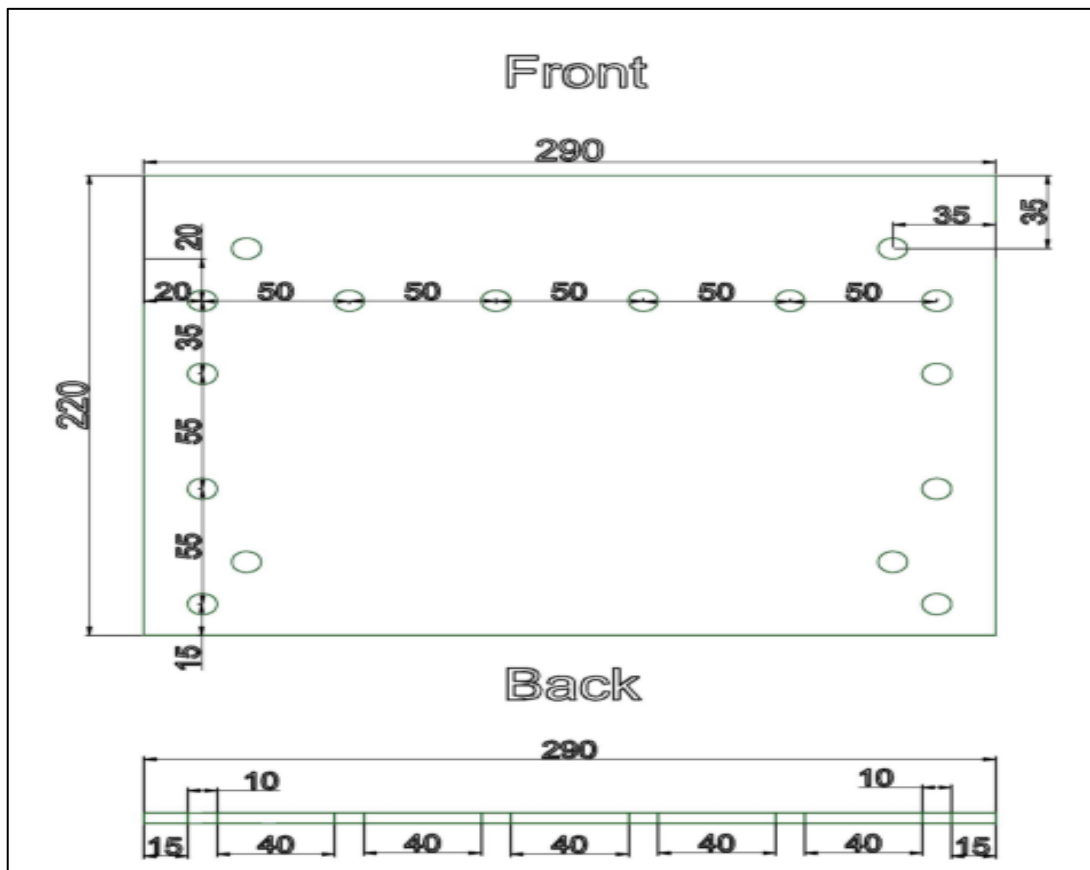
Fig. A13: Plan view and front view of cover plate for top casing.

APPENDIX B

PHOTOS OF FIELD TEST AND LAB-SCALE TEST

Fig. B1: Full assembly of FBT.

Fig. B2: Photo taken during calibration.
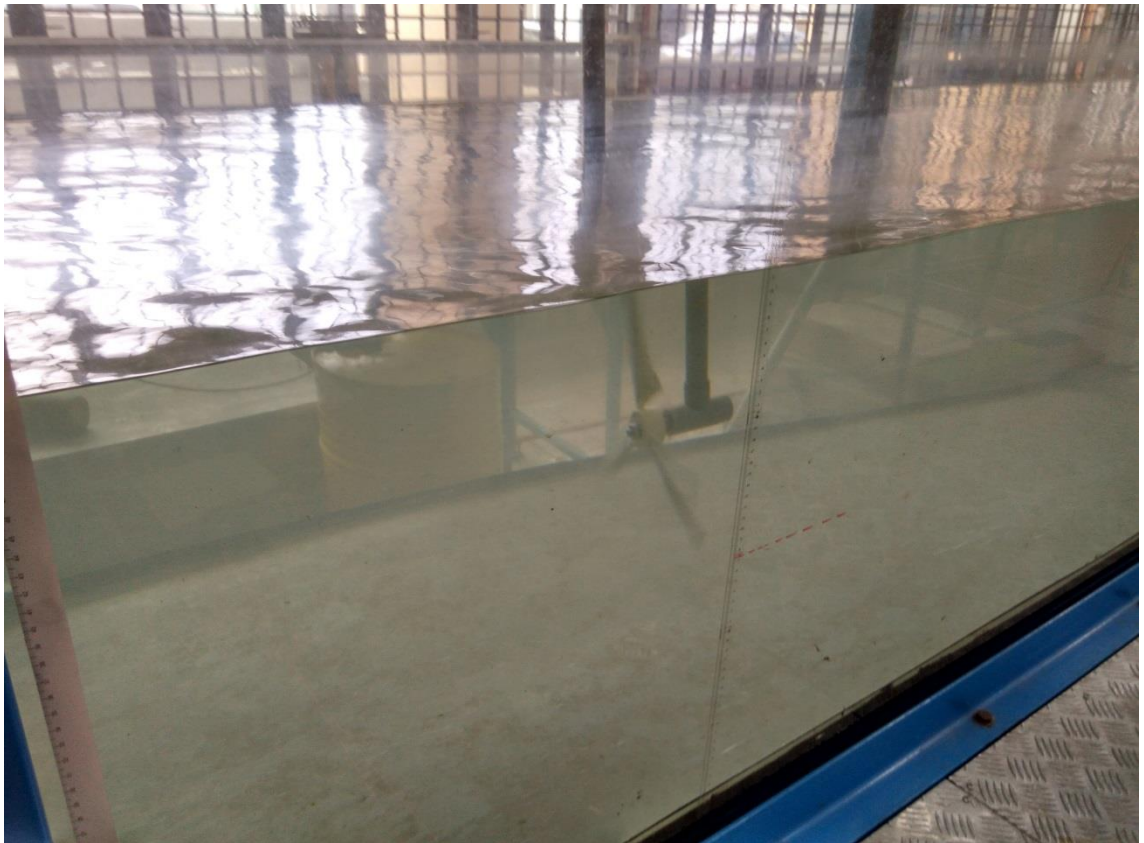
Fig B3. Photo taken for lab-scale three-bladed turbine (front)

Fig B4. Photo taken for lab-scale three-bladed turbine (back)
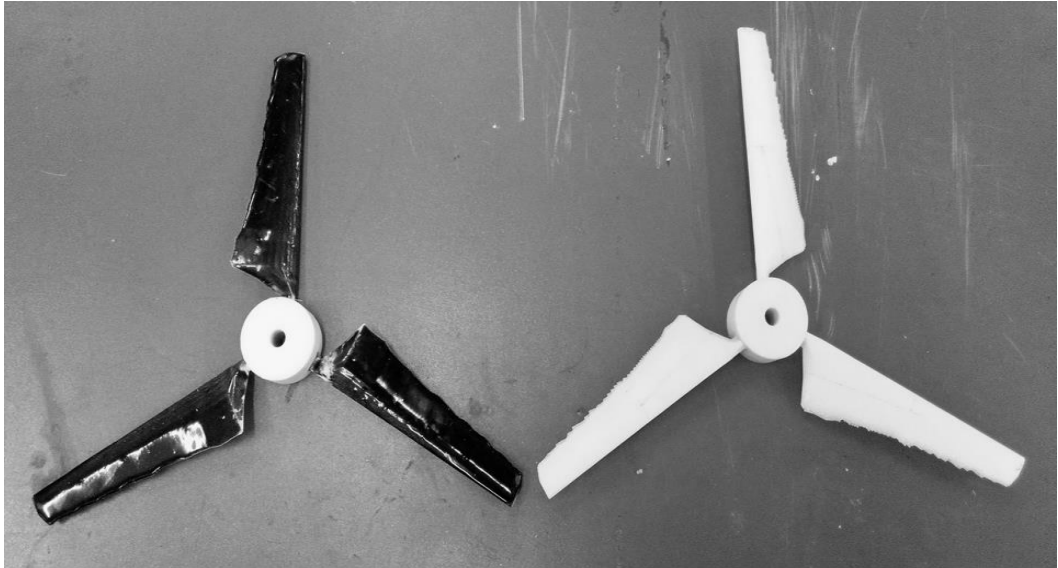
Fig B5. Three-bladed turbines used for lab-test.
(left coated with hydrophobic coating and right without hydrophobic coating

APPENDIX C

RAW DATA FOR ALL TESTS
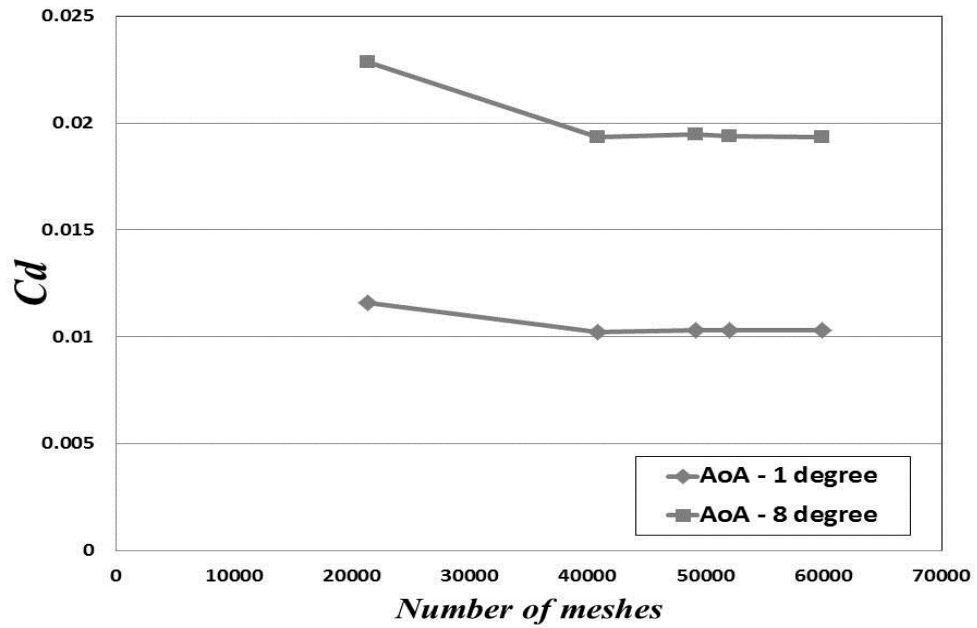
Fig. C1: Mesh Independence Test for NACA 63418

Table C1: Simulated lift and drag forces by ANSYS Fluent
for NACA 63418 without coating.

AoA	Lift Forces (N)	Drag Forces (N)
1	0.12190	0.012748
2	0.15045	0.013324
3	0.17831	0.014126
4	0.20523	0.015148
5	0.23106	0.016389
6	0.25565	0.017850
7	0.27897	0.019538
8	0.30100	0.021463
9	0.32141	0.023627
10	0.33985	0.026066
11	0.35636	0.028769

Table C2: Simulated lift and drag forces by ANSYS Fluent
for NACA 63418 with coating on upper surface.

AoA	Lift Forces (N)	Drag Forces (N)
1	0.12371	0.012324
2	0.15225	0.012900
3	0.18015	0.013692
4	0.20715	0.014698
5	0.23306	0.015917
6	0.25773	0.017350
7	0.28118	0.019009
8	0.30319	0.020902
9	0.32342	0.023043
10	0.34141	0.025483

Table C3: Lift forces measured for NACA 63418 without coating.

AoA (°)	Lift Forces (N)										Average
	1	2	3	4	5	6	7	8	9	10	
1	0.087	0.088	0.088	0.090	0.089	0.091	0.091	0.088	0.089	0.089	0.089
2	0.108	0.110	0.108	0.108	0.108	0.109	0.111	0.109	0.109	0.110	0.109
3	0.132	0.132	0.128	0.127	0.129	0.130	0.127	0.128	0.129	0.128	0.129
4	0.149	0.150	0.150	0.149	0.148	0.149	0.149	0.150	0.147	0.149	0.149
5	0.167	0.169	0.170	0.169	0.167	0.167	0.167	0.169	0.168	0.167	0.168
6	0.186	0.184	0.186	0.187	0.186	0.187	0.187	0.186	0.186	0.185	0.186
7	0.205	0.203	0.202	0.203	0.202	0.202	0.203	0.204	0.202	0.204	0.203
8	0.218	0.225	0.224	0.217	0.220	0.218	0.217	0.221	0.220	0.220	0.220
9	0.234	0.235	0.235	0.234	0.233	0.235	0.236	0.236	0.236	0.236	0.235
10	0.249	0.248	0.248	0.246	0.249	0.248	0.247	0.248	0.248	0.249	0.248
11	0.258	0.261	0.262	0.258	0.258	0.258	0.259	0.261	0.262	0.263	0.260

Table C4: Drag forces measured for NACA 63418 without coating.

AoA (°)	Drag Forces (N)										Average
	1	2	3	4	5	6	7	8	9	10	
1	0.011	0.010	0.011	0.011	0.010	0.011	0.011	0.011	0.011	0.011	0.0108
2	0.011	0.011	0.012	0.011	0.012	0.010	0.011	0.010	0.011	0.011	0.0110
3	0.012	0.012	0.011	0.011	0.012	0.011	0.011	0.012	0.012	0.011	0.0115
4	0.013	0.012	0.012	0.011	0.012	0.011	0.012	0.012	0.011	0.013	0.0119
5	0.013	0.012	0.013	0.012	0.013	0.013	0.012	0.012	0.012	0.012	0.0124
6	0.014	0.014	0.012	0.012	0.013	0.013	0.014	0.014	0.014	0.013	0.0133
7	0.015	0.015	0.014	0.015	0.014	0.013	0.013	0.014	0.013	0.014	0.0140
8	0.016	0.015	0.015	0.015	0.015	0.014	0.014	0.016	0.015	0.015	0.0150
9	0.015	0.016	0.015	0.016	0.017	0.016	0.016	0.017	0.016	0.016	0.0160
10	0.018	0.017	0.017	0.018	0.017	0.018	0.018	0.017	0.017	0.018	0.0175
11	0.020	0.021	0.020	0.020	0.021	0.022	0.021	0.022	0.021	0.022	0.0210

Table C5: Lift forces measured for NACA 63418 coated with Biocyl on upper surface.

AoA (º)	Lift Forces (N)										Average
	1	2	3	4	5	6	7	8	9	10	
1	0.089	0.090	0.089	0.088	0.089	0.089	0.091	0.089	0.091	0.090	0.0895
2	0.109	0.108	0.107	0.107	0.110	0.108	0.109	0.110	0.109	0.108	0.1085
3	0.130	0.129	0.132	0.129	0.130	0.129	0.131	0.130	0.131	0.129	0.1300
4	0.149	0.150	0.149	0.148	0.150	0.149	0.148	0.149	0.149	0.148	0.1490
5	0.166	0.167	0.168	0.167	0.167	0.168	0.166	0.166	0.167	0.168	0.1670
6	0.187	0.184	0.186	0.185	0.184	0.186	0.185	0.186	0.187	0.185	0.1855
7	0.204	0.204	0.203	0.204	0.203	0.204	0.204	0.203	0.204	0.202	0.2035
8	0.220	0.223	0.224	0.220	0.220	0.221	0.219	0.220	0.221	0.222	0.2210
9	0.233	0.232	0.233	0.234	0.235	0.234	0.236	0.234	0.235	0.234	0.2340
10	0.250	0.249	0.248	0.249	0.247	0.250	0.249	0.249	0.251	0.248	0.2490
11	0.259	0.257	0.258	0.259	0.260	0.259	0.257	0.258	0.256	0.257	0.2580

Table C6: Drag forces measured for NACA 63418 coated with Biocyl on upper surface.

AoA (°)	Drag Forces (N)										Average
	1	2	3	4	5	6	7	8	9	10	
1	0.010	0.011	0.009	0.010	0.011	0.010	0.011	0.011	0.009	0.011	0.0103
2	0.010	0.010	0.011	0.011	0.011	0.011	0.010	0.010	0.010	0.011	0.0105
3	0.011	0.011	0.010	0.011	0.011	0.012	0.010	0.011	0.011	0.012	0.0110
4	0.011	0.010	0.012	0.012	0.012	0.012	0.012	0.011	0.012	0.012	0.0116
5	0.012	0.011	0.012	0.011	0.012	0.012	0.013	0.012	0.012	0.013	0.0120
6	0.013	0.012	0.013	0.012	0.014	0.013	0.013	0.013	0.013	0.014	0.0130
7	0.014	0.014	0.013	0.013	0.014	0.014	0.013	0.013	0.014	0.013	0.0135
8	0.015	0.015	0.014	0.014	0.015	0.015	0.014	0.014	0.015	0.015	0.0146
9	0.016	0.016	0.015	0.015	0.016	0.015	0.016	0.016	0.015	0.017	0.0157
10	0.017	0.018	0.016	0.017	0.018	0.017	0.017	0.018	0.017	0.017	0.0172
11	0.021	0.020	0.021	0.021	0.021	0.021	0.020	0.020	0.021	0.021	0.0207

Table C7: Lift forces measured for NACA 63418 fully coated with Biocyl.

AoA (°)	1	2	3	4	5	6	7	8	9	10	Average
	Lift Forces (N)										
1	0.090	0.089	0.089	0.090	0.090	0.088	0.090	0.090	0.090	0.089	0.0895
2	0.108	0.110	0.108	0.108	0.109	0.109	0.108	0.108	0.108	0.109	0.1085
3	0.128	0.130	0.131	0.132	0.131	0.130	0.129	0.128	0.129	0.132	0.1300
4	0.150	0.151	0.148	0.149	0.148	0.148	0.149	0.149	0.148	0.150	0.1490
5	0.168	0.168	0.167	0.166	0.168	0.166	0.167	0.167	0.166	0.167	0.1670
6	0.185	0.186	0.184	0.186	0.185	0.185	0.186	0.187	0.185	0.186	0.1855
7	0.202	0.204	0.201	0.203	0.200	0.202	0.202	0.201	0.202	0.203	0.2020
8	0.218	0.220	0.220	0.219	0.219	0.218	0.221	0.218	0.218	0.219	0.2190
9	0.234	0.233	0.232	0.233	0.234	0.234	0.235	0.235	0.234	0.236	0.2340
10	0.245	0.243	0.244	0.245	0.246	0.246	0.245	0.246	0.244	0.246	0.2453
11	0.257	0.255	0.257	0.256	0.255	0.256	0.255	0.256	0.257	0.256	0.2560

Table C8: Drag forces measured for NACA 63418 fully coated with Biocyl.

AoA (°)	Drag Forces (N)										Average
	1	2	3	4	5	6	7	8	9	10	
1	0.010	0.009	0.010	0.009	0.011	0.011	0.010	0.010	0.011	0.010	0.0101
2	0.010	0.011	0.010	0.010	0.010	0.011	0.010	0.010	0.011	0.010	0.0103
3	0.010	0.011	0.011	0.012	0.011	0.011	0.011	0.010	0.011	0.011	0.0109
4	0.012	0.012	0.011	0.011	0.011	0.011	0.012	0.011	0.012	0.011	0.0114
5	0.013	0.012	0.013	0.012	0.013	0.013	0.012	0.012	0.012	0.012	0.0119
6	0.012	0.013	0.013	0.013	0.013	0.014	0.013	0.012	0.013	0.013	0.0129
7	0.013	0.013	0.014	0.013	0.013	0.014	0.014	0.014	0.013	0.014	0.0135
8	0.014	0.015	0.015	0.014	0.015	0.015	0.014	0.015	0.015	0.014	0.0146
9	0.016	0.016	0.016	0.016	0.015	0.015	0.016	0.016	0.016	0.015	0.0157
10	0.017	0.017	0.018	0.018	0.017	0.017	0.017	0.017	0.017	0.017	0.0172
11	0.022	0.021	0.020	0.020	0.020	0.022	0.021	0.020	0.020	0.021	0.0207

Table C9: Lift forces measured for NACA 63418 coated with Biocyl on front half of upper surface.

AoA (°)	Lift Forces (N)										Average
	1	2	3	4	5	6	7	8	9	10	
1	0.089	0.089	0.090	0.090	0.091	0.090	0.090	0.090	0.089	0.089	0.0897
2	0.108	0.108	0.109	0.109	0.110	0.109	0.108	0.108	0.107	0.108	0.1084
3	0.130	0.130	0.131	0.131	0.129	0.130	0.129	0.131	0.130	0.131	0.1302
4	0.148	0.149	0.148	0.149	0.149	0.150	0.149	0.148	0.149	0.149	0.1488
5	0.168	0.166	0.167	0.168	0.168	0.169	0.168	0.168	0.167	0.167	0.1676
6	0.186	0.187	0.187	0.187	0.186	0.185	0.187	0.185	0.186	0.186	0.1862
7	0.202	0.203	0.204	0.203	0.204	0.203	0.203	0.204	0.203	0.203	0.2032
8	0.222	0.221	0.221	0.222	0.222	0.223	0.221	0.222	0.220	0.220	0.2214
9	0.234	0.234	0.235	0.235	0.234	0.235	0.234	0.235	0.234	0.235	0.2345
10	0.249	0.247	0.250	0.250	0.249	0.247	0.248	0.250	0.248	0.249	0.2487
11	0.260	0.259	0.257	0.258	0.259	0.257	0.260	0.260	0.259	0.260	0.2589

Table C10: Drag forces measured for NACA 63418 coated with Biocyl on front half of upper surface.

AoA (°)	Drag Forces (N)										Average
	1	**2**	**3**	**4**	**5**	**6**	**7**	**8**	**9**	**10**	
1	0.011	0.009	0.011	0.011	0.010	0.011	0.010	0.009	0.011	0.011	0.0104
2	0.011	0.011	0.010	0.011	0.010	0.010	0.011	0.010	0.011	0.011	0.0106
3	0.010	0.011	0.011	0.012	0.012	0.011	0.011	0.010	0.010	0.011	0.0109
4	0.012	0.012	0.011	0.010	0.012	0.011	0.011	0.011	0.012	0.012	0.0114
5	0.011	0.012	0.011	0.013	0.013	0.011	0.012	0.013	0.013	0.013	0.0122
6	0.012	0.013	0.013	0.013	0.012	0.014	0.012	0.014	0.013	0.012	0.0128
7	0.014	0.013	0.012	0.014	0.013	0.014	0.014	0.012	0.013	0.014	0.0133
8	0.014	0.016	0.016	0.015	0.014	0.014	0.015	0.015	0.014	0.015	0.0148
9	0.015	0.015	0.016	0.015	0.015	0.016	0.015	0.016	0.016	0.015	0.0154
10	0.018	0.017	0.017	0.016	0.016	0.018	0.018	0.017	0.016	0.017	0.0170
11	0.021	0.021	0.022	0.020	0.020	0.020	0.021	0.021	0.021	0.022	0.0209

Table C11: Lift forces measured for NACA 63418 coated with Always Dry on upper surface.

AoA (°)	Lift Forces (N)										Average
	1	2	3	4	5	6	7	8	9	10	
1	0.090	0.090	0.088	0.089	0.088	0.090	0.090	0.090	0.089	0.089	0.0893
2	0.108	0.107	0.108	0.108	0.108	0.109	0.110	0.109	0.108	0.107	0.1084
3	0.129	0.129	0.129	0.130	0.131	0.130	0.129	0.1.29	0.130	0.130	0.1296
4	0.148	0.149	0.149	0.150	0.149	0.148	0.149	0.150	0.149	0.148	0.1489
5	0.168	0.166	0.167	0.168	0.166	0.167	0.167	0.168	0.168	0.168	0.1673
6	0.185	0.185	0.187	0.186	0.186	0.187	0.186	0.185	0.185	0.185	0.1857
7	0.203	0.203	0.204	0.205	0.204	0.203	0.203	0.202	0.203	0.203	0.2033
8	0.222	0.221	0.221	0.221	0.223	0.222	0.220	0.221	0.220	0.221	0.2212
9	0.234	0.235	0.234	0.235	0.234	0.233	0.234	0.235	0.234	0.235	0.2343
10	0.248	0.250	0.249	0.248	0.249	0.248	0.250	0.249	0.248	0.249	0.2488
11	0.258	0.258	0.259	0.260	0.258	0.258	0.259	0.259	0.257	0.257	0.2583

Table C12: Drag forces measured for NACA 63418 coated with Always Dry on upper surface.

AoA (°)	Drag Forces (N)										Average
	1	2	3	4	5	6	7	8	9	10	
1	0.009	0.010	0.011	0.011	0.010	0.010	0.011	0.010	0.011	0.010	0.0103
2	0.011	0.010	0.010	0.011	0.010	0.010	0.011	0.011	0.011	0.011	0.0106
3	0.010	0.010	0.011	0.012	0.010	0.011	0.012	0.011	0.011	0.012	0.0110
4	0.012	0.012	0.011	0.012	0.011	0.011	0.011	0.012	0.011	0.011	0.0114
5	0.012	0.012	0.011	0.012	0.011	0.012	0.012	0.013	0.013	0.012	0.0120
6	0.014	0.013	0.014	0.013	0.013	0.013	0.014	0.014	0.013	0.013	0.0129
7	0.013	0.014	0.014	0.013	0.013	0.013	0.014	0.014	0.014	0.015	0.0136
8	0.014	0.014	0.015	0.013	0.014	0.015	0.015	0.015	0.016	0.015	0.0146
9	0.017	0.015	0.016	0.016	0.015	0.016	0.015	0.015	0.016	0.015	0.0156
10	0.018	0.017	0.017	0.018	0.017	0.017	0.018	0.017	0.017	0.017	0.0173
11	0.020	0.020	0.020	0.022	0.020	0.021	0.021	0.021	0.021	0.020	0.0206

Table C13: Lift forces measured for NACA 63418 fully coated with Always Dry.

AoA (º)	Lift Forces (N)										Average
	1	2	3	4	5	6	7	8	9	10	
1	0.089	0.089	0.090	0.090	0.090	0.091	0.090	0.090	0.089	0.089	0.0897
2	0.108	0.109	0.108	0.108	0.109	0.108	0.108	0.107	0.109	0.109	0.1083
3	0.129	0.128	0.129	0.130	0.131	0.130	0.129	0.130	0.131	0.131	0.1298
4	0.150	0.148	0.148	0.150	0.149	0.151	0.150	0.150	0.149	0.148	0.1493
5	0.167	0.167	0.168	0.167	0.168	0.168	0.167	0.167	0.168	0.167	0.1674
6	0.186	0.185	0.185	0.184	0.184	0.186	0.186	0.185	0.186	0.186	0.1853
7	0.201	0.202	0.202	0.203	0.202	0.202	0.203	0.202	0.203	0.202	0.2022
8	0.219	0.219	0.220	0.219	0.218	0.219	0.220	0.219	0.220	0.220	0.2193
9	0.233	0.233	0.234	0.233	0.234	0.235	0.235	0.234	0.233	0.235	0.2339
10	0.245	0.246	0.245	0.244	0.244	0.243	0.244	0.245	0.246	0.245	0.2447
11	0.256	0.256	0.255	0.257	0.256	0.256	0.255	0.255	0.256	0.256	0.2558

Table C14: Drag forces measured for NACA 63418 fully coated with Always Dry.

AoA (º)	Drag Forces (N)										Average
	1	2	3	4	5	6	7	8	9	10	
1	0.010	0.011	0.009	0.010	0.010	0.010	0.011	0.010	0.010	0.009	0.0100
2	0.010	0.009	0.010	0.011	0.011	0.010	0.010	0.011	0.010	0.011	0.0102
3	0.011	0.011	0.010	0.011	0.010	0.011	0.011	0.011	0.010	0.011	0.0107
4	0.011	0.012	0.012	0.011	0.010	0.012	0.011	0.012	0.011	0.010	0.0112
5	0.012	0.012	0.012	0.011	0.012	0.012	0.012	0.011	0.011	0.012	0.0117
6	0.013	0.012	0.013	0.014	0.013	0.013	0.012	0.013	0.013	0.012	0.0128
7	0.014	0.013	0.013	0.014	0.014	0.013	0.013	0.013	0.014	0.013	0.0134
8	0.015	0.015	0.014	0.015	0.014	0.014	0.014	0.015	0.015	0.015	0.0146
9	0.015	0.015	0.016	0.015	0.016	0.016	0.015	0.016	0.016	0.016	0.0156
10	0.018	0.018	0.017	0.016	0.017	0.016	0.018	0.018	0.017	0.016	0.0171
11	0.021	0.020	0.020	0.021	0.021	0.021	0.022	0.020	0.021	0.020	0.0207

Table C15: Lift forces measured for NACA 63418 coated with Always Dry on front half of upper surface.

AoA (°)	Lift Forces (N)										Average
	1	2	3	4	5	6	7	8	9	10	
1	0.090	0.089	0.090	0.089	0.090	0.089	0.089	0.090	0.090	0.090	0.0896
2	0.109	0.109	0.108	0.109	0.108	0.108	0.109	0.109	0.109	0.109	0.1087
3	0.130	0.129	0.129	0.130	0.131	0.131	0.130	0.130	0.129	0.130	0.1299
4	0.149	0.149	0.148	0.148	0.149	0.149	0.149	0.149	0.148	0.149	0.1487
5	0.167	0.166	0.168	0.167	0.167	0.168	0.168	0.167	0.168	0.169	0.1675
6	0.185	0.186	0.185	0.187	0.187	0.186	0.186	0.185	0.185	0.186	0.1858
7	0.204	0.204	0.203	0.202	0.203	0.204	0.204	0.203	0.203	0.204	0.2034
8	0.220	0.220	0.221	0.222	0.221	0.222	0.221	0.220	0.221	0.220	0.2208
9	0.235	0.234	0.234	0.234	0.235	0.234	0.234	0.235	0.235	0.234	0.2344
10	0.249	0.248	0.248	0.249	0.250	0.249	0.247	0.248	0.249	0.248	0.2485
11	0.259	0.258	0.259	0.259	0.258	0.259	0.259	0.258	0.258	0.259	0.2586

Table C16: Drag forces measured for NACA 63418 coated with Always Dry on front half of upper surface.

AoA (°)	Drag Forces (N)										Average
	1	**2**	**3**	**4**	**5**	**6**	**7**	**8**	**9**	**10**	**Average**
1	0.010	0.010	0.010	0.011	0.011	0.011	0.010	0.009	0.010	0.011	0.0103
2	0.010	0.011	0.011	0.010	0.011	0.011	0.011	0.010	0.011	0.011	0.0107
3	0.011	0.010	0.010	0.011	0.011	0.012	0.011	0.012	0.011	0.010	0.0109
4	0.011	0.011	0.012	0.011	0.012	0.011	0.011	0.011	0.012	0.011	0.0113
5	0.013	0.013	0.012	0.011	0.011	0.012	0.011	0.012	0.013	0.012	0.0120
6	0.013	0.012	0.013	0.013	0.014	0.013	0.012	0.013	0.013	0.014	0.0130
7	0.014	0.014	0.013	0.014	0.013	0.014	0.013	0.013	0.014	0.013	0.0135
8	0.015	0.015	0.014	0.014	0.013	0.014	0.015	0.014	0.015	0.015	0.0144
9	0.016	0.016	0.015	0.015	0.016	0.017	0.016	0.016	0.015	0.015	0.0157
10	0.017	0.018	0.018	0.017	0.016	0.016	0.017	0.017	0.018	0.017	0.0171
11	0.021	0.020	0.021	0.020	0.021	0.022	0.022	0.021	0.020	0.020	0.0208

Table C17: Power output for the TBT without coating at different TSR.

TSR	Power Output (W)			
	1	2	3	Average
1	0.045	0.042	0.045	0.044
2	0.320	0.300	0.300	0.307
3	0.738	0.746	0.742	0.742
4	0.841	0.832	0.845	0.839
5	0.756	0.765	0.769	0.763

Table C18: Power output for the TBT fully coated with Biocyl at different TSR.

TSR	Power Output (W)			
	1	2	3	Average
1	0.045	0.045	0.048	0.046
2	0.300	0.320	0.300	0.307
3	0.746	0.749	0.742	0.745
4	0.836	0.849	0.841	0.842
5	0.769	0.761	0.789	0.773

Table C19: Power output for the TBT coated with Biocyl
on suction side at different TSR.

TSR	Power Output (W)			
	1	2	3	Average
1	0.045	0.045	0.045	0.045
2	0.300	0.300	0.300	0.300
3	0.728	0.742	0.735	0.735
4	0.845	0.841	0.845	0.842
5	0.769	0.777	0.766	0.771

Table C20: Power output for the TBT fully coated with Always Dry at different TSR.

TSR	Power Output (W)			
	1	2	3	Average
1	0.045	0.048	0.042	0.044
2	0.300	0.320	0.320	0.313
3	0.742	0.746	0.746	0.744
4	0.853	0.845	0.849	0.849
5	0.765	0.778	0.769	0.770

Table C21: Power output for the TBT coated with Always Dry
on suction side at different TSR.

TSR	Power Output (W)			
	1	2	3	Average
1	0.048	0.045	0.045	0.046
2	0.320	0.300	0.320	0.313
3	0.731	0.746	0.738	0.738
4	0.845	0.841	0.853	0.846
5	0.761	0.769	0.769	0.766

Table C22: Simulated power coefficient by WT_Perf for the TBT with different assumption of drag reduction.

TSR	Power Coefficients (Cp)		
	Without coating	10% drag reduction	30% drag reduction
2	0.155696	0.161057	0.171953
3	0.392272	0.394297	0.404875
4	0.443950	0.445635	0.449007
5	0.453549	0.456196	0.461491
6	0.448844	0.453128	0.461712

Table C23: Power output of the FBT with 8x gearing at different velocities.

Velocity (m/s)	Power Output (W)		
	1	2	3
0.100	0.0405	0.0416	-
0.105	0.0449	0.0424	-
0.110	0.0441	0.0432	-
0.115	0.0424	0.0441	-
0.120	0.0615	0.0677	-
0.125	0.0729	0.0762	-
0.130	0.0807	0.0784	-
0.135	0.0936	0.0876	-
0.140	0.1024	0.1089	-
0.145	0.1296	0.1444	-
0.150	0.1681	0.1599	-
0.155	0.2304	0.2116	-
0.160	0.2497	0.2304	-
0.165	0.2916	0.3136	-
0.170	0.3249	0.3091	-
0.175	0.3364	0.3318	-
0.180	0.4096	0.4356	-
0.185	0.4225	0.4898	-
0.190	0.5476	0.5296	-
0.195	0.5958	0.5685	-
0.200	0.5837	0.5929	-
0.201	0.6022	0.5776	-
0.202	0.5715	0.6084	-
0.203	0.6399	0.6086	-
0.204	0.6147	0.6304	-
0.205	0.6496	0.6724	-
0.206	0.6561	0.6724	0.6399
0.207	0.6823	0.6755	0.6659
0.208	0.6922	0.7056	0.6889
0.209	0.6989	0.7123	0.7024
0.210	0.7225	0.7121	0.7056
0.211	0.7228	0.7396	0.7157
0.212	0.7498	0.7396	0.7604
0.213	0.7597	0.7674	0.7569
0.214	0.7327	0.7744	0.7885
0.215	0.8028	0.7957	0.8094

0.216	0.8208	0.8102	0.7885
0.217	0.8172	0.8353	0.8281
0.218	0.8391	0.8208	0.8281
0.219	0.8464	0.8427	0.8575
0.220	0.8354	0.8612	0.8649
0.221	0.8464	0.8644	0.8724
0.222	0.8612	0.8836	0.8706
0.223	0.8761	0.8686	0.8836
0.224	0.9063	0.9216	0.9025
0.225	0.9254	0.9178	0.9332
0.226	0.9526	0.9487	0.9607
0.227	0.9722	0.9801	0.9604
0.228	0.9841	0.9997	0.9761
0.229	1.0120	1.0323	1.0282
0.230	1.0445	1.0241	1.0609
0.231	1.0527	1.0816	1.0733
0.232	1.0899	1.0983	1.1025
0.233	1.1236	1.1067	1.1151
0.234	1.1278	1.4062	1.1321
0.235	1.1492	1.1406	1.1492
0.236	1.1664	1.1751	1.1578
0.237	1.1794	1.1881	1.2012
0.238	1.2188	1.1967	1.1881
0.239	1.2232	1.2321	1.2103
0.240	1.2277	1.2455	1.2365
0.241	1.2544	1.2455	1.2633
0.242	1.2679	1.2905	1.2899
0.243	1.2814	1.2769	1.2773
0.244	1.2814	1.2769	1.2774
0.245	1.2996	1.3087	1.2992
0.246	1.2905	1.3042	1.3133
0.247	1.3271	1.3317	1.3179
0.248	1.3409	1.3225	1.3363
0.249	1.3549	1.3456	1.3225
0.250	1.3545	1.3596	1.3454

Table C24: Power output of the FBT with 4x gearing at different velocities.

Velocity (m/s)	Power Output (W)		
	1	**2**	**3**
0.100	0.0064	0.0068	-
0.105	0.0064	0.0067	-
0.110	0.0071	0.0069	-
0.115	0.0074	0.0081	-
0.120	0.0077	0.0085	-
0.125	0.0102	0.0104	-
0.130	0.0101	0.0108	-
0.135	0.0121	0.0116	-
0.140	0.0149	0.0139	-
0.145	0.0174	0.0185	-
0.150	0.0225	0.0219	-
0.155	0.0256	0.0269	-
0.160	0.0361	0.0346	-
0.165	0.0416	0.0402	-
0.170	0.0449	0.0467	-
0.175	0.0502	0.0484	-
0.180	0.0529	0.0520	-
0.185	0.0511	0.0529	-
0.190	0.0548	0.0557	-
0.195	0.0538	0.0576	-
0.200	0.0577	0.0621	-
0.201	0.0635	0.0615	-
0.202	0.0645	0.0639	-
0.203	0.0655	0.0645	-
0.204	0.0676	0.0635	-
0.205	0.0666	0.0676	-
0.206	0.0673	0.0686	0.0708
0.207	0.0666	0.0635	0.0676
0.208	0.0673	0.0697	0.0666
0.209	0.0697	0.0686	0.0697
0.210	0.0676	0.0683	0.0667
0.211	0.0676	0.0708	0.0676
0.212	0.0665	0.0704	0.0718
0.213	0.0697	0.0691	0.0715
0.214	0.0708	0.0704	0.0676
0.215	0.0729	0.0740	0.0719
0.216	0.0729	0.0751	0.0740
0.217	0.0727	0.0762	0.0773
0.218	0.0751	0.0753	0.0762
0.219	0.0795	0.0784	0.0762
0.220	0.0784	0.0773	0.0765
0.221	0.0786	0.0796	0.0818
0.222	0.0841	0.0829	0.0833
0.223	0.0843	0.0830	0.0864
0.224	0.0829	0.0864	0.0888
0.225	0.0876	0.0876	0.0885

0.226	0.0901	0.0924	0.0888
0.227	0.0912	0.0921	0.0899
0.228	0.0936	0.0924	0.0949
0.229	0.0924	0.0937	0.0945
0.230	0.0961	0.0986	0.0957
0.231	0.0986	0.0973	0.0988
0.232	0.0999	0.0993	0.1024
0.233	0.1037	0.1011	0.0998
0.234	0.1050	0.1037	0.1024
0.235	0.1063	0.1089	0.1076
0.236	0.1089	0.1089	0.1102
0.237	0.1129	0.1116	0.1102
0.238	0.1125	0.1142	0.1129
0.239	0.1156	0.1147	0.1170
0.240	0.1156	0.1140	0.1183
0.241	0.1185	0.1197	0.1181
0.242	0.1225	0.1211	0.1220
0.243	0.1207	0.1253	0.1225
0.244	0.1239	0.1236	0.1251
0.245	0.1241	0.1253	0.1267
0.246	0.1296	0.1325	0.1310
0.247	0.1296	0.1323	0.1311
0.248	0.1340	0.1320	0.1324
0.249	0.1354	0.1369	0.1352
0.250	0.1369	0.1371	0.1334

Table C25: RPM of the TBT without coating at different velocity.

Velocity (m/s)	RPM										Average
	1	**2**	**3**	**4**	**5**	**6**	**7**	**8**	**9**	**10**	**Average**
0.280	74.60	74.90	74.70	74.70	74.50	74.65	74.83	74.77	74.74	74.68	74.71
0.300	78.01	78.20	78.20	77.90	77.80	77.75	77.79	79.53	78.71	77.59	78.15
0.333	89.94	89.50	89.70	90.08	90.13	89.45	89.20	89.40	89.93	89.41	89.67
0.350	94.24	94.16	94.15	94.23	94.20	94.26	94.17	94.17	94.21	94.19	94.20

Table C26: RPM of the TBT coated with Biocyl on suction side at different velocity.

Velocity (m/s)	RPM										Average
	1	**2**	**3**	**4**	**5**	**6**	**7**	**8**	**9**	**10**	**Average**
0.280	76.23	76.49	76.88	76.54	76.62	76.54	76.23	76.27	76.31	76.65	76.48
0.300	79.63	79.57	79.78	80.09	80.04	79.92	79.55	79.61	79.89	79.93	79.80
0.333	91.29	91.36	91.11	91.17	91.25	90.88	90.94	91.06	90.95	90.93	91.10
0.350	96.07	96.18	96.31	95.83	95.18	95.75	95.83	95.92	96.04	95.72	95.88

Table C27: RPM of the TBT fully coated with Biocyl at different velocity.

Velocity (m/s)	RPM										Average
	1	**2**	**3**	**4**	**5**	**6**	**7**	**8**	**9**	**10**	**Average**
0.280	75.22	75.78	75.74	75.68	75.38	75.59	75.51	75.62	75.49	75.57	75.56
0.300	78.82	79.08	79.13	79.01	79.18	79.12	79.03	78.89	79.11	79.14	79.05
0.333	90.37	90.71	90.58	90.67	90.48	90.79	90.56	90.73	90.69	90.53	90.61
0.350	94.74	94.81	95.12	95.19	94.98	95.08	94.98	94.92	94.89	95.07	94.98

Table C28: RPM of the TBT coated with Always Dry on suction side at different velocity.

Velocity (m/s)	RPM										Average
	1	**2**	**3**	**4**	**5**	**6**	**7**	**8**	**9**	**10**	
0.280	76.5	76.68	76.94	77.17	77.21	76.83	76.52	76.22	76.34	77.18	76.76
0.300	80.05	80.09	80.12	79.97	80.1	81.02	79.91	79.88	79.93	80.35	80.14
0.333	91.99	92.07	92.13	92.1	91.68	91.83	91.85	92.17	91.89	92.07	91.98
0.350	96.57	96.70	96.80	96.30	95.70	96.55	96.24	96.10	96.26	96.48	96.37

Table C29: RPM of the TBT fully coated with Always Dry at different velocity.

Velocity (m/s)	RPM										Average
	1	**2**	**3**	**4**	**5**	**6**	**7**	**8**	**9**	**10**	
0.280	75.51	75.33	76.05	76.00	76.21	75.26	75.78	75.92	75.45	76.07	75.76
0.300	78.99	79.15	78.92	78.74	79.21	79.13	79.07	79.20	79.11	78.99	79.05
0.333	90.84	90.62	91.10	90.96	90.78	90.71	90.69	90.72	90.93	90.67	90.80
0.350	95.31	95.72	95.03	95.12	95.18	95.57	95.43	95.47	96.44	95.26	95.35